ISSN 1023-9855

Thoracic Medicine

Volume 36 • Number 2 • June 2021

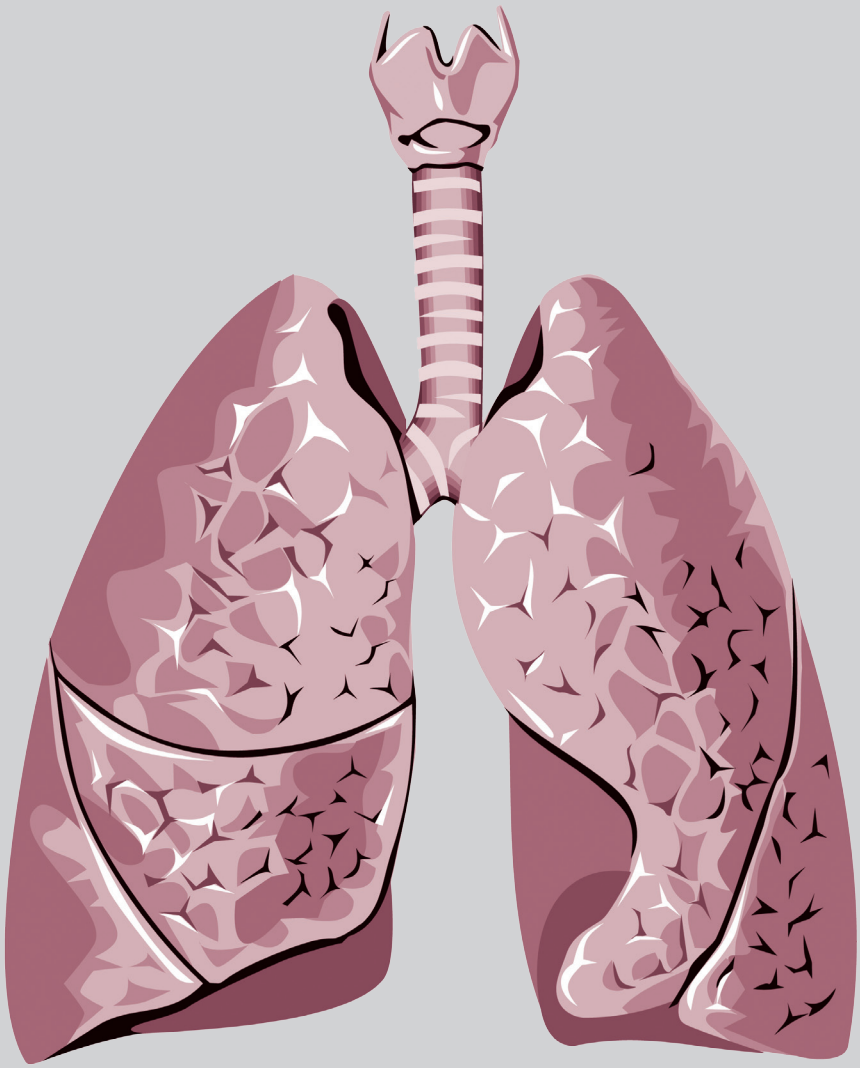

The Official Journal of

Taiwan Society of Pulmonary and Critical Care Medicine

Taiwan Society of Sleep Medicine

Taiwan Society for Respiratory Therapy

Taiwan Society of Tuberculosis and Lung Diseases

Thoracic Medicine

The Official Journal of
Taiwan Society of Pulmonary and Critical Care Medicine
Taiwan Society for Respiratory Therapy
Taiwan Society of Sleep Medicine
Taiwan Society of Tuberculosis and Lung Diseases

Thoracic Medicine

The Official Journal of
Taiwan Society of Pulmonary and Critical Care Medicine
Taiwan Society for Respiratory Therapy
Taiwan Society of Sleep Medicine
Taiwan Society of Tuberculosis and Lung Diseases

Volume 36
Number 2
June 2021

CONTENTS

Progression of Ventilator-Induced Lung Injury in COVID-19-Related Acute Respiratory Distress Syndrome, and Therapeutic Strategies

Chung-Sheng Shi[1,2,*], Shih-Hsing Yang[3,*], Chieh-Mo Lin[1,4,5], Chin-Kuo Lin[1,4], Tzu-Hsiung Huang[1,6,#]

Introduction: A common and obvious complication of progressive COVID-19 is acute hypoxemic respiratory insufficiency or failure, leading to acute respiratory distress syndrome (ARDS) and requiring oxygen therapy and mechanical ventilation. However, the pathological changes in ARDS resulting from COVID-19 are different from those of typical ARDS, and mechanically ventilated patients with COVID-19-related ARDS exhibit a higher mortality rate than do typical ARDS patients.

Objective: To review published articles on this topic with the objective of determining how to minimize the progression of patient self-inflicted lung injury or ventilator-induced lung injury (VILI) and improving the survival rate of mechanically ventilated patients with COVID-19-related ARDS.

Data Source: A literature search was undertaken in the PubMed database on all related studies up to August 2020. There were no restrictions on publication date, study design or language.

Study Selection: Included studies involved those that investigated the pathological changes of COVID-19-related ARDS and that proposed strategies to prevent and treat VILI in patients with COVID-19-related ARDS. Thirty-two relevant articles were selected for final review.

Results: We summarized the current research on the pathophysiology of COVID-19-related ARDS and the suggested therapeutic strategies to deal with the progression of patient self-inflicted lung injury or VILI.

Conclusion: According to the pathogenesis of mechanically ventilated patients with COVID-19-related ARDS, lung-protective ventilation strategies and early pharmacologic intervention may be considered not only as supportive therapy but also as preventive therapy.
(Thorac Med 2021; 36: 60-70)

Key words: COVID-19; acute respiratory distress syndrome; ventilator-induced lung injury; mechanical ventilation

[1]Graduate Institute of Clinical Medicine Sciences, College of Medicine, Chang Gung University, Taoyuan, Taiwan, [2]Division of Colon and Rectal Surgery, Department of Surgery, Chang Gung Memorial Hospital, Chiayi, Taiwan, [3]Department of Respiratory Therapy, Fu Jen Catholic University, New Taipei City, Taiwan, [4]Division of Pulmonary Infection and Critical Care, Department of Pulmonary and Critical Care Medicine, Chang Gung Memorial Hospital, Puzi City, Chiayi County, Taiwan, [5]Department of Nursing, Chang Gung University of Science and Technology, Chiayi Campus, Puzi City, Chiayi County, Taiwan, [6]Department of Respiratory Therapy, Chang Gung Memorial Hospital, Chiayi County, Taiwan, [*]Contributed equally to the study, [#]Correspondence to Tzu-Hsiung Huang

Introduction

An unexplainable increase in the incidence of pneumonia was observed in Wuhan, Hubei Province, China in December 2019. These cases of pneumonia were found to be caused by a new beta-coronavirus called severe acute respiratory syndrome coronavirus 2 (SARS-CoV-2). SARS-CoV-2 causes an infectious disease given the name "coronavirus disease 2019 (COVID-19)" by the World Health Organization (WHO). COVID-19 rapidly leads to cluster spreading and affects the respiratory system, resulting in pneumonia, respiratory failure, and ultimately multiple organ failure [1]. According to a WHO dashboard presented on 8 November 2020, the pandemic has 49,578,590 confirmed cases and has caused 1,245,717 deaths worldwide. The mortality rate of COVID-19 patients requiring mechanical ventilation, including subjects with COVID-19 infection and with all underlying illnesses (mixed group), is high [2].

In some patients diagnosed with COVID-19, the respiratory system is affected, which quickly leads to respiratory distress and hypoxemia, thus meeting the Berlin criteria for acute respiratory distress syndrome (ARDS) [3]. In addition to the virus-host interaction and the comorbidities of patients with COVID-19 respiratory distress, we speculate that mechanical ventilation also worsens the severity of the existing disease. While mechanical ventilation is required for patients suffering from ARDS, it could potentially impair the condition by overly distending regional pulmonary alveoli, especially with large tidal volumes, and trigger ventilator-induced lung injury (VILI).

However, the pathological changes of COVID-19-related ARDS are different from those of typical ARDS, and some studies consider that COVID-19-related ARDS is not typical ARDS [4]. In this review, we analyzed the differences in the pathological characteristics of typical ARDS and those of COVID-19-related ARDS, and the proposed strategies to prevent and treat VILI in patients with COVID-19-related ARDS.

Methods

Data sources and search strategy

We performed a comprehensive search via the PubMed database for relevant articles up to August 2020. Studies were not limited to human or other animal species. There were no restrictions on publication date, language or study type; and non-original studies, such as editorials and letters, were also included. We used the following search terms: COVID-19, acute respiratory distress syndrome, ventilator-induced lung injury, angiotensin-converting enzyme 2, coagulation abnormalities, cytokine storm, lung-protective ventilation, prone positioning, corticosteroids, inflammatory monocyte, and precision medicine.

Study selection

We selected articles for our literature review based on our research question and search keywords (Figure 1). Three reviewers (CSS, SHY, and THH) independently conducted the primary search and screened the titles and abstracts of the articles. They retrieved the full text of potentially relevant studies and inde-

Address reprint requests to: Dr. Tzu-Hsiung Huang, Department of Respiratory Therapy, Chang Gung Memorial Hospital, No. 6, Sec. West, Jiapu Rd., Puzi City, Chiayi County, 61363, Taiwan

pendently assessed them. Minor disagreements were resolved by discussion between review authors without the requirement for a mediator.

Results

Literature review

A summary of the results of this literature review were recorded in the flow chart (Figure 1). In searching the PubMed database, 6438 potential articles or abstracts were identified. After removal of duplicates, 5863 articles were screened for relevance and 575 were found to require further review. In the end, 32 relevant

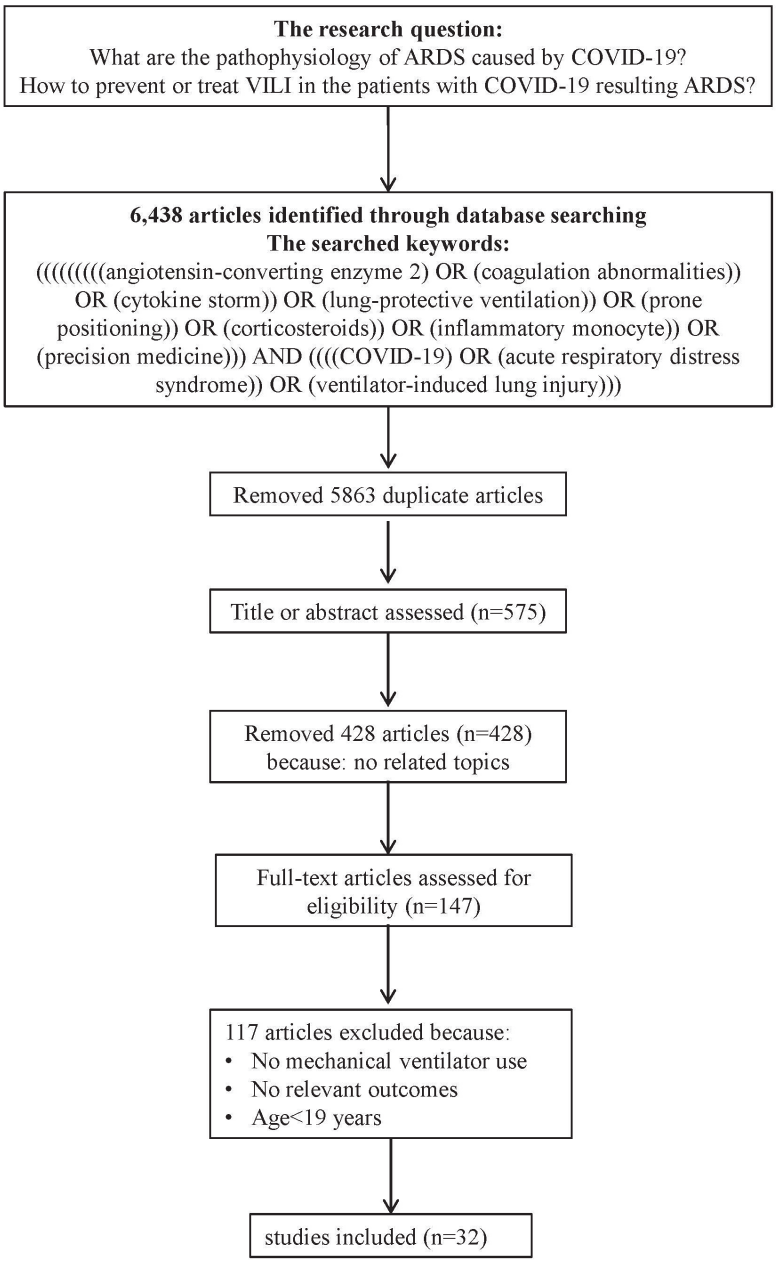

Fig. 1. Process for study inclusion in this literature review.

articles were selected for final review.

Clinical features of COVID-19-related ARDS

Although there are many causes of ARDS, most patients have similar clinical characteristics [5]. However, recent studies have found that the clinical characteristics of patients with COVID-19-related ARDS are different from those of patients with typical ARDS [4]. Clinicians and respiratory therapists must understand the differences in physiological and pathological conditions for distinguishing COVID-19-related ARDS from typical ARDS. This is critically important to providing appropriate mechanical ventilation to patients in critical/intensive care. The common clinical features of COVID-19-related ARDS are described in the subsequent sections.

Lung mechanics in COVID-19-related ARDS

ARDS is characterized generally as low respiratory system compliance in association with noncardiogenic pulmonary edema, shunt-related hypoxemia, and baby lung with a decreasing aerated lung volume [5]. The ventilator settings for patients at this stage should minimize high transpulmonary pressure-induced overstretched alveoli by using a low tidal volume and allowing permissive hypercapnia [6]. Furthermore, in order to improve oxygenation, the application of higher positive end-expiratory pressure (PEEP) is considered useful [6]. In the early stages of COVID-19-related ARDS, most patients do not develop obvious dyspnea and decreased lung compliance, but show the early features of deterioration in oxygenation [7]. At this stage, computed tomography (CT) reveals bilateral ground-glass opacities, and the lung infiltration is located mainly in the interstitium, rather than the alveoli of the lung [7]. These COVID-19-related ARDS patients are referred to as having the "L-type" phenotype, characterized by low lung elastance (high compliance), low lung weight as estimated by CT scan, and low response to PEEP [4, 7]. For many patients, the disease may stabilize at this stage without further deterioration. However, with the development of serious disease, some patients will progress to clinical manifestations with more typical ARDS characteristics, including CT showing extensive lung consolidation, high elastance (low compliance), high lung weight and good response to PEEP [7]. This is referred to as the "H-type" phenotype The clinical management of the 2 types of patients is different, because H-type patients preferentially develop pneumonia-like thickening that demands ventilator support, but L-type patients display clearer lungs that can be damaged by the use of ventilation. Although the 2 types are 2 extremes, the timing of their occurrence often overlaps with each other [7], demonstrating the complexity of clinical management of COVID-19-related ARDS. It is crucial that H- and L-type patients are correctly categorized, because the treatment protocols are very different for these 2 types.

Systemic coagulation abnormalities

Another frequently reported feature is a highly activated coagulation cascade with widespread micro- and macro-thromboses in the lung and in other organs [7, 8]. Extremely elevated levels of serum fibrin degradation product, D-dimer, are a consistent finding associated with adverse outcomes [7, 8]. A highly activated coagulation pathway with pulmonary disseminating thrombosis is a constant feature in most severe COVID-19 patients, and results in systemic coagulation abnormalities [7, 8]. Furthermore, autopsies of COVID-19 patients

reveal blood clots not only in the lungs, but also in the liver and kidneys. A study also showed that an elevated serum concentration of D-dimer is significantly related to mortality in hospitals [9]. Moreover, SARS-CoV-2 can bind to the angiotensin-converting enzyme 2 (ACE2) receptor on vascular endothelial cells, causing coagulation problems [10]. This may damage the pulmonary vascular endothelium, leading to destruction of pulmonary vascular regulation, ventilation-perfusion disorders, and hypoxemia.

Cytokine storm syndrome in patients with COVID-19-related ARDS

The pathophysiology of severe COVID-19 is similar to that of severe community-acquired pneumonia caused by various viruses or bacteria [11]. SARS-CoV-2 infection can overstimulate the immune system, triggering an out-of-control immune response and the development of macrophage activation syndrome or secondary hemophagocytic lymphohistiocytosis, which leads to a cytokine storm and further multiple organ failure in patients [11]. During a SARS-CoV-2 attack, a patient's immune system exhibits systemic hyper-inflammation, T lymphocyte activation, an increase in hemophagocytic macrophages, profound hyperferritinemia, and the release of a variety of proinflammatory cytokines, including monocyte chemoattractant protein 1, macrophage inflammatory protein 1-α, interleukin (IL)-1β, IL-6, and tumor necrosis factor-α (TNF-α) [11]. IL-6 and IL-1β are related to the poor prognosis/mortality of ARDS patients. Overproduction of acute response proinflammatory cytokines (TNF-α, IL-6, and IL-1β) results in an increased risk of vascular hyperpermeability, multiple organ failure, and eventual death in patients with COVID-19 [11].

Increased risk of mortality/complications in ventilated COVID-19 patients

While mechanical ventilation is required for ARDS patients, large tidal volumes of ventilation could potentially aggravate pulmonary function by overly distending regional pulmonary alveoli, and lead to VILI [6]. VILI may occur not only in healthy lungs but also in cases of deteriorating pre-existing pulmonary disease, such as ARDS [6]. It is characterized by upregulating the recruitment of numerous subsets of leukocytes that overproduce the inflammatory mediators that increase pulmonary vasculature permeability, triggering protein-rich pulmonary edema and eventually a deteriorating gaseous exchange. Clinical studies have shown that using a lower tidal volume during mechanical ventilation can mitigate lung injury, decrease mortality, and reduce VILI [12]. However, the incidence of VILI and VILI-associated mortality remains high in patients. Pre-existing lung infections also increase patient susceptibility to VILI, even with the application of more protective ventilation strategies using lower tidal volume settings. We suggest that mechanical ventilation may amplify the cytokine storm syndrome leading to increased mortality of COVID-19 patients.

How can we prevent or treat VILI in patients with COVID-19-related ARDS?

Since there is no specific antiviral treatment for COVID-19 at present, the current management of COVID-19 is supportive, including supplemental oxygen and mechanical ventilation. However, the strategies for providing lung protective mechanical ventilation to COVID-19 patients without worsening the severity of respiratory failure is clinically problematic and controversial. The critical issues of using venti-

lators in COVID-19 patients are discussed subsequently.

Lung-protective ventilation strategies

COVID-19-related ARDS is similar to the early stage of typical ARDS. A previous study has defined this group as "L-type" [7]. Hypoxic or perfusion-related problems in patients lead to the high transpulmonary pressures associated with spontaneous vigorous inspiratory effort. This may contribute to lung damage (the so-called “patient self-induced lung injury” [P-SILI]) [6, 7]. During mechanical ventilation, the progressive deterioration of lung function indicates the possibility of a VILI vortex. At this stage, effective sedation and/or paralysis may reduce the risk of patient-induced high transpulmonary pressure. A previous study suggested that, in this situation, it is appropriate to target a lower PEEP (8-10 cmH_2O), proper tidal volume (7-9 ml/kg), and driving pressure below 13–15 cmH2O [7].

COVID-19 "L-type" with disease progression and/or P-SILI leads to increased pulmonary edema and a reduced number of aerated alveoli (so-called "baby lung"). "L-type" will gradually develop into typical ARDS of an "H-type" phenotype [7]. In the H-type phase, the development of collapsed or consolidated alveoli will reduce the number of aerated alveoli, leading to hypercapnia and hypoxemia. Lung-protective ventilation strategies, including permissive hypercapnia, higher PEEP (≤15 cm H_2O), and lower tidal volume (6 ml/kg), and targeting driving pressure below 13–15 cmH_2O, are recommended during this period. Despite the use of a lung-protective ventilation strategy, it may be very difficult to accurately measure and control respiratory parameters in ventilated patients, and some ventilated patients with COVID-19 may still develop VILI. Therefore, besides applying personalized clinical strategies to prevent VILI, exploration of other potential pathological mechanisms or related pharmaceutical interventions to prevent or treat VILI may be required.

Prone positioning

Prone ventilation can be used to treat typical ARDS, mainly as a strategy to improve gaseous exchange, thereby increasing the survival rate of patients using traditional mechanical ventilation [13]. Numerous physiological studies have shown that placing a person in a prone position can diminish pleural pressure gradients, reestablish aeration to dorsal lung segments, and support more homogeneous aeration of the lung in ARDS [13]. Multiple studies suggest that the prone position can facilitate the redistribution of pulmonary blood flow and the maintenance of matching between ventilation and perfusion in COVID-19-related ARDS [13]. A meta-analysis found that use of the prone position can decrease mortality in ARDS patients when implemented in the initial hours of disease manifestation in patients with prolonged severely impaired oxygenation [14]. And, the minimum duration of prone positioning was suggested to be 12 hours a day for COVID-19-related ARDS patients [15]. These studies indicate that early initiation and prolonged use of the prone position can be considered a lung-protective ventilation strategy in COVID-19 patients requiring ventilation [14-15].

Corticosteroids

Corticosteroids have been considered a potential treatment for ARDS due to their role in reducing inflammation; however, their benefit is controversial [16]. Some studies have

found that corticosteroids can reduce morbidity and mortality in ARDS patients [16], but other studies have shown that corticosteroids can significantly increase the risk of influenza A virus H1N1-related ARDS death [17], and may affect the rate of virus clearance in COVID-19 patients. The Randomized Evaluation of COVID-19 Therapy (RECOVERY) trial involving severe COVID-19 patients requiring mechanical ventilation reported that dexamethasone reduced mortality compared with usual care or a placebo [18]. A new meta-analysis review of data also showed that for patients with severe COVID-19, administration of systemic corticosteroids, compared with usual care or a placebo, was associated with lower 28-day all-cause mortality [19]. On September 4, 2020, and based on new evidence, the WHO published guidance for clinicians and health care decision-makers on the use of corticosteroids in patients with COVID-19. The WHO recommended the use of corticosteroids to treat patients with severe and critical COVID-19, but did not recommend corticosteroids for patients with non-severe COVID-19 because the treatment would not be beneficial and might even prove to be harmful.

Pharmacologic intervention using a cytokine inhibitor

At present, no antiviral drugs or vaccines have been proven to treat COVID-19. Scientists around the world are testing whether previously developed drugs used to treat other viral infections can also effectively fight COVID-19. The pathophysiology of severe COVID-19 is similar to that of severe community-acquired pneumonia caused by infections of viruses or bacteria. The cytokine storm, an overproduction of early-phase proinflammatory cytokines, amplified by mechanical ventilation, leads to increased vascular hyperpermeability, multiple organ failure, and eventually death. Therefore, therapeutic measures that suppress the over-activation of cytokines may function as protective strategies to improve the survival rate of COVID-19 patients using ventilation. Elevated interleukin-6 (IL-6) is involved in COVID-19 and induces pneumonia and macrophage activation syndrome-like disease [20]. Tocilizumab, a monoclonal antibody against IL-6, recently showed a potential for treating COVID-19 patients with a risk of cytokine storm [21]. A multicenter, randomized and controlled trial of tocilizumab for treatment of patients with COVID-19 pneumonia and elevated IL-6 has been approved in China (ChiCTR2000029765). Moreover, clinical data have suggested that IL-6 plays a critical role in the pathogenesis of VILI [12, 22]. Based on the above studies, we can speculate that inhibitors and/or signal inhibitions of cytokines may have therapeutic value in preventing or treating VILI in COVID-19 respiratory failure. At present, a period of testing is still needed to know whether blockage of specific cytokines has therapeutic value in treating COVID-19-related ARDS.

Pharmacologic intervention using ACE2 inhibitors

The renin-angiotensin-aldosterone system (RAAS) is an important class of vasoactive peptides that can coordinate multiple physiological functions in the body. Angiotensin-converting enzyme (ACE), one of the RAAS members, is responsible for converting angiotensin I into angiotensin II for regulating blood pressure and fluid balance. ACE2 is a highly homologous metalloproteases of ACE that disables angiotensin II and is a RAAS negative regulator. A pre-

vious paper reported that ACE2 and angiotensin II type 2 receptor protected mice from acid aspiration or sepsis-induced severe acute lung injury [23]. Furthermore, ACE2 is a necessary receptor for cell fusion and infection of severe acute respiratory syndrome (SARS) coronavirus, the cause of SARS [24]. Moreover, ACE2 is also a co-receptor of SARS-CoV-2 infection for cell entry in the COVID-19 pathogenesis [25]. ACE inhibitors (ACE-1 inhibitors, such as enalapril and ramipril) and angiotensin receptor antagonists (angiotensin receptor blockers [ARBs], such as candesartan and valsartan) may be of value in preventing and treating COVID-19. On the other hand, previous studies have found that RAAS is also involved in the pathogenesis of VILI, and ACE inhibitors or angiotensin receptor antagonists can attenuate VILI in animal models [26]. Therefore, we conjecture that ACE inhibitors or angiotensin receptor antagonists may have therapeutic value in preventing and treating VILI in ARDS resulting from COVID-19. However, ACE inhibitors and ARBs have different effects on angiotensin II, and the overall results of using them may be difficult to predict in COVID-19 patients with ARDS.

Regulation of monocyte-macrophage responses

Due to the importance of monocytic lineage cells in inflammation, regulation of the function of macrophages and monocytes is a promising therapeutic strategy against ARDS. Future studies need to explore whether monocytic cells are involved in the pathogenesis of VILI in severe COVID-19, and if targeting specific monocytic subsets can lead to basic research into a viable clinical treatment for severe COVID-19. The subsets of monocytes are heterogeneous and pluripotent cells, which phenotypically consist of at least 2 distinct subcategories that can be distinguished by the expression level of Ly6C, a specific marker of monocytic lineage in mice. Monocytes expressing high levels of Ly6C (Ly-6C^{high}) and C-C chemokine receptor 2 (CCR2^{high}) and low levels of CX3C chemokine receptor 1 (CX3CR1^{low}) are designated as the Ly6C^{high} CCR2^{high} CX3CR1^{low} monocytes, which are the inflammatory subset of monocytes. Ly6C^{high} CCR2^{high} CX3CR1low monocytes are derived from bone marrow macrophage-dendritic precursor cells and can be recruited to sites of inflammation and injury. However, the Ly6C^{low}-CCR2^{low}CX3CR1^{high} monocyte is the tissue resident subset, which enters tissues with or without inflammation.

Our recent study found that Ly6C^{high} monocytes can enlarge the pulmonary vascular permeability of the resulting VILI by enriching vascular endothelial growth factor (VEGF) expression [27], indicating the critical Ly6C^{high} monocytes-VEGF axis during VILI. A previous study showed that mechanical ventilation with a high tidal volume, rather than a low tidal volume, notably prompts the expression and activity of cyclooxygenase-2 (COX-2) in both the lungs and the systemic circulation of mice [28]. The study further revealed the expression of COX-2 in monocytes and macrophages of the alveoli of lung sections [28]. The pharmacologic suppression of COX-2 with CAY10404 significantly reduced IL-6 production in bronchoalveolar lavage fluid and attenuated VILI in mice [28]. Furthermore, the contribution of COX-2-dependent recruitment of VEGF-secreting Ly6C^{high} monocytes is critical in the increment of total protein in bronchoalveolar lavage fluid during VILI development [29]. Therefore, we speculate that inhibiting COX-2

activity to regulate the mobilization of inflammatory monocytes may have therapeutic value in preventing or treating VILI in patients with COVID-19.

Precision medicine to prevent or treat VILI

The differences in people's genes and target genes of illness that are taken into account to implement prevention or treatment strategies are also used to define precision medicine. Since the heterogeneity of ARDS is a key factor leading to the failure of many clinical trials [30] and most ARDS patients require mechanical ventilation, understanding the changes in candidate genes affecting VILI may reduce lung damage caused by the ventilator and lower the mortality rate of patients with different types of ARDS. COVID-19 patients also have other comorbidities that may limit the development of precision medicine, and therefore, the detection of target genes of VILI can potentially address the individual data of ventilated patients for the implementation of personalized treatment and improvement of outcomes. However, human experimental models could not be used to verify VILI in this study, and most lung gene expression data come from cell models (for example, human epithelial and endothelial cells under mechanical stress) [31] or animal models (for example, the lungs of VILI mice) [32]. Hence, the genomic information collected from these models (especially gene expression) needs to be confirmed by extensive research in the human disease platform.

Conclusion

In this review, we summarized the current research on clinical features, cytokine storm syndrome, and the risks of mechanical ventilation use in patients with COVID-19-related ARDS. Based on the pathophysiology of COVID-19-related ARDS, we suggest that lung-protective ventilation strategies for L- or H-type, and early pharmacological interventions can be appropriately applied (Figure 2). This would be expected to minimize patient self-inflicted lung injury or VILI, and improve the survival rate of mechanically ventilated patients with COVID-19-related ARDS.

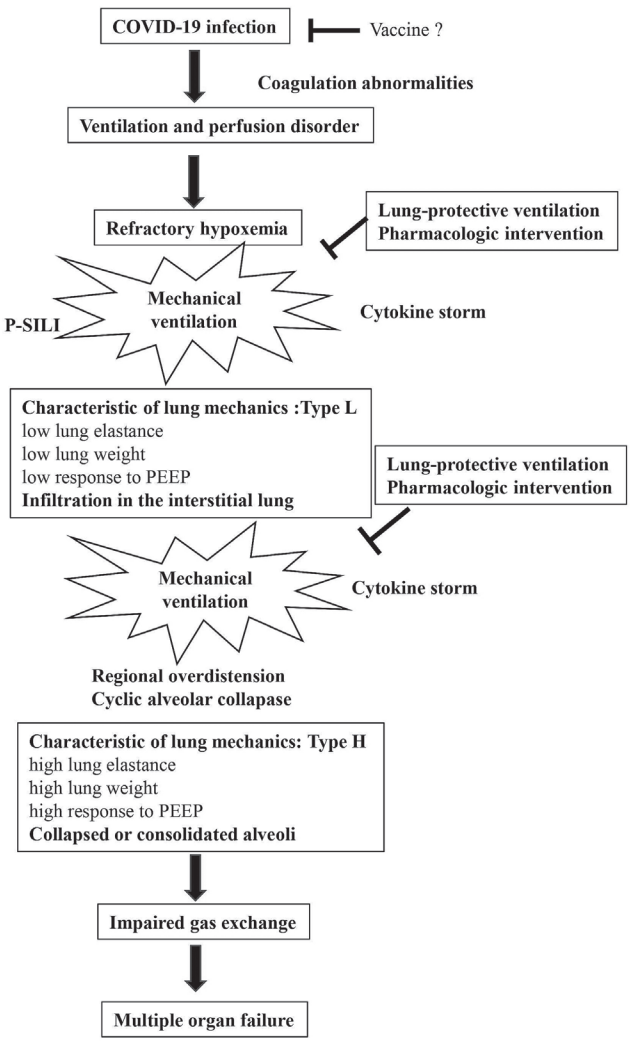

Fig. 2. Illustration of ventilator-induced lung injury present in COVID-19-related ARDS patients.

Author contributions

CSS, SHY, and THH drafted the manuscript, ZML and CKL provided clinical discussion, and THH edited and revised the manuscript. All authors have read and approved the final manuscript.

Acknowledgements

This work was supported in part by grants from the Chang Gung Memorial Hospital Research Foundation (CMRPG6G0361 and CMRPG6I0041).

Conflicts of Interest

The authors declare that they have no competing interests.

References

1. Cao Y, Liu X, Xiong L, *et al*. Imaging and clinical features of patients with 2019 novel coronavirus SARS-CoV-2: A systematic review and meta-analysis. J Med Virol 2020; Sep; 92(9): 1449-1459.
2. Richardson S, Hirsch JS, Narasimhan M, *et al*. Presenting characteristics, comorbidities, and outcomes among 5700 patients hospitalized with COVID-19 in the New York City area. JAMA 2020; 22(2765184).
3. Ranieri VM, Rubenfeld GD, Thompson BT, *et al*. Acute respiratory distress syndrome: the Berlin Definition. JAMA 2012; 307(23): 2526-33.
4. Gattinoni L, Coppola S, Cressoni M, *et al*. Covid-19 does not lead to a "typical" acute respiratory distress syndrome. Am J Respir Crit Care Med 2020; 30(10): 202003-0817LE.
5. Thompson BT, Chambers RC, Liu KD. Acute respiratory distress syndrome. N Engl J Med 2017; 377(6): 562-72.
6. Brochard L, Slutsky A, Pesenti A, *et al*. Mechanical ventilation to minimize progression of lung injury in acute respiratory failure. Am J Respir Crit Care Med 2017; 195(4): 438-42.
7. Marini JJ, Gattinoni L. Management of COVID-19 respiratory distress. JAMA 2020 Apr 24; doi: 10.1001/jama.2020.6825.
8. Connors JM, Levy JH. COVID-19 and its implications for thrombosis and anticoagulation. Blood 2020; 135(23): 2033-40.
9. Zhang Y Xiao M, Zhang S, *et al*. Coagulopathy and antiphospholipid antibodies in patients with Covid-19. N Engl J Med 2020 Apr 8;382(17): e38. doi: 10.1056/NEJMc2007575.
10. MOmar MB. Covid-19 and the angiotensin-converting enzyme (ACE2): areas for research. Heart Lung 2020 Apr 20; pii: S0147-9563(20)30146-1. doi: 10.1016/j.hrtlng.2020.04.012.
11. Mehta P, McAuley DF, Brown M, *et al*. COVID-19: consider cytokine storm syndromes and immunosuppression. Lancet 2020 Mar 28; 395(10229):1033-1034. doi: 10.1016/S0140-6736(20)30628-0. Epub 2020 Mar 16.
12. Brower RG, Matthay MA, Morris A, *et al*. Ventilation with lower tidal volumes as compared with traditional tidal volumes for acute lung injury and the acute respiratory distress syndrome. N Engl J Med 2000; 342(18): 1301-8.
13. Scholten EL, Beitler JR, Prisk GK, *et al*. Treatment of ARDS with prone positioning. Chest 2017; 151(1): 215-24.
14. Mora-Arteaga JA, Bernal-Ramirez OJ, Rodriguez SJ, *et al*. The effects of prone position ventilation in patients with acute respiratory distress syndrome. A systematic review and metaanalysis. Med Intensiva 2015; 39(6): 359-72.
15. Ghelichkhani P, Esmaeili M. Prone position in management of COVID-19 patients; a commentary. Archiv Academ Emerg Med 2020; 8(1): e48-e.
16. Zhao Q, Shi J-X, Hu R, *et al*. Effect of glucocorticoids on mortality in patients with acute respiratory distress syndrome: A meta-analysis. Experiment Therapeut Med. 2019; 18(6): 4913-20.
17. Brun-Buisson C, Richard JC, Mercat A, *et al*. Early corticosteroids in severe influenza A/H1N1 pneumonia and acute respiratory distress syndrome. Am J Respir Crit Care Med 2011; 183(9): 1200-6.
18. Horby P, Lim WS, Emberson JR, *et al*. Dexamethasone

in hospitalized patients with Covid-19 - preliminary report. N Engl J Med 2020; 17(10): doi:10.1056/NEJMoa2021436.

19. Sterne JAC, Murthy S, Diaz JV, *et al*. Association between administration of systemic corticosteroids and mortality among critically Ill patients with COVID-19: a meta-analysis. JAMA 2020; 324(13): 1330-41.
20. McGonagle D, Sharif K, O'Regan A, *et al*. The role of cytokines including interleukin-6 in COVID-19-induced pneumonia and macrophage activation syndrome-like disease. Autoimmun Rev 2020; 3(102537):102537.
21. Luo P, Liu Y, Qiu L, *et al*. Tocilizumab treatment in COVID-19: a single center experience. J Med Virol 2020; 6(10): 25801.
22. Ranieri VM, Suter PM, Tortorella C, *et al*. Effect of mechanical ventilation on inflammatory mediators in patients with acute respiratory distress syndrome: a randomized controlled trial. JAMA 1999; 282(1): 54-61.
23. Imai Y, Kuba K, Rao S, *et al*. Angiotensin-converting enzyme 2 protects from severe acute lung failure. Nature 2005; 436(7047): 112-6.
24. Li W, Moore MJ, Vasilieva N, *et al*. Angiotensin-converting enzyme 2 is a functional receptor for the SARS coronavirus. Nature 2003; 426(6965): 450-4.
25. Vaduganathan M, Vardeny O, Michel T, *et al*. Renin-angiotensin-aldosterone system inhibitors in patients with Covid-19. N Engl J Med 2020; 382(17): 1653-9.
26. Wang D, Chai XQ, Magnussen CG, *et al*. Renin-angiotensin-system, a potential pharmacological candidate, in acute respiratory distress syndrome during mechanical ventilation. Pul Pharmacol Therapeut 2019; 58: 101833-.
27. Shi CS, Huang TH, Lin CK, *et al*. VEGF production by Ly6C+high monocytes contributes to ventilator-induced lung injury. PLOS ONE 2016; 11(10): e0165317.
28. Robertson JA, Sauer D, Gold JA, *et al*. The role of cyclooxygenase-2 in mechanical ventilation-induced lung injury. Am J Respir Cell Mol Biol 2012; 47(3): 387-94.
29. Huang TH, Fang PH, Li JM, *et al*. Cyclooxygenase-2 activity regulates recruitment of VEGF-secreting Ly6C(high) monocytes in ventilator-induced lung injury. Int J Mol Sci 2019; 20(7).
30. Silva PL, Pelosi P, Rocco PRM, *et al*. Personalized pharmacological therapy for ARDS: a light at the end of the tunnel. Expert Opin Investig Drugs 2020; 29(1): 49-61.
31. Wang T, Gross C, Desai AA, *et al*. Endothelial cell signaling and ventilator-induced lung injury: molecular mechanisms, genomic analyses, and therapeutic targets. Am J Physiol Lung Cell Mol Physiol 2017; 312(4): L452-l76.
32. Wurfel MM. Microarray-based analysis of ventilator-induced lung injury. Proc Am Thorac Soc 2007; 4(1): 77-84.

Feasibility of Re-biopsy by Endobronchial Ultrasound-guided Transbronchial Needle Aspiration (EBUS-TBNA) in Patients with Previously Treated Lung Cancer

Kai-Lun Yu[1,2], Han-Ching, Yang[1], Jen-Chung Ko[1], Chao-Chi Ho[3], Jin-Yuan Shih[3]

Background: Re-biopsy is paramount for further treatment of lung cancer patients with recurrent or progressive disease. Endobronchial ultrasound-guided transbronchial needle aspiration (EBUS-TBNA) is an important method for tissue sampling of mediastinal lesions. However, the role of EBUS-TBNA in re-biopsy of lung cancer is not clear. In this study, we investigated the feasibility of re-biopsy by EBUS-TBNA of pretreated lung cancer patients.

Methods: Consecutive patients with pretreated lung cancer with suspected progression or recurrence that underwent EBUS-TBNA between October 2015 and December 2019 were enrolled. The diagnostic yield, specimen adequacy, and complications were assessed.

Results: A total of 72 lesions from 45 patients with suspected lung cancer recurrence (n=11) or progression (n=34) were sampled by EBUS-TBNA. The diagnostic yield and specimen adequacy rate was 73.3% (33/45) and 95.6% (43/45), respectively. There was no major complication, but 7 (15.6%) minor complications were noted in these patients. Twenty-one patients had EGFR testing results from both the initial diagnosis and from re-biopsy specimens. The acquired T790M mutation was identified in 5 (38.5%) of 13 patients with EGFR-mutant lung adenocarcinoma.

Conclusion: EBUS-TBNA is a feasible and safe method of re-biopsy for pretreated lung cancer patients. ***(Thorac Med 2021; 36: 71-80)***

Key words: endobronchial ultrasound-guided transbronchial biopsy, re-biopsy, lung cancer

Introduction

Lung cancer is the leading cause of cancer-related mortality worldwide [1]. Treatment for lung cancer has seen great advances in the most recent 15 years, largely due to a greater understanding of the underlying genomic alterations and tumor growth, and factors such as epidermal growth factor receptor (EGFR) [2-3]. The use of EGFR-tyrosine kinase inhibitors (EGFR-TKIs) has seen a good response rate and good progression-free survival for patients with

[1]Department of Internal Medicine, National Taiwan University Hospital, Hsin-Chu Branch, Taiwan
[2]Graduate Institute of Clinical Medicine, College of Medicine, National Taiwan University, Taiwan
[3]Department of Internal Medicine, National Taiwan University Hospital, Taiwan
Address reprint requests to: Dr. Jin-Yuan Shih, Department of Internal Medicine National Taiwan University Hospital No. 7, Chung-Shan South Road, Taipei 10002, Taiwan

sensitizing EGFR mutations [3]. However, drug resistance often developed after 10-12 months of treatment [3]. This resistance may come from acquired point mutations, small cell transformation, or other factors [4]. When disease progression or recurrence is observed clinically, re-biopsy is often required to confirm current disease status and molecular alternations to optimize subsequent treatment [4-5].

Endobronchial ultrasound-guided transbronchial needle aspiration (EBUS-TBNA) is a bronchoscopic method that provides real-time images of mediastinal lesions, leading to accurate tissue sampling of the mediastinum. EBUS-TBNA has been reported to have good diagnostic efficacy, and has been an important technique for pathological diagnosis, nodal staging, and tissue acquisition for molecular and immune condition analysis of lung cancer [6]. EBUS-TBNA is also a safe technique with a low complication rate, and has a diagnostic yield ranging between 61% and 91% [6-8]. However, most studies investigating the efficacy and clinical usefulness of EBUS-TBNA were focused on newly diagnosed lung cancer patients. Reports on the clinical role of EBUS-TBNA in re-biopsy of previously treated lung cancers are relatively rare [9]. To our knowledge, there is no local data on EBUS-TBNA for re-biopsy in Taiwan.

In this retrospective study, we aimed to evaluate the clinical role and safety of EBUS-TBNA for re-biopsy of patients with suspected recurrent or progressive lung cancer after treatment.

Methods

Study design and subjects

This retrospective study was conducted at National Taiwan University Hospital, Hsin-Chu Branch, between October 2015 and December 2019. Consecutive patients with progressive or recurrent lung cancer after treatment who underwent re-biopsy using EBUS-TBNA were enrolled. Disease progression was determined by the physician's clinical evaluation, using RECIST ver1.1 [10]. Written informed consent was obtained before the procedures. The study was approved by the Institutional Review Board of National Taiwan University Hospital Hsin-Chu Branch.

EBUS-TBNA procedure

All procedures were performed in the bronchoscopy room by an experienced pulmonologist. Patients received local anesthesia with lidocaine and mild-to-moderate sedation with intravenous fentanyl and midazolam in the supine position. The bronchoscopy, equipped with a convex probe EBUS (BF-UC260-OL8; Olympus, Tokyo, Japan), was inserted orally. The bronchoscopy and ultrasound images (ultrasound processor, EU-ME2; Olympus) were shown on the integrated monitor. After examination by convex EBUS and the target aspirate lesion was selected, EBUS-TBNA was performed using a 22-gauge needle (NA-201SX-4022; Olympus). Under real-time EBUS imaging, the needle was inserted via the working channel of the bronchoscopy, and then penetrated the tracheobronchial wall to the target lesion. The TBNA needle was moved back and forth around 20 times with negative pressure. After closing the negative pressure, the needle was removed from the bronchoscopy for further specimen preparation.

First, the stylet was inserted into the aspiration needle and the aspiration tissue was pushed out. Histological examination of the specimen

was performed when a solid tissue core was obtained. Then, the fluid specimen was spread onto the slides for further preparation of air-dried and alcohol-fixed slides for cytological examination. Rapid on-site evaluation (ROSE) was not routinely performed in our institution. Procedure-related complications were recorded. Respiratory failure, severe bleeding, hypotension, arrhythmia, consciousness disturbance after recovery from sedation, or any condition requiring intensive care unit admission were considered major complications.

Pathological and cytological results and molecular diagnosis

The histology and cytology specimens were evaluated by a qualified pathologist. The overall diagnostic yield rate was the combination of positive diagnoses of pathological or cytological specimens. The specimens were regarded as diagnostic when a specific diagnosis, such as malignancy or granulomatous inflammation, was established. Pathological specimens that led to a definite diagnosis or to the obtaining of a sufficient number of lymphocytes were considered adequate. The specimens were considered inadequate if they showed only blood, epithelial cells, cartilage cells, or no materials (dry tapping). False negative was established when re-biopsy specimens were negative for malignancy, but malignancy was proved by other sampling methods or by clinical follow-up, at least 6 months after EBUS-TBNA. If the clinical physician requested further molecular testing (EGFR) or special staining (anaplastic lymphoma kinase, ALK), these results were recorded.

Statistical analysis

Descriptive data were assessed as the mean (standard deviation) or count (percentage), as appropriate. The chi-squared test or Fisher's exact test for categorical variables, and Student's t-test or Mann-Whitney U test for continuous variables were used as appropriate to assess differences between 2 groups. A 2-tailed P-value <0.05 was considered statistically significant. All analyses were performed using SPSS, version 18.0 (SPSS Inc., Chicago, IL, US).

Results

From October 2015 to December 2019, 45 previously-treated lung cancer patients with suspected progressive disease (n=34) or recurrence (n=11) underwent re-biopsy using EBUS-TBNA. Thirty-seven patients (82.2%) had lung adenocarcinoma and 19 (42.2%) had received targeted therapy. A total of 34 patients were finally diagnosed as having lung cancer progression, 5 had lung cancer recurrence, and 6 had no lung cancer recurrence. The overall diagnostic yield of re-biopsy by EBUS-TBNA was 73.3% (33/45), and the specimen adequacy rate was 95.6% (43/45). Sensitivity and specificity were 82.1% and 100%, respectively (Table 1). The detailed pathological results of initial diagnosis and re-biopsy by EBUS-TBNA are summarized in Table 2.

A total of 72 lesion punctures were performed for these 45 patients. The mean lesion size was 1.5 cm. The mean procedure time was 29.0 minutes. The mean puncture site per patient and puncture times per lesion were 1.6 and 3.3, respectively. No patients had major complications, and 7 (15.6%) had minor complications due to the procedures. Four patients (8.9%) had fever after the procedure and were given antibiotics; their fever subsided 1 day later. Bleeding was noted in 1 patent during the

Table 1. Characteristics of the Patients

Variable	Number	(%)
Total	45	(100)
Age, years		
Mean	61.7	
Range	36-83	
Sex		
Male	28	(62.2)
Female	17	(37.8)
Smoking history		
Never	25	(55.6)
Former/current	20	(44.4)
Initial cancer type		
Adenocarcinoma	37	(82.2)
Squamous cell carcinoma	5	(11.1)
NSCLC, NOS	1	(2.2)
Small cell lung cancer	1	(2.2)
Others	1	(2.2)
ECOG PS		
0-1	41	(91.1)
>=2	4	(8.9)
Stage		
I	5	(11.1)
II	4	(8.9)
III	17	(37.8)
IV	19	(42.2)
Previous treatment		
TKIs	19	(42.2)
Chemotherapy	30	(66.7)
Radiotherapy	18	(40.0)
Surgery	14	(31.1)
Indication of EBUS-TBNA		
Progression	34	(75.6)
Recurrence	11	(24.4)
PET-CT before EBUS-TBNA		
Yes	5	(11.1)
No	40	(88.9)

Acronyms: NSCLC, NOS, non-small cell lung cancer, not otherwise specified; ECOG PS, Eastern Cooperative Oncology Group performance status; TKIs, tyrosine kinase inhibitors; EBUS-TBNA, endobronchial ultrasound-guided transbronchial needle aspiration; PET-CT, positron emission tomography-computed tomography.

procedure. Endotracheal epinephrine was given, and the bleeding then ceased. One patient had desaturation during the procedure (SpO_2 < 80% for around 10 seconds). We terminated the procedure and oxygenation improved soon thereafter. Another patient had moderate hemosputum. Intravenous transamine was administered, and the hemosputum resolved in 1 day (Table 3).

Table 2. Pathology results of patients with progressive disease

Cell types at initial diagnosis	N	Cell types of EBUS-TBNA re-biopsy specimens	N
Adenocarcinoma	27	Adenocarcinoma	17
		NSCLC	1
		Carcinoma	2
		Atypical cells	2
		Negative for malignancy	5
Squamous cell carcinoma	4	Squamous cell carcinoma	2
		Poorly differentiated carcinoma	1
		Necrosis	1
NSCLC	1	Squamous cell carcinoma	1
Lymphoepithelioma-like carcinoma	1	Lymphoepithelioma-like carcinoma	1
Small cell lung cancer	1	Small cell lung cancer	1

Acronyms: NSCLC, non-small cell lung cancer; EBUS-TBNA, endobronchial ultrasound-guided transbronchial needle aspiration.

Table 3. Characteristics of Target Lesions and Procedures, and Diagnostic Yields of the Locations

Lesion and procedure characteristics	Values	Diagnostic yield
Total lesion number, n (%)	72 (100)	
Lesion size, cm, mean ± SD	1.5 ± 0.8	
Puncture times per lesion, mean ± SD	3.3 ± 1.3	
Puncture site per patient, mean ± SD	1.6 ± 0.8	
Puncture times per patient, mean ± SD		
Lesion Location, n (%)		
2R	1 (1.4)	1 (100)
2L	1 (1.4)	1(100)
4R	20 (27.8)	14 70.0)
4L	13 (18.1)	11(84.6)
3P	1 (1.4)	1 (100)
7	18 (25)	10 (55.6)
10R	1 (1.4)	1 (100.0)
11Rs	10 (13.4)	3 (30.0)
11Ri	2 (2.8)	1 (50.0)
11L	3 (4.2)	0 (0.0)
Right upper lung lesion	1 (1.4)	1 (100)
Right lower lung lesion	1 (1.4)	1 (100)
Procedure time, minutes, mean ± SD	29.0 ± 10.9	
Fentanyl, mcg, mean ± SD	68.9 ± 23.9	
Midazolam, mg, mean ± SD	8.6 ± 5.2	
Complications, n (%)	7 (15.6)	
Fever	4 (8.9)	
Bleeding	1 (2.2)	
Hemosputum and IV transamine use	1 (2.2)	
Desaturation and termination of the procedure	1 (2.2)	

Acronym: SD, standard deviation.

We investigated possible factors affecting the diagnostic yield of re-biopsy. After assessing age, sex, smoking, ECOG PS, lymph node size, stage of lung cancer, total puncture times per person, previous cancer treatment modalities, and cancer types, we found there were no identifiable factors that significantly affected the diagnostic yield (Table 4).

Table 4. Factors Affecting the Diagnostic Yield of re-biopsy by EBUS-TBNA

Factors	Success(n=33)	Failure(n=12)	*P*-value
Mean age			0.205
>65	14	6	
≤65	19	6	
Sex			0.096*
Male	18	10	
Female	15	2	
Smoking			0.258
Current	13	7	
Never or former	20	5	
ECOG PS			0.561
0-1	29	12	
≥2	4	0	
Lymph node size#			0.466*
<20 mm	23	10	
≥20 mm	10	2	
Stage of lung cancer			
I~IIIA	10	5	0.252
IIB~IV	23	5	
Total puncture times per patient			
<5	13	5	0.890
≥5	20	7	
Previous treatment history			
TKIs use			0.158
Yes	17	9	
No	16	3	
Chemotherapy use			0.722*
Yes	21	9	
No	12	3	
Radiotherapy use			0.891
Yes	13	5	
No	20	7	
Surgery use			0.356
Yes	9	5	
No	24	7	
Cancer type			0.419
Adenocarcinoma	26	11	
Non-adenocarcinoma	7	1	

*Fisher's exact test. Other variables were calculated with Pearson chi-square test.

Lymph node size was recorded as the short axis diameter of the maximal lesion per patient.

Acronyms: NSCLC, non-small cell lung cancer; EBUS-TBNA, endobronchial ultrasound-guided transbronchial needle aspiration; ECOG PS, Eastern Cooperative Oncology Group performance status; TKIs, tyrosine kinase inhibitors.

Table 5. EGFR profiles of 21 patients with initial and re-biopsy results

Initial EGFR profile ➔ EGFR results from re-biopsy specimens	n
Exon 19 del ➔Exon 19 del + T790M	3
Exon 19 del ➔Exon 19	1
L858R ➔L858L + T790M	2
L858R ➔L858R	3
L861Q ➔L861Q	2
G719A + L861Q ➔G719A + L861Q	1
G719S + T790M ➔G719S/G719S/G719C + T790M	1
Wild-type ➔Wild-type	8

Acronyms: EBUS-TBNA, endobronchial ultrasound-guided transbronchial needle aspiration; EGFR, epidermal growth factor receptor.

Twenty-one patients had EGFR genotyping results at the initial diagnosis and from EBUS-TBNA re-biopsy specimens. Eight patients had wild-type EGFR at the initial diagnosis, and the EGFR from re-biopsy specimens were all wild-type. Thirteen patients had EGFR mutations at the initial diagnosis, and the T790M mutation was identified in 5 (38.5%) of them (Table 5). Sixteen patients had ALK IHC results from re-biopsy specimens and 3 had an ALK alternation. One of these 3 patients had an ALK alternation at the initial diagnosis and 2 did not.

Discussion

For this study, we retrospectively collected patients with previously treated lung cancer who underwent EBUS-TBNA for re-biopsy. The diagnostic yield was 73.3% and the specimen adequacy rate was 95.6%. There was no major complication in our study.

EBUS-TBNA is an important method for tissue proof and nodal staging in patients with suspected lung cancer. Previously published articles reported the diagnostic yield of EBUS-TBNA was 61-91% [6-8]. The diagnostic yield of our study (73.3%) was fair, but not as high as in some other studies. There are some possible reasons for this. First, most patients in previous studies were newly diagnosed with lung cancer without any treatment. In these cases, anatomy of the mediastinum, cellularity of the malignant cells, and fibrosis condition of the lesions may change with treatment. Second, in our institution, patients underwent EBUS-TBNA via the oral route under light-to-moderate sedation, rather than via an endotracheal tube under general anesthesia. Agitation, airway secretion, and intermittent short-term desaturation of patients may distract the bronchoscopist and compromise the fluency of the procedure and even sampling accuracy. Third, ROSE was not routinely used in our institution. If ROSE was performed, it was examined by the pulmonologist rather than a pathologist or cytologist. Hence, the diagnostic yield may decrease without ROSE. Fourth, 5 of 11 patients with suspected cancer recurrence were finally diagnosed as not having recurrence. These patients also partially contributed to a decrease in the diagnostic yield.

The adequacy rate in our study was 95.6% (43/45). In other words, there were 2 patients with inadequate specimens. The procedure was terminated in 1 patient because of desaturation during the procedure, and we could not obtain adequate specimens. The lymph node size of

the other patient was only 1 cm. The pathological result revealed some anthracnosis and inflammatory cells. The relatively small size of the target lesion might be the reason for the inadequate specimen.

We also investigated factors potentially affecting the diagnostic yield, and found none that were significant. Kim *et al* reported 367 previously treated lung cancer patients who underwent re-biopsy by EBUS-TBNA [9]. The overall diagnostic yield was 76.3%. Sensitivity was lower in the radiation group than in the palliation (chemotherapy or EGFR-TKIs) group (83.3% vs 97.7%, p=0.012). We could not group patients in this simple way because most of our patients received multiple lines and multiple modalities (chemotherapy, TKIs, radiation therapy, surgery) of treatment before re-biopsy. Only a few patients (n=2) had received only radiotherapy or concurrent chemoradiotherapy before re-biopsy. Hence, further studies with larger case numbers are needed to confirm the factors that affect diagnostic yield in re-biopsy patients.

Complications were another important issue. EBUS-TBNA could be performed safely in patients with initially diagnosed lung cancer [8, 11-12]. However, the complication rate in re-biopsy patients remains unclear. In the current study, the minor complication rate was 15.6% and the most common complication was fever (8.9%). Kim *et al* reported 367 patients that underwent EBUS-TBNA for re-biopsy [9]. There were no major complications; the minor complications rate was 3.3% and fever was noted only in 3 (0.8%) patients. The complication rate in patients with EBUS-TBNA re-biopsy may need further prospective study.

Liquid biopsy, a recently developed technique, is used for detecting tumor-derived genomic alterations from blood or other body fluid. To date, several advantages of liquid biopsy have been investigated [4, 13-14]. First, liquid biopsy is less invasive than tissue biopsy, despite the advances in minimally invasive techniques to obtain tissue specimens. Hence, liquid biopsy could be performed in patients with a poor performance status. Second, liquid biopsy can be tested repeatedly, thus enabling disease status monitoring. Third, liquid biopsy might overcome the spatial heterogeneity of the tumor, and provide us a landscape of genetic alterations [15]. However, recent studies have found that liquid biopsy could not detect ~30% of T790M-positive tissue specimens [15], partially due to the lack of tumor/DNA shed from tumor to blood. In addition, a false positive condition was reported because of clonal hematopoiesis of bone marrow cells [16]. Moreover, a histologic shift may occur in some patients, resulting in an inability to detect changes in tissue level by liquid biopsy [17, 18], although a histologic shift was not noted in our study. Hence, liquid biopsy and tissue biopsy for detecting genomic alternations are complementary rather than alternatives for each other.

Most published studies reporting on EBUS-TBNA specimens for molecular testing focused on newly diagnosed lung cancer [19-22]. Few articles mentioned the clinical use of EBUS-TBNA re-biopsy specimens for molecular testing. In the current study, 21 patients had EGFR genotyping results at the initial diagnosis and re-biopsy. We noted that 5 (38.5%) of 13 patients with an initial EGFR mutation had acquired the T790M mutation detected from the re-biopsy specimens. The proportion of acquired T790M mutations was lower than that of previously published data (~50%) [17, 23-24]. This may be because the current study, for the

most part, used lymph nodes for EGFR testing rather than primary lung lesions or distant metastasis lesions. The discrepancy in EGFR genotyping between the primary tumor and the lymph nodes has been reported [25-26].

Conclusion

In summary, the current study found that using EBUS-TBNA for re-biopsy in previously treated lung cancer had a satisfactory diagnostic yield and could be conducted safely. Moreover, in some patients, further molecular testing was successfully conducted using a re-biopsy sample. This is the first local study to investigate the role of EBUS-TBNA for re-biopsy in Taiwan. Further large prospective studies may be needed to validate the efficacy.

References

1. Barta JA, Powell CA, Wisnivesky JP. Global epidemiology of lung cancer. An Global Health 2019; 85.
2. Paez JG, Jänne PA, Lee JC, *et al*. EGFR mutations in lung cancer: correlation with clinical response to gefitinib therapy. Science 2004; 304: 1497-500.
3. Mok TS, Wu Y-L, Thongprasert S, *et al*. Gefitinib or carboplatin–paclitaxel in pulmonary adenocarcinoma. N Engl J Med 2009; 361:947-57.
4. Del Re M, Crucitta S, Gianfilippo G, *et al*. Understanding the mechanisms of resistance in EGFR-positive NSCLC: from tissue to liquid biopsy to guide treatment strategy. Int J Mol Sci 2019; 20: 3951.
5. Chouaid C, Dujon C, Do P, *et al*. Feasibility and clinical impact of re-biopsy in advanced non-small-cell lung cancer: a prospective multicenter study in a real-world setting (GFPC study 12-01). Lung Cancer 2014; 86: 170-3.
6. Silvestri GA, Gonzalez AV, Jantz MA, *et al*. Methods for staging non-small cell lung cancer: diagnosis and management of lung cancer: American College of Chest Physicians evidence-based clinical practice guidelines. Chest 2013; 143: e211S-e50S.
7. Gu P, Zhao Y-Z, Jiang L-Y, *et al*. Endobronchial ultrasound-guided transbronchial needle aspiration for staging of lung cancer: a systematic review and meta-analysis. Eur J Cancer 2009; 45: 1389-96.
8. Dhooria S, Sehgal IS, Gupta N, *et al*. Diagnostic yield and complications of EBUS-TBNA performed under bronchoscopist-directed conscious sedation. J Bronchol Intervent Pulmonol 2017; 24: 7-14.
9. Kim J, Kang HJ, Moon SH, *et al*. Endobronchial ultrasound-guided transbronchial needle aspiration for re-biopsy in previously treated lung cancer. Cancer Res Treatment: Official Journal of the Korean Cancer Association 2019; 51: 1488.
10. Eisenhauer EA, Therasse P, Bogaerts J, *et al*. New response evaluation criteria in solid tumours: revised RECIST guideline (version 1.1). Eur J Cancer 2009; 45: 228-47.
11. Asano F, Aoe M, Ohsaki Y, *et al*. Complications associated with endobronchial ultrasound-guided transbronchial needle aspiration: a nationwide survey by the Japan Society for Respiratory Endoscopy. Respir Res 2013; 14: 1-8.
12. Casal RF, Lazarus DR, Kuhl K, *et al*. Randomized trial of endobronchial ultrasound–guided transbronchial needle aspiration under general anesthesia versus moderate sedation. Am J Respir Crit Care Med 2015; 191:796-803.
13. Siravegna G, Mussolin B, Venesio T, *et al*. How liquid biopsies can change clinical practice in oncology. Ann Oncol 2019; 30: 1580-90.
14. Guibert N, Pradines A, Favre G, *et al*. Current and future applications of liquid biopsy in nonsmall cell lung cancer from early to advanced stages. Eur Respir Rev 2020; 29.
15. Oxnard GR, Thress KS, Alden RS, *et al*. Association between plasma genotyping and outcomes of treatment with osimertinib (AZD9291) in advanced non–small-cell lung cancer. J Clin Oncol 2016; 34: 3375.
16. Hu Y, Ulrich BC, Supplee J, *et al*. False-positive plasma genotyping due to clonal hematopoiesis. Clin Cancer Res 2018; 24: 4437-43.
17. Helena AY, Arcila ME, Rekhtman N, *et al*. Analysis of tumor specimens at the time of acquired resistance to EGFR-TKI therapy in 155 patients with EGFR-mutant lung cancers. Clin Cancer Res 2013; 19:2240-7.
18. Oser MG, Niederst MJ, Sequist LV, *et al*. Transformation

from non-small-cell lung cancer to small-cell lung cancer: molecular drivers and cells of origin. The Lancet Oncol 2015; 16:e165-e72.

19. Nakajima T, Yasufuku K, Suzuki M, *et al*. Assessment of epidermal growth factor receptor mutation by endobronchial ultrasound-guided transbronchial needle aspiration. Chest 2007; 132:597-602.
20. Sakairi Y, Nakajima T, Yasufuku K, *et al*. EML4-ALK fusion gene assessment using metastatic lymph node samples obtained by endobronchial ultrasound-guided transbronchial needle aspiration. Clin Cancer Res 2010; 16: 4938-45.
21. Navani N, Brown JM, Nankivell M, *et al*. Suitability of endobronchial ultrasound-guided transbronchial needle aspiration specimens for subtyping and genotyping of non–small cell lung cancer: a multicenter study of 774 patients. Am J Respir Crit Care Med 2012; 185: 1316-22.
22. Nakajima T, Yasufuku K, Nakagawara A, *et al*. Multigene mutation analysis of metastatic lymph nodes in non-small cell lung cancer diagnosed by endobronchial ultrasound-guided transbronchial needle aspiration. Chest 2011; 140: 1319-24.
23. Sequist LV, Waltman BA, Dias-Santagata D, *et al*. Genotypic and histological evolution of lung cancers acquiring resistance to EGFR inhibitors. Sci Transl Med 2011; 3: 75ra26-75ra26.
24. Campo M, Gerber D, Gainor JF, *et al*. Acquired resistance to first-line afatinib and the challenges of prearranged progression biopsies. J Thorac Oncol 2016; 11: 2022-6.
25. Wang F, Fang P, Hou D-Y, *et al*. Comparison of epidermal growth factor receptor mutations between primary tumors and lymph nodes in non-small cell lung cancer: a review and meta-analysis of published data. Asian Pac J Cancer Prev 2014; 15: 4493-7.
26. Kang HJ, Hwangbo B, Lee JS, *et al*. Comparison of epidermal growth factor receptor mutations between metastatic lymph node diagnosed by EBUS-TBNA and primary tumor in non-small cell lung cancer. PLoS One 2016; 11: e0163652.

Comparison of Effectiveness of Proportional Assist Ventilation and Pressure Support Ventilation for Weaning Adult Patients from Prolonged Mechanical Ventilation: A Randomized Controlled Trial

Pi-Hua Lin[1], Chiu-Fan Chen[2,3], David Lin Lee[2,4]

Background: Proportional assist ventilation with load-adjustable gain factors (PAV+) is a promising mode with better patient synchrony and weaning advantages. This study aimed to compare the effectiveness of PAV+ and pressure support ventilation (PSV) for weaning adult patients from prolonged mechanical ventilation (PMV).

Methods: Patients with PMV were recruited for this prospective trial. Patients were randomly assigned to receive PAV+ or PSV as a weaning mode. Weaning outcomes and mortality were evaluated.

Results: A total of 36 patients completed the study (18 in the PAV+ group and 18 in the PSV group). The peak inspiratory pressure and tidal volume initially were significantly lower in the PAV+ group than in the PSV group. Both peak inspiratory pressure and tidal volume decreased during the weaning process in both groups, and the PAV+ group showed a smaller tidal volume change. Outcome analysis showed that the PAV+ group possibly had better results in the 28-day weaning success rate, weaning duration, and hospital mortality than the PSV group, but significance was not achieved.

Conclusion: This study proved the effectiveness of the PAV+ mode for weaning patients with PMV. PAV+ may be a potential mode for weaning patients with PMV in the future. ***(Thorac Med 2021; 36: 81-94)***

Key words: pressure support ventilation, prolonged mechanical ventilation, proportional assist ventilation, respiratory failure, weaning

Introduction

Approximately 1 in 3 patients admitted to intensive care units (ICUs) will receive mechanical ventilation (MV) [1]. Of these, 5%–10% will transition from acute to chronic critical illness and require prolonged MV (PMV), resulting in poor quality of life, pervasive functional and cognitive disabilities, intense caregiving needs, high mortality, and a high cost

[1]Division of Respiratory Therapy, Kaohsiung Veterans General Hospital, Kaohsiung, Taiwan
[2]Division of Chest Medicine, Kaohsiung Veterans General Hospital, Kaohsiung, Taiwan
[3]Department of Internal Medicine, Taitung Branch, Taipei Veterans General Hospital, Taitung, Taiwan
[4]Department of Medicine, National Yang-Ming University, Taipei, Taiwan
Address reprint requests to: Dr. Chiu-Fan Chen, Division of Chest Medicine, Kaohsiung Veterans General Hospital No. 386 Dazhong First Rd., Zuoying Dist., Kaohsiung City 81362, Taiwan

for care [2]. Pressure support ventilation (PSV) is the most frequently used ventilator weaning mode, especially for patients with PMV [3-4]. However, this conventional mode has several disadvantages, including patient-ventilator asynchrony, over- and under-assistance, and subsequent diaphragm weakness [5-7]. Diaphragm weakness has been reported to be associated with prolonged weaning and decreased survival [8-10].

Proportional assist ventilation (PAV), designed and developed by Younes, is a promising mode that improves patient-ventilator synchrony [11-12]. It provides synchronized partial ventilator assistance in proportion to a patient's instantaneous effort, amplifying the patient's ventilatory effort and giving the patient the freedom to adapt to his or her own breathing pattern [11,13]. The initial version of PAV required clinicians to measure lung compliance and airway resistance manually. PAV with load-adjustable gain factors (PAV+) was developed subsequently, to automatically and frequently measure compliance and resistance using noninvasive methods, making the mode more convenient for clinical use [14]. A recent meta-analysis of randomized controlled trials (RCTs) showed that PAV+ was associated with significantly lower patient-ventilator asynchrony, a lower weaning failure rate, and shorter MV duration than PSV for weaning ICU patients from MV [15].

According to a small-scale physiologic study, PAV+ also resulted in significantly fewer asynchronies than PSV in difficult-to-wean patients [16]. However, the clinical effectiveness of PAV+ on weaning outcomes for patients with PMV has not yet been evaluated. Therefore, this study aimed to compare weaning outcomes between PAV+ and PSV in adult patients with PMV in Taiwan.

Methods

Patients, randomization, and masking

This randomized controlled trial was conducted over an 11-month period in a 16-bed respiratory care center (RCC) of a tertiary medical center in southern Taiwan. Patients who transferred to the RCC due to PMV were screened for enrollment. PMV was defined as MV use >21 days. The study was approved by the Institutional Review Board of Kaohsiung Veterans General Hospital (VGHKS99-CT14–15), and written informed consent was obtained from all patients before enrolling them into the study.

The RCC is a specialized weaning unit for patients with PMV, with the primary aim of liberating patients from MV and improving ICU turnover. It was established in accordance with the integrated delivery system policy of Taiwan's National Health Insurance Bureau. The system includes 4 stages of care for patients on MV support: 1st stage, ICU care at 1–21 days of MV; 2nd stage, RCC care at 21–63 days; 3rd stage, chronic respiratory care unit for patients on long-term MV support >63 days; and 4th stage, an optional choice: home care for MV-dependent patients. In the RCC, 24-hour vital sign monitoring and nursing care is performed, and the nurse-to-patient ratios are 1:4 during both daytime and nighttime.

Patients meeting the following inclusion criteria and who had been admitted to the RCC were enrolled in the study: age ≥20 years, extubation failure or spontaneous breathing trial (SBT) failure at least once in the ICU, conditions requiring PMV or patients who were expected to receive PMV, stable hemodynamics, no vasopressor, inspired oxygen (FiO_2) ≤0.40, external positive end-expiratory

pressure (PEEP) ≤5 cmH2O, partial pressure of oxygen (PaO_2) >60 mmHg, and body temperature <38ºC (within 24 hours). Patients with the following characteristics were excluded: bronchopleural fistulas, central neurological disorders, hemodialysis, and patients with a pressure support level already <15 cmH_2O. The patients were enrolled and randomly assigned to the PAV+ group or the PSV group, using a computer-generated random number list. All patients were ventilated via endotracheal tube or tracheostomy tube. Both groups (PAV+ and PSV mode) used the same Puritan-Bennett 840 ventilators (Nellcor Puritan Bennett LLC, Gosport, UK). Blinding after randomization was not possible in this study. The withdrawal criteria used in this study were: (1) the patient developed severe or intolerable adverse events, (2) the patient had new medical problems requiring further treatment and intervention, and therefore had to discontinue the weaning process, (3) the patient had poor cooperation, and (4) the patient was not obeying the study protocol.

Measurement

Before the weaning trial, the following information was collected for each patient: age, sex, body mass index, MV duration before this trial, number of reintubations, Acute Physiology and Chronic Health Evaluation II (APACHE II) score at RCC admission, PaO_2/FiO_2, lung compliance, airway resistance, maximal inspiratory pressure (MIP), tidal volume (VT) at spontaneous breathing, respiratory rate (RR) at spontaneous breathing, rapid shallow breath index (RSBI), tracheostomy rate, initial cause of MV, and MV mode at enrollment. MV duration before the trial was defined as the time from the start of ventilation support to the time of randomization. Lung compliance and airway resistance were measured at volume control ventilation, with tidal volume setting of 10 ml/kg, flow of 60 L/min, square wave, and plateau pressure measured at 1-1.5 seconds after the end of inspiration. The lung compliance calculation formula was: Static compliance = VT/(Pplat-PEEP), ml/cm H_2O. The airway resistance (Raw) calculation formula was: Raw = (PIP-Pplat)/flow, cm H_2O/L/sec (PIP = peak inspiratory pressure, Pplat = plateau pressure). The patient was removed from the ventilator for 3-5 minutes, then RR and minute ventilation were measured during 1 minute of spontaneous breathing, to calculate RSBI. Minute ventilation was measured using a Wright Respirometer (Ferraris Medical Ltd, UK). Later, MIP was measured using an Inspiratory Force Meter (Boehringer Laboratories, USA).

The following data were collected 1 hour after the first setting for MV weaning (PAV+ or PSV) and after each adjustment of the support level, which included the support level, FiO_2, PEEP, VT, RR, RSBI, minute ventilation, peak inspiratory pressure (PIP), mean airway pressure, inspiratory time (Ti), ratio of inspiratory time and respiratory cycle time (Ti/Ttot), heart rate, and peripheral oxygen saturation. At this stage, VT, RR and RSBI were obtained when the patient was under PAV+ or PSV support.

The primary outcome was 28-day weaning success rate. The secondary outcomes were weaning duration, hospital length of stay (LOS), RCC LOS, weaning success rate at discharge, and hospital mortality. Weaning duration was defined as the time from randomization to successful liberation from MV. For those who failed to liberate themselves from MV throughout the course of the weaning trial, the weaning duration was defined from randomization to the end of the study (discharge or up to 28 days).

Weaning success was defined as being alive and liberated from MV for more than 48 hours.

Weaning protocol

The weaning protocol for this study was similar to the ICU difficult weaning protocol (stepwise adjustment of the MV support level). The flowchart of the weaning protocol is shown in Figure 1. Weaning was attempted at least twice a day. Under similar baseline conditions (PEEP ≤5 cmH_2O, FiO_2 ≤0.4), the goal of the initial weaning mode setting was to maintain VT above 5–8 ml/kg and RR between 8 and 25/min. Therefore, the initial support level was dependent on each patient's lung condition at that moment. For patients with adequate VT and stable RR for 1–2 hours, the ventilator support level was tapered gradually (reduction of 5%–10% in PAV+ and 2–4 cmH_2O in PSV). For patients with tachypnea (>35–40/min) or low VT <5 ml/kg, the ventilator support level was titrated up (increased 5%–10% in PAV+ and 2–5 cmH_2O in PSV). If the patient still had tachypnea (>35–40/min) and low VT (<5 ml/

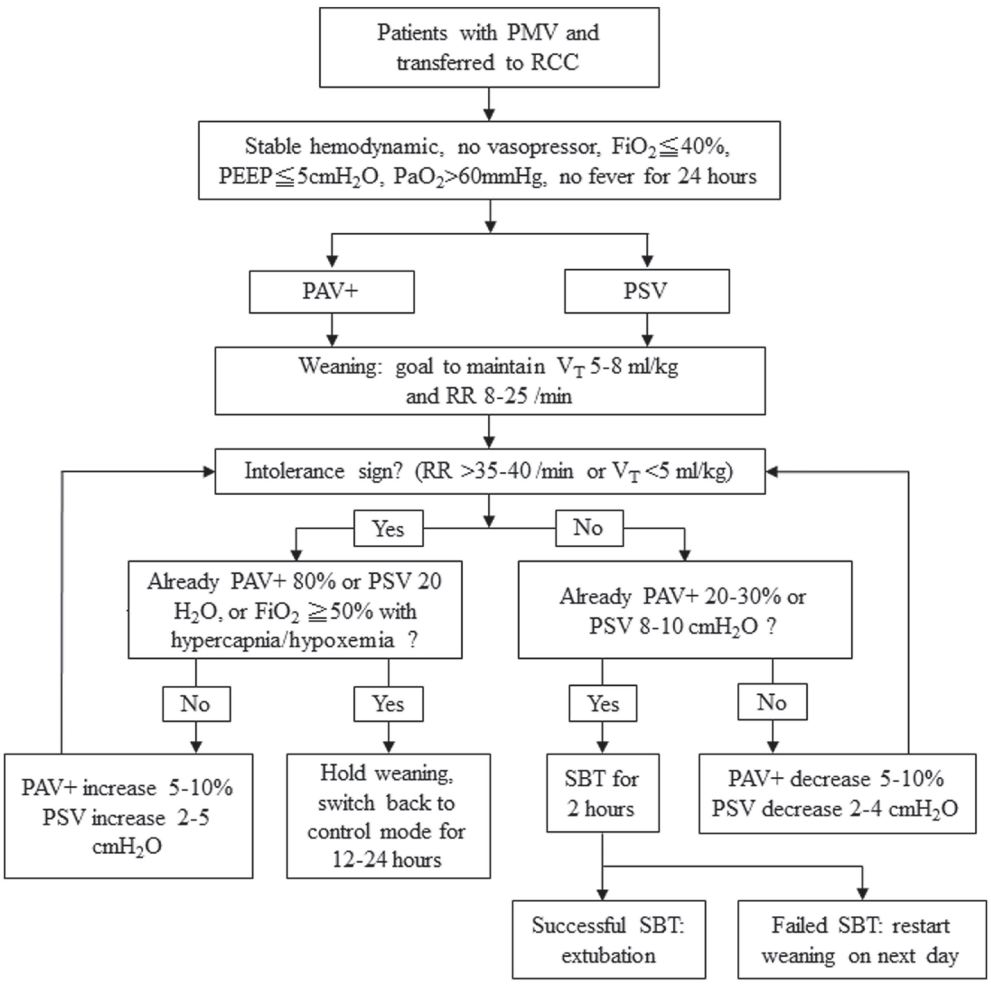

Fig. 1. Flowchart of the weaning protocol for patients with PMV

PAV+ = proportional assist ventilation with load-adjustable gain factors, PEEP = positive end-expiratory pressure, PMV = prolonged mechanical ventilation, PSV = pressure support ventilation, RCC = respiratory care center, RR = respiratory rate, SBT = spontaneous breathing trial, VT = tidal volume

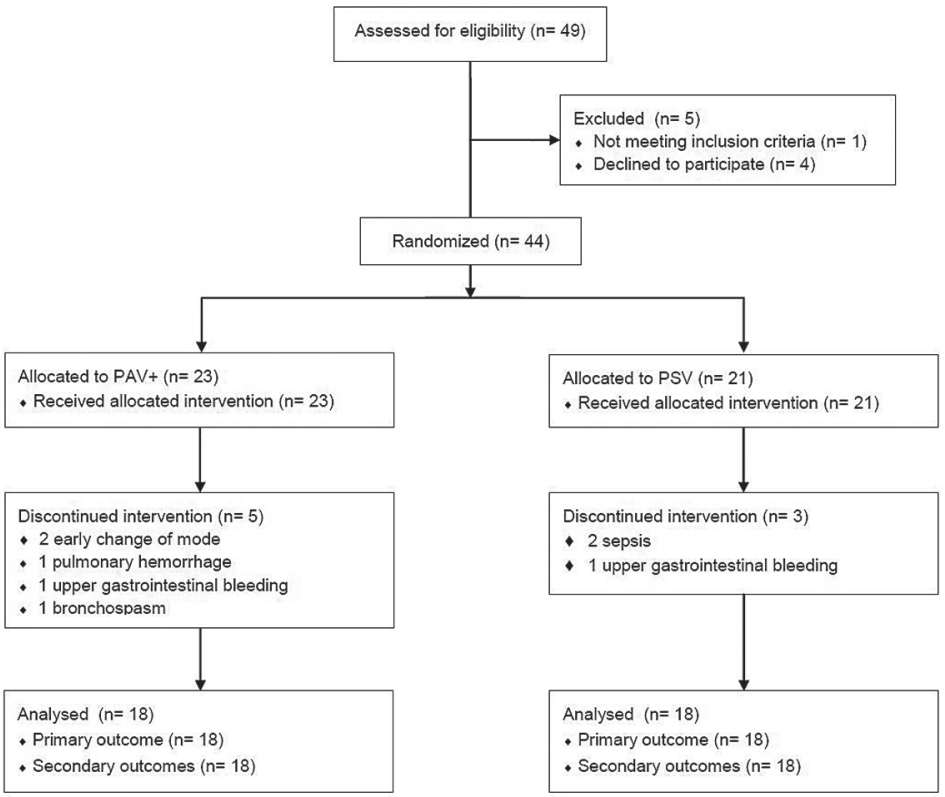

Fig. 2. Flowchart of patient selection and randomization
PAV+ = proportional assist ventilation with load-adjustable gain factors, PSV = pressure support ventilation.

kg) despite PAV+ 80% or PSV 20 cmH_2O, or FiO_2 increased to 50% with hypercapnia or hypoxemia, then the weaning process was held and switched back to control mode for 12–24 hours. Once the patient had a ventilator support level tapered to 20%–30% in PAV+ or 8–10 cmH_2O in PSV, a SBT was performed to evaluate the readiness for extubation.

The SBT was performed by discontinuing MV and connecting a T-tube to the patient to deliver oxygen; respiration then was observed for 2 hours. For patients that could tolerate the SBT, the clinician would perform extubation. If the SBT failed, MV would be continued, and the weaning process would be restarted on the next day. SBT failure was determined using the following indices: (1) objective indices of failure, such as tachypnea (RR >35/min for more than 5 minutes), hypoxemia (SPO_2 <90%), arrhythmia (heart rate >140 beats/min and/or ≥ 20% change from baseline), and hypertension/hypotension (systolic pressure >180 or <90 mmHg or ≥20% change from baseline), and (2) subjective indices, such as agitation, depressed mental status, diaphoresis, and evidence of increasing respiratory effort [1,17].

Statistical analysis

Continuous variables were expressed as mean ± standard deviation and were compared using independent t-tests and paired t-tests. Dichotomous variables were expressed as number (percentage) and were compared using Pearson's chi-squared tests. Time from randomiza-

tion to weaning from MV was evaluated using the Kaplan-Meier method, and the log-rank test was used to compare differences between the 2 groups. SPSS software (version 20.0; IBM Corp., Armonk, NY) was used for statistical analysis. A 2-tailed p value <0.05 was considered statistically significant.

Results

From 1 May 2010 to 31 March 2011, a total of 44 patients who transferred to the RCC due to PMV or expected PMV were enrolled in the study and were randomly assigned to the PAV+ or the PSV group (Table 2). Of the original 44 patients, 36 completed the study (18 in the PAV+ group and 18 in the PSV group), and 8 discontinued the study (2 for ventilator-associated pneumonia, 1 for severe bronchospasm, 1 for pulmonary hemorrhage, 2 for upper gastrointestinal bleeding, and 2 for early change of ventilation mode). The mean age of the patients was 73 ± 13.6 years, the APACHE II score at RCC admission was 14.7 ± 3.8, and the MV duration before enrollment was 26 ± 15.5 days. The baseline physiologic parameters before enrollment were as follows: PaO_2/FiO_2 ratio, 293.2 ± 110; lung compliance, 29.8 ± 12.2 ml/cmH_2O; maximal inspiratory pressure, -33.2 ± 11.1 cmH_2O; and RSBI, 111.7 ± 53.9. The tracheostomy rate was 55.6% at baseline. The most common cause of MV was pneumonia, followed by chronic obstructive pulmonary disease and sepsis. There was no significant difference between the 2 groups in terms of baseline clinical features and MV mode at enrollment (Table 1). The majority of patients were on control modes (volume control ventilation, 36.1%; pressure control ventilation, 33.3%) before randomization.

After randomization, the support level after the first MV setting for weaning was 60.8 ± 9.3% in the PAV+ group and 15.4 ± 1.8 cmH_2O in the PSV group. Analyses of the physiologic parameters of the first MV setting for weaning revealed the following: the PAV+ group had significantly lower PIP (14.7 ± 4.5 vs. 21.3 ± 2.4 cmH_2O, $p < 0.001$), longer Ti (0.97 ± 0.17 vs. 0.68 ± 0.16 sec, $p < 0.001$), higher Ti/Ttot (0.41 ± 0.06 vs. 0.29 ± 0.06, $p < 0.001$), lower VT (356.3 ± 61.4 vs. 431.5 ± 103.8 ml, $p = 0.013$), and lower VT/ideal body weight (6.6 ± 1.3 vs. 7.6 ± 1.7 ml/kg, $p = 0.047$) than the PSV group. There was a borderline significant trend of higher RSBI in the PAV+ group (81.6 ± 27.5 vs. 64.2 ± 24.7 breath/min/L, $p = 0.053$) (Table 2).

A comparison of the physiologic parameters of the lowest ventilator setting for the weaning trial showed that the support level was 32.5 ± 6.2% in the PAV+ group and 10.1 ± 0.8 cmH_2O in the PSV group. The PAV+ group also had significantly lower PIP (11.4 ± 2.4 vs. 16 ± 1 cmH_2O, $p < 0.001$), longer Ti (0.86 ± 0.16 vs. 0.67 ± 0.13 sec, $p = 0.001$), and higher Ti/Ttot (0.39 ± 0.06 vs. 0.31 ± 0.06, $p < 0.001$) and RSBI (89.4 ± 27.9 vs. 70.7 ± 23.5, $p = 0.037$) than the PSV group. Moreover, the PAV+ group had a trend toward lower VT than the PSV group (334.2 ± 64.4 vs. 388.5 ± 95.6, $p = 0.054$). However, patient heart rate was higher in the PAV+ group than in the PSV group (97.4 ± 17.5 vs. 85.8 ± 12.6, $p = 0.031$) (Table 3).

A comparison of physiologic parameter changes between the initial and the lowest support level is shown in Figure 3. In the PAV group, there were significant decreases in PIP (mean difference, -3.2 ± 4.3 cmH_2O; p = 0.006) and Ti (mean difference, -0.11 ± 0.17 sec; $p = 0.017$). In the PSV group, there was a signifi-

Table 1. Comparison of Baseline Clinical Features of PAV+ and PSV Groups

Variables	All (n=36)	PAV+ (n=18)	PSV (n=18)	*p* value
Age, years	73 ± 13.6	74.8 ± 12.2	71.1 ± 15.1	0.421
Sex, males, n (%)	23 (63.9)	12 (66.7)	11 (61.1)	0.729
BMI, kg/m^2	24.9 ± 6.1	23.9 ± 4.9	25.9 ± 7.1	0.325
MV duration before enrollment, days	26 ± 15.5	23.5 ± 10	28.4 ± 19.5	0.348
Number of reintubations before enrollment	0.75 ± 0.91	0.83 ±1.1	0.67 ± 0.69	0.589
APACHE II	14.7 ± 3.8	14.8 ± 3.4	14.7 ± 4.2	0.931
PaO_2/FiO_2 ratio*	293.2 ± 110	263.4 ± 97	321.41 ± 117.2	0.163
C_L^+, ml/cmH_2O	29.8 ± 12.2	27.6 ± 7.8	31.9 ±15.3	0.312
Raw$^+$, sec・cmH_2O/L	11.2 ± 6.5	11.9 ± 7.8	10.5 ± 5	0.561
MIP$^+$, cmH_2O	-33.2 ± 11.1	-31.7 ± 10.4	-34.4 ± 11.8	0.518
VTsb^{II}, ml	298.6 ± 98.5	292.8 ± 58	304.4 ± 128.9	0.744
RRsb^{II}, /min	29.2 ± 8.1	27.5 ± 7.6	30.9 ± 8.5	0.248
RSBI^{II}, breath/min/L	111.7 ± 53.9	101.5 ± 47.6	121.9 ± 59.4	0.292
Tracheostomy, n (%)	20 (55.6)	10 (55.6)	10 (55.6)	1.000
Reason for MV, n (%)				
Pneumonia	19 (52.8)	10 (55.6)	9 (50)	0.275
COPD	5 (13.9)	3 (16.7)	2 (11.1)	
Sepsis	4 (11.1)	2 (11.1)	2 (11.1)	
Heart failure	3 (8.3)	1 (5.6)	2 (11.1)	
Postoperative state	2 (5.6)	0 (0)	2 (11.1)	
Post-CPR	1 (2.8)	0 (0)	1 (5.6)	
Other	2 (5.6)	2 (11.1)	0 (0)	
MV mode at enrollment, n (%)				
VCV	13 (36.1)	9 (50)	4 (22.2)	0.178
PCV	12 (33.3)	4 (22.2)	8 (44.4)	
PRVC	2 (5.6)	2 (11.1)	0 (0)	
SIMV	3 (8.3)	1 (5.6)	2 (11.1)	
PSV	6 (16.7)	2 (11.1)	4 (22.2)	

Data presented as mean ± SD or n (%).

APACHE II = acute physiology and chronic health evaluation II, BMI = body mass index, CL = lung compliance, COPD = chronic obstructive pulmonary disease, CPR = cardiopulmonary resuscitation, Raw = airway resistance, MIP = maximal inspiratory pressure, MV = mechanical ventilation, PAV+ = proportional assist ventilation with load-adjustable gain factors, PCV = pressure-controlled ventilation, PSV = pressure-support ventilation, PRVC = pressure-regulated volume control, RRsb = respiratory rate at spontaneous breathing, RSBI = rapid shallow breathing index, SD = standard deviation, SIMV = synchronized intermittent mandatory ventilation, VCV = volume-controlled ventilation, VTsb = tidal volume at spontaneous breathing.

*PaO_2/FiO_2: 29 cases, $^+$CL and Raw: 34 cases, $^+$MIP: 31 cases, ^{II}VTsb, RRsb and RSBI: 32 cases

cant decrease in PIP (mean difference, -5.2 ± 2.4 cmH_2O; $p < 0.001$). The-PSV group showed a wide range of RR and VT variations at the initial support level, but the variations decreased at the lowest support level. The PAV group showed a wide range of RR and RSBI variation at both the initial and the lowest support levels; however, VT remained in a narrow range at both the initial and the lowest support levels of PAV+.

For all patients, the weaning duration was 15.3 ± 9.4 days, the RCC LOS was 29.7 ± 22 days, the hospital LOS was 57.8 ± 21 days, the weaning success rate at 28 days was 61.1%, the

Table 2. Comparison of Physiologic Parameters 1 Hour After the First Vventilator Setting for Weaning

Parameters	PAV+ (n=18)‖	PSV (n=18)	*p* value
PAV+ level, %	60.8 ± 9.3		
PSV level, cmH_2O		15.4 ± 1.8	
FiO_2, %	35.8 ± 3.5	36.1 ± 3.2	0.807
PEEP, cmH_2O	5 ± 0	4.6 ± 1.2	0.202
RR, /min	26.4 ± 5.5	25 ± 5.4	0.448
VT, ml	356.3 ± 61.4	431.5 ± 103.8	0.013*
VT/IBW, ml/kg	6.6 ± 1.3	7.6 ± 1.7	0.047*
RSBI, breath/min/L	81.6 ± 27.5	64.2 ± 24.7	0.053
Minute ventilation, L	8.9 ± 1.8	10.2 ± 3.3	0.156
PIP, cmH_2O	14.7 ± 4.5	21.3 ± 2.4	<0.001*
Pmean, cmH_2O	8.2 ± 1.2	9.1 ± 1.3	0.059
Ti^+, sec	0.97 ± 0.17	0.68 ± 0.16	<0.001*
$Ti/Ttot^+$	0.41 ± 0.06	0.29 ± 0.06	<0.001*
Heart rate, beat/min	95.2 ± 15.8	89.1 ± 16.6	0.267
SpO_2,%	96.7 ± 3.2	95.2 ± 2.1	0.585

Data presented as mean ± SD, *$p < 0.05$

$^+$n = 35, $^+$n = 34

IBW = ideal body weight, min = minute, PAV+ = proportional assist ventilation with load-adjustable gain factors, PEEP = external positive end-expiratory pressure, PIP = peak inspiratory pressure, Pmean = mean airway pressure, PSV = pressure support ventilation, RR = respiratory rate, RSBI = rapid shallow breathing index, SD = standard deviation, SpO_2 = peripheral oxygen saturation, Ti = inspiration time, Ttot = total cycle time, VT = tidal volume

Table 3. Comparison of Physiologic Parameters of the Lowest Levels of Ventilator Settings for Weaning

Parameters	PAV+ (n=18)‖	PSV (n=18)	*p value*
PAV+ level, %	32.5 ± 6.2		
PSV level, cmH_2O		10.1 ± 0.8	
Days of weaning	8.3 ± 7.2	6.6 ± 5	0.412
FiO_2, %	34.7 ± 4.7	34.7 ± 3.6	1.000
PEEP, cmH_2O	5 ± 0	5 ± 0	1.000
RR, /min	28.1 ± 4.8	26.1 ± 4.7	0.218
VT, ml	334.2 ± 64.4	388.5 ± 95.6	0.054
VT/IBW, ml/kg	6.2 ± 1.5	6.9 ± 1.9	0.228
RSBI, breath/min/L	89.4 ± 27.9	70.7 ± 23.5	0.037*
Minute ventilation, L	8.9 ± 2.2	9.9 ± 2.8	0.249
Ti^+, sec	0.86 ± 0.16	0.67 ± 0.13	0.001*
$Ti/Ttot^+$	0.39 ± 0.06	0.31 ± 0.06	<0.001*
PIP^+, cmH_2O	11.4 ± 2.4	16 ± 1	<0.001*
$Pmean^+$, cmH_2O	7.2 ± 0.6	8.5 ± 0.7	<0.001*
Heart $rate^+$, beat/min	97.4 ± 17.5	85.8 ± 12.6	0.031*
SpO_2^+, %	97.3 ± 2.6	97.4 ± 2	0.888

Data presented as mean ± SD, *$p < 0.05$

+n = 35

IBW = ideal body weight, min = minute, PAV+ = proportional assist ventilation with load-adjustable gain factors, PEEP = external positive end-expiratory pressure, PIP = peak inspiratory pressure, Pmean = mean airway pressure, PSV = pressure support ventilation, RR = respiratory rate, RSBI = rapid shallow breathing index, SD = standard deviation, SpO_2 = peripheral oxygen saturation, Ti =inspiration time, Ttot = total cycle time, VT = tidal volume

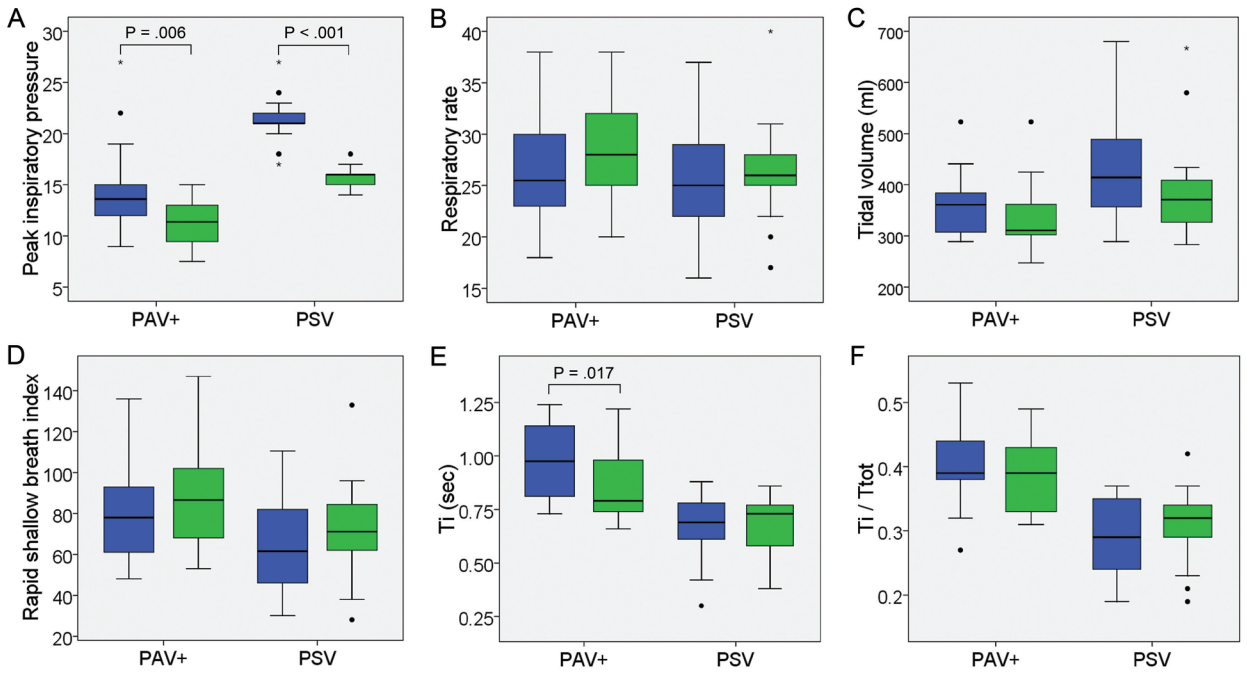

Fig. 3. Comparison of physiologic parameters of the first (blue) and the lowest (green) ventilator support level during weaning
In the PAV group, there was a significant decrease in PIP (-3.2 ± 4.3 cmH2O; p = 0.006) and Ti (-0.11 ± 0.17 sec; p = 0.017). In the PSV group, there was a significant decrease in PIP (-5.2 ± 2.4 cmH2O; p < 0.001).
PAV+ = proportional assist ventilation with load-adjustable gain factors, PIP = peak inspiratory pressure, PSV = pressure support ventilation, Ti = inspiration time, Ttot = total cycle time

Table 4. Comparison of PAV+ and PSV Group Outcomes

	All (n=36)	PAV+ (n=18)	PSV (n=18)	*p* value
Weaning duration, days	15.3 ± 9.4	14.6 ± 9.2	16.1 ± 9.8	0.652
RCC LOS, days	29.7 ± 22	24.5 ± 13.7	34.9 ± 27.5	0.160
Hospital LOS, days	57.8 ± 21	53.9 ± 14.6	61.7 ± 25.7	0.268
Weaning success at 28 days, n (%)	22 (61.1)	13 (72.2)	9 (50)	0.171
Weaning success at discharge, n (%)	24 (66.7)	14 (77.8)	10 (55.6)	0.157
Hospital mortality, n (%)	4 (11.1)	0 (0)	4 (22.2)	0.104

Data presented as mean ± SD or n (%)
LOS = length of stay, PAV+ = proportional assist ventilation with load-adjustable gain factors, PSV = pressure support ventilation, RCC = respiratory care center, SD = standard deviation

weaning success rate at discharge was 66.7%, and hospital mortality was 11.1%. The PAV+ group had a nonsignificant trend toward a higher weaning success rate at 28 days (72.2% vs. 50%, $p = 0.171$) and at discharge (77.8% vs. 55.6%, $p = 0.157$) than the PSV group (Table 4). The Kaplan-Meier curve of time-to-successful weaning for the PAV+ and PSV groups also showed a trend toward greater weaning success and shorter weaning duration in the PAV+ group than in the PSV group (Figure 4), although the difference between the 2 groups was not significant (log-rank test, $p = 0.294$).

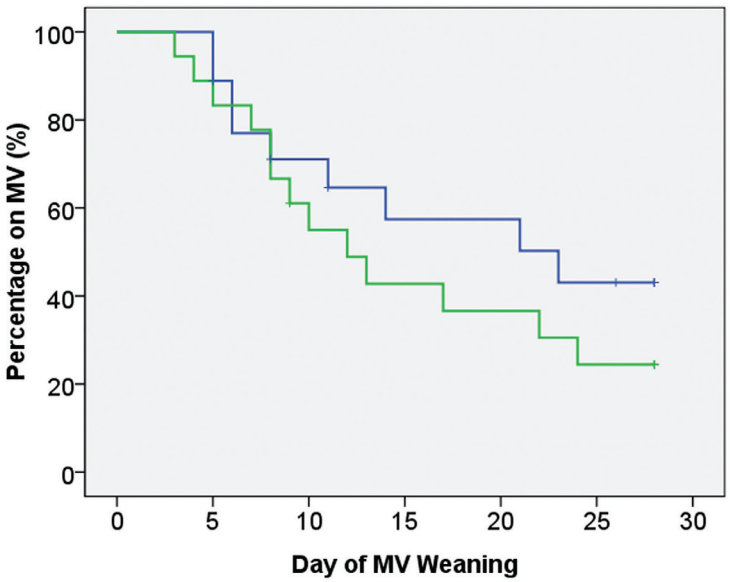

Fig. 4. Kaplan-Meier curve for comparison of time to successful weaning between the PAV+ and PSV groups
The PAV+ group (green line) had a nonsignificant trend toward a higher weaning success rate and shorter weaning duration than the PSV group (blue line). Log-rank test: p = 0.294.
PAV+ = proportional assist ventilation with load-adjustable gain factors, PSV = pressure support ventilation

Discussion

This is the first RCT comparing the weaning outcomes of PAV+ and PSV in patients with PMV. This study found that PAV+ is as effective as PSV for weaning adult patients from PMV. The 28-day weaning success rates were 72.2% in the PAV+ group and 50% in the PSV group, and the weaning durations were 14.6 days in the PAV+ group and 16.1 days in the PSV group, suggesting a potential advantage of PAV+ for weaning from PMV. Although statistical significance was not achieved due to the small sample size and inadequate statistical power, our results are consistent with recent literature evaluating the efficacy of PAV+ for weaning MV patients in the ICU [15].

PSV is the most commonly used ventilator mode for weaning patients from MV, specifically for those patients with difficult or prolonged MV weaning [3-4]. However, PSV has several disadvantages, including patient-ventilator asynchrony, and inability to evaluate and match the patient's breathing effort, which results in over- or under-assist of MV. Both over- and under-assist of MV in PSV may result in diaphragm weakness [5], and diaphragm weakness has been reported to be associated with weaning failure, prolonged weaning, and extubation failure [8-10]. Moreover, gradual tapering of the PSV level is also a poor predictor of the patient's ability to sustain ventilation after extubation [18].

Asynchrony is common in PSV and the assist-control mode, with 18%–24% of patients having an asynchrony index >10% [19-20]. Asynchrony is unfavorable to weaning and was found to result in prolonged MV duration, increased need of sedation, extended ICU stay, and increased ICU and hospital mortality [21-

22]. Asynchrony was reported to be more common in PSV of a high support level and high VT, and to improve in PSV of a low support level and decreased VT [19,23-24]. Ineffective triggers are the most common type of asynchrony in PSV and other MV modes [21,25-26]. A higher PSV support level was associated with significantly higher VT and lower RR of MV than a lower PSV support level, because patients are unable to compensate for the initial high assist in PSV [24]. Furthermore, the initial high VT in PSV may contribute to an ineffective effort by increasing intrinsic PEEP, resulting in lower RR of MV [19,26]. It was also reported that lowering VT by decreasing the pressure support level or Ti in PSV can effectively reduce ineffective triggers in patients with weaning difficulties [23].

PAV+ is designed to adjust the inspiratory pressure proportionally to the patient's inspiratory demand (instantaneous flow, volume, and pressure generated by the respiratory muscles), and is a form of partial ventilator support, like additional inspiratory muscles, for the patient [11,14-15]. PAV+ delivers support proportional to lung mechanics and allows the patient to maintain his or her own breathing pattern, without targeting inspiratory flow, VT, or pressure [11]. PAV+ is reported to be a more user-friendly mode than PSV, with less need of intervention for ventilator settings and sedative dose changes [12,27]. There is emerging evidence that the PAV+ mode is a promising mode for MV weaning in the ICU. A recent meta-analysis evaluating RCTs comparing the effectiveness of PAV+ and PSV in ICU patients found that PAV+ had a significantly lower incidence of an asynchrony index >10%, a lower rate of weaning failure, and shorter MV duration than PSV [15]. Recent literature also suggested that PAV+ had more stable VT and thus prevented over-assistance and diaphragm dysfunction [6,28].

A similar proportional mode, neurally adjusted ventilatory assist (NAVA), is also designed to improve patient-ventilator asynchrony, but via methods different from PAV+. While PAV+ operates via ongoing assessment of lung mechanics and the work of breathing (by air pressure, flow, volume), NAVA operates via measurement of diaphragmatic electromyography to control gas delivery [12,15]. Therefore, NAVA provides ventilator support proportional to electrical signals directly from the diaphragmatic muscles [12]. According to a recent meta-analysis of RCTs comparing NAVA and PSV in the ICU, NAVA also had a significantly lower incidence of an asynchrony index >10% than PSV. However, the effectiveness of NAVA on the weaning rate and MV duration was insignificant after pooling the RCT results [15]. Furthermore, NAVA requires the placement of a special nasogastric tube to monitor diaphragmatic electrical signals, while PAV+ does not require this invasive device [12]. Therefore, PAV+ is considered a more practical proportional mode, with more evidence on outcome benefits compared to NAVA.

Evaluating both the percentage of ventilator support and the patient's own respiratory effort is difficult under the PSV mode. In current practice, adjustment of the PSV support level during the weaning process relies mainly on clinical markers, such as RR, respiratory pattern, VT, and heart rate. However, previous literature reported that these clinical markers were poor predictors for assessing the work of breathing in patients with PSV, and titrating the PSV level according to the respiratory pattern may result in inappropriate respiratory muscle workloads [29-30].

PAV+ monitors both total workload and the patient's respiratory workload, and the RCC staff can properly adjust the ventilator support percentage to keep the patient's work of breathing within the comfort zone (0.3–0.7 J/L). In PAV+, the work of breathing is calculated using noninvasive measurement of resistance and elastance of the pulmonary system [20,31]. Using measurement of the work of breathing, PAV+ can guarantee an appropriate ventilator support level to match the patient's requirement, preventing over- or under-assistance. This effort-adapted mode of MV helps improve patient-ventilator synchrony and effectively unload the respiratory muscles [6,32].

In our study, both groups showed a significant PIP decrease during the weaning process. However, PIP was significantly lower in the PAV+ group than in the PSV group, at both the first and the lowest levels of MV setting. A previous study reported that PAV+ had consistently lower PIP than PSV [20]. The marked reduction in PIP, while achieving similar VT, suggests that patients using PAV+ assumed a greater total respiratory workload than patients using PSV [20]. In the PSV group, there was a wider range of VT at the initial assist level, with a considerable number of patients with high VT. This phenomenon was consistent with the literature showing that PSV was prone to over-assist in the initial stage, which may result in air trapping and increase the ineffective trigger [7,12]. In contrast, in the PAV+ group, VT was lower and more stable among different assist levels, consistent with previous literature, implying that this mode better matches the patient's demand and prevents over-assistance [7,12,20,24,28].

Our study has some limitations. This was a single-center study consisting of a small sample size and with inadequate statistical power; therefore, the generalizability of the results is limited. Blinding was impossible for the MV patients and healthcare staffs. Our study did not evaluate the patient's work of breathing, patient-ventilator asynchrony, and the use of sedation. We evaluated weaning duration, rather than MV duration, because the MV duration before the trial was long and highly variable. Moreover, some patients remained on MV support despite the 28 days of the weaning trial during the study. The patients included in this study were in a prolonged MV status and were difficult to wean. Not all patients can successfully taper the MV support level to PAV+ 30% or PSV 10 cmH_2O and proceed to SBT. Therefore, the average lowest support level was slightly higher than PAV+ 30% and PSV 10 cmH_2O.

Conclusion

In this study, the use of PAV+ was associated with a significantly lower PIP and a more stable VT than with the use of PSV for patients with PMV. The 2 modes had a similar weaning duration and weaning success rate. Although the clinical use of this mode for MV weaning is still uncommon, evidence supporting the better efficacy of PAV+ with MV weaning is increasing. Moreover, a large multicenter RCT comparing PAV+ and PSV for weaning patients with acute respiratory failure is already ongoing (NCT02447692). Our study demonstrated the effectiveness of the PAV+ mode for weaning patients with PMV. And with its additional advantages of patient-ventilator synchrony and matching of the patient's effort requirement, we suggest the PAV+ mode is a promising weaning mode for PMV patients in the future.

Acknowledgments

We thank Mrs. Yu-Jung Chang for her opinions on manuscript revision.

References

1. Esteban A, Anzueto A, Frutos F, *et al*. Characteristics and outcomes in adult patients receiving mechanical ventilation: a 28-day international study. JAMA 2002; 287: 345-355.
2. Cox CE, Martinu T, Sathy SJ, *et al*. Expectations and outcomes of prolonged mechanical ventilation. Crit Care Med 2009; 37: 2888-2894; quiz 2904.
3. Esteban A, Anzueto A, Alía I, *et al*. How is mechanical ventilation employed in the intensive care unit? An international utilization review. Am J Respir Crit Care Med 2000; 161: 1450-1458.
4. Boles JM, Bion J, Connors A, *et al*. Weaning from mechanical ventilation. Eur Respir J 2007; 29: 1033-1056.
5. Dres M, Goligher EC, Heunks LMA, *et al*. Critical illness-associated diaphragm weakness. Intensive Care Med 2017; 43: 1441-1452.
6. Vaporidi K. NAVA and PAV+ for lung and diaphragm protection. Curr Opin Crit Care 2020; 26: 41-46.
7. Pletsch-Assuncao R, Caleffi Pereira M, Ferreira JG, *et al*. Accuracy of invasive and noninvasive parameters for diagnosing ventilatory overassistance during pressure support ventilation. Crit Care Med 2018; 46: 411-417.
8. Kim WY, Suh HJ, Hong SB, *et al*. Diaphragm dysfunction assessed by ultrasonography: influence on weaning from mechanical ventilation. Crit Care Med 2011; 39: 2627-2630.
9. Jung B, Moury PH, Mahul M, *et al*. Diaphragmatic dysfunction in patients with ICU-acquired weakness and its impact on extubation failure. Intensive Care Med 2016; 42: 853-861.
10. Dres M, Dubé BP, Mayaux J, *et al*. Coexistence and impact of limb muscle and diaphragm weakness at time of liberation from mechanical ventilation in medical intensive care unit patients. Am J Respir Crit Care Med 2017; 195: 57-66.
11. Younes M. Proportional assist ventilation. In: Mancebo J, Net A, Brochard L, eds. Mechanical Ventilation and Weaning. Update in Intensive Care Medicine. Berlin, Heidelberg; Springer, 2003: 39-73.
12. Kacmarek RM. Proportional assist ventilation and neurally adjusted ventilatory assist. Respir Care 2011; 56: 140-148.
13. Ambrosino N, Rossi A. Proportional assist ventilation (PAV): a significant advance or a futile struggle between logic and practice? Thorax 2002; 57: 272-276.
14. Xirouchaki N, Kondili E, Vaporidi K, *et al*. Proportional assist ventilation with load-adjustable gain factors in critically ill patients: comparison with pressure support. Intensive Care Med 2008; 34: 2026-2034.
15. Kataoka J, Kuriyama A, Norisue Y, *et al*. Proportional modes versus pressure support ventilation: a systematic review and meta-analysis. Ann Intensive Care 2018; 8: 123.
16. Costa R, Spinazzola G, Cipriani F, *et al*. A physiologic comparison of proportional assist ventilation with load-adjustable gain factors (PAV+) versus pressure support ventilation (PSV). Intensive Care Med 2011; 37: 1494-1500.
17. Bosma K, Ferreyra G, Ambrogio C, *et al*. Patient-ventilator interaction and sleep in mechanically ventilated patients: pressure support versus proportional assist ventilation. Crit Care Med 2007; 35: 1048-1054.
18. Nathan SD, Ishaaya AM, Koerner SK, *et al*. Prediction of minimal pressure support during weaning from mechanical ventilation. Chest 1993; 103: 1215-1219.
19. Thille AW, Rodriguez P, Cabello B, *et al*. Patient-ventilator asynchrony during assisted mechanical ventilation. Intensive Care Med 2006; 32: 1515-1522.
20. Bosma KJ, Read BA, Bahrgard Nikoo MJ, *et al*. A pilot randomized trial comparing weaning from mechanical ventilation on pressure support versus proportional assist ventilation. Crit Care Med 2016; 44: 1098-1108.
21. Blanch L, Villagra A, Sales B, *et al*. Asynchronies during mechanical ventilation are associated with mortality. Intensive Care Med 2015; 41: 633-641.
22. de Wit M, Miller KB, Green DA, *et al*. Ineffective triggering predicts increased duration of mechanical ventilation. Crit Care Med 2009; 37: 2740-2745.
23. Thille AW, Cabello B, Galia F, *et al*. Reduction of patient-ventilator asynchrony by reducing tidal volume during

pressure-support ventilation. Intensive Care Med 2008; 34: 1477-1486.
24. Giannouli E, Webster K, Roberts D, *et al*. Response of ventilator-dependent patients to different levels of pressure support and proportional assist. Am J Respir Crit Care Med 1999; 159: 1716-1725.
25. Mellott KG, Grap MJ, Munro CL, *et al*. Patient ventilator asynchrony in critically ill adults: frequency and types. Heart Lung 2014; 43: 231-243.
26. 歐芷瑩、陳昌文、張漢煜，使用呼吸器病患與呼吸器不同步的介紹及改善方式。內科學誌 2009; 20: 497-505。
27. Xirouchaki N, Kondili E, Klimathianaki M, *et al*. Is proportional-assist ventilation with load-adjustable gain factors a user-friendly mode? Intensive Care Med 2009; 35: 1599-1603.
28. Su PL, Kao PS, Lin WC, *et al*. Limited predictability of maximal muscular pressure using the difference between peak airway pressure and positive end-expiratory pressure during proportional assist ventilation (PAV). Crit Care 2016; 20: 382.
29. Berger KI, Sorkin IB, Norman RG, *et al*. Mechanism of relief of tachypnea during pressure support ventilation. Chest 1996; 109: 1320-1327.
30. Banner MJ, Kirby RR, Kirton OC, *et al*. Breathing frequency and pattern are poor predictors of work of breathing in patients receiving pressure support ventilation. Chest 1995; 108: 1338-1344.
31. Bellani G, Pesenti A. Assessing effort and work of breathing. Curr Opin Crit Care 2014; 20: 352-358.
32. Moerer O. Effort-adapted modes of assisted breathing. Curr Opin Crit Care 2012; 18: 61-69.

Disseminated Intravascular Coagulation in Sepsis is Associated with Specific Infection and Organ Dysfunction

Yao-Wen Kuo[1], Kuei-Pin Chung[2], Hou-Tai Chang[3-5], Chong-Jen Yu[6-8]

Introduction: The failure of randomized controlled trials to demonstrate the efficacy of treatments targeting disseminated intravascular coagulation (DIC) in sepsis may imply that DIC develops under specific clinical contexts in patients with sepsis. However, the clinical features associated with DIC development in sepsis are not well understood yet.

Methods: We conducted a prospective study and enrolled 126 patients with sepsis admitted to medical intensive care units (ICUs) in 2 medical centers. DIC was determined based on the Japanese Association for Acute Medicine (JAAM) or the International Society on Thrombosis and Haemostasis (ISTH) scoring systems.

Results: Using the JAAM score, we identified 39 patients (31%) with DIC at ICU admission. Multivariate analysis indicated that clinical features significantly associated with increased risk of JAAM DIC included hypotension (odds ratio [OR] 8.037, 95% confidence interval [CI] 1.496–43.175, $P = 0.015$) and infections other than pneumonia, particularly intra-abdominal infections (OR 8.952, 95% CI 1.765–43.395, $P = 0.008$). Meanwhile, 10 patients (7.9%) were diagnosed with overt DIC according to the ISTH score, and multivariate analysis indicated that congestive heart failure (OR 9.192, 95% CI 1.665–50.761, $P = 0.011$) and hyperbilirubinemia (OR 6.525, 95% CI 1.311–32.481, $P = 0.022$) were significantly associated with increased risk of overt DIC.

Conclusion: Our results suggest that, rather than being a common phenomenon in sepsis, DIC may be a unique complication under certain clinical conditions. The exact mechanisms that explain the association between these clinical features and DIC are unknown, and warrant further investigation. ***(Thorac Med 2021; 36: 95-105)***

Key words: critical illness, coagulation, sepsis, septic shock, outcome

[1]Department of Integrated Diagnostics & Therapeutics, National Taiwan University Hospital, Taipei, Taiwan
[2]Department of Laboratory Medicine, National Taiwan University Hospital and National Taiwan University Cancer Center, Taipei, Taiwan
[3]Department of Critical Care Medicine, Far Eastern Memorial Hospital, New Taipei, Taiwan
[4]Department of Industrial Engineering and Management, Yuan Ze University, Taoyuan, Taiwan
[5]Institute of Health Policy and Management, National Taiwan University, Taipei, Taiwan
[6]Department of Internal Medicine, National Taiwan University Hospital, Taipei, Taiwan
[7]Department of Internal Medicine, College of Medicine, National Taiwan University, Taipei, Taiwan
[8]Department of Internal Medicine, National Taiwan University Hospital Biomedical Park Hospital, Zhubei City, Hsinchu County, Taiwan
Address reprint requests to: Dr. Kuei-Pin Chung, Department of Laboratory Medicine, National Taiwan University Hospital and National Taiwan University Cancer Center, No. 7, Chung Shan S. Rd., Zhongzheng Dist., Taipei 100, Taiwan

Introduction

Systemic inflammatory response syndrome can cause an imbalance between coagulation and fibrinolytic pathways through endothelial dysfunction and the systemic release of inflammatory cytokines [1-2]. Abnormal activation of the coagulation system can provoke disseminated intravascular coagulation (DIC), which is characterized by extensive formation of intravascular microthrombi in the microvasculature, leading to compromised microcirculation and tissue perfusion [3-4]. Previous studies have indicated that DIC in critically ill patients is associated with multi-organ dysfunction and poor survival [5-6], and that sepsis is the most common etiology of DIC in critically ill patients [7]. In murine models of sepsis, treatments to correct abnormal coagulation activation have been shown to improve organ dysfunction and host survival [8-9]. However, to date, randomized controlled studies have all failed to demonstrate the efficacy of DIC-targeted treatments in sepsis, including antithrombin III, tissue factor pathway inhibitors, activated protein C and thrombomodulin [10-13].

The failure of these clinical trials raises doubts as to whether DIC is a common pathophysiological phenomenon in all patients with sepsis, since 40% to 75% of patients with sepsis will not develop overt DIC [14-17]. Dhainaut *et al*. reported that overt DIC in sepsis was associated with non-Caucasian ethnicity and surgical intensive care unit (ICU) admission, but not acute respiratory distress syndrome [14]. The findings thus implicated that sepsis-related DIC may develop under particular clinical contexts. However, the clinical features associated with DIC development in sepsis are not yet clear. Therefore, we conducted this prospective study to explore the clinical characteristics, including comorbidities, infection diagnoses, and dysfunction of specific organ systems, significantly associated with DIC in sepsis, and further investigated the prognostic significance of DIC.

Materials and Methods

Settings and study population

This study was carried out at 2 tertiary medical centers in northern Taiwan; the patient enrollment process was described in our previous study [18]. The Institutional Review Board of each institution approved the protocol (200907064R and 098014-3), and the patients were enrolled after informed consent had been obtained. Consecutive adult patients (≥18 years of age) who were admitted to medical ICUs for sepsis or septic shock from August 2010 through January 2012 were screened for eligibility. Sepsis was defined as that associated with acute organ dysfunction, including hypotension (systolic blood pressure < 90 mmHg, mean arterial pressure < 65 mmHg, or reduction in systolic blood pressure > 40 mmHg), respiratory dysfunction (bilateral pulmonary infiltrates with a partial pressure of arterial oxygen to fraction of inspired oxygen ratio [PaO_2/FiO_2 ratio] < 300 mmHg), renal dysfunction (serum creatinine level>2 mg/dL or urine output<0.5 $mL \cdot kg^{-1} \cdot h^{-1}$ for 2 h), hyperbilirubinemia (total serum bilirubin level > 2 mg/dL), thrombocytopenia (platelet count < $100 \times 10^3/\mu L$), coagulation abnormalities (activated partial thromboplastin time [aPTT] > 60 s or international normalized ratio > 1.5), and hypoperfusion (serum lactate level > 2 mmol/L) [19-20]. Septic shock was defined as sepsis with systolic blood pressure < 90 mmHg, mean arterial pressure < 65 mmHg, or reduction in systolic blood pressure > 40 mmHg

despite an adequate volume resuscitation or use of vasopressors. The exclusion criteria were pregnancy, Child-Pugh C cirrhosis, presence of acute cerebral vascular events, primary diagnosis of arrhythmia or acute cardiogenic lung edema, massive gastrointestinal bleeding, status epilepticus, need for immediate surgery, hematologic malignancies, febrile neutropenia, treatment with immunosuppressive agents before admission, advanced malignancy with poor preadmission performance status and inevitable short-term mortality, human immunodeficiency virus infection, and refusal to consent to participate in the study. Patients who had abnormal coagulation or had received anticoagulants before admission were also excluded.

The patients' clinical parameters, including demographic data, baseline comorbidities, and infection diagnoses, were obtained. Disease severity was evaluated according to the Acute Physiology and Chronic Health Evaluation (APACHE II) score. Sequential Organ Failure Assessment (SOFA) scores were calculated at admission to evaluate the severity of global organ dysfunction.

Diagnosis of DIC

We measured prothrombin time (PT), aPTT, d-dimer, fibrin degradation products (FDP), and fibrinogen at ICU admission. Platelet count was determined at admission and again 24 h after admission. The definition of DIC was based on the scoring systems developed by the International Society on Thrombosis and Haemostasis (ISTH) or the Japanese Association for Acute Medicine (JAAM) [21,22]. The occurrence of DIC was thus determined according to both JAAM DIC and ISTH overt DIC scores, as described in previous reports [21,23]. Patients with a JAAM DIC score ≥ 4 or ISTH overt DIC score ≥ 5 were considered to have JAAM DIC or ISTH overt DIC, respectively.

Statistical analysis

Data are reported as mean ± standard deviation (SD), median [minimum–maximum], or number (proportion). Comparisons of proportions were performed using Pearson's χ^2 test or Fisher's exact test, while continuous variables were compared with Student's *t*-test or the Mann-Whitney U test, as appropriate. Multivariate logistic regression analysis was used to investigate specific organ dysfunction, infection diagnoses or other clinical parameters independently associated with JAAM DIC or ISTH overt DIC. Statistically significant variables ($P < 0.05$) in univariate analysis were included in multivariate logistic regression analysis with backward variable selection. The criteria of *P* values for entry into and remaining in the regression models were set at 0.05 and 0.2, respectively. Kaplan–Meier curves for 28-day survival were plotted, and survival differences were compared using a log-rank test. Two-sided P values < 0.05 were considered to be statistically significant. All analyses were performed using SPSS (version 17.0 for Windows; IBM Corporation, Armonk, NY, USA) or GraphPad Prism (version 5.0; GraphPad Software, La Jolla, CA, USA).

Results

Diagnosis of DIC

From August 2010 through January 2012, 126 consecutive patients admitted to medical ICUs for sepsis or septic shock were enrolled as the study population. The clinical features of these 126 patients are described in Table 1. None of the study population received drotreco-

Table 1. Clinical Characteristics of the Study Population

Parameters	Entire group	28-day survival		
		Survived	Died	*P*+
Number	126	94	32	
Age	70.5 ± 15.5	70.1 ± 16.0	71.8 ± 14.3	0.609
Sex		0.733		0.733
Male	78 (61.9)	59 (62.8)	19 (59.4)	
Female	48 (38.1)	35 (37.2)	13 (40.6)	
Comorbidities				
Congestive heart failure	10 (7.9)	6 (6.4)	4 (12.5)	0.273
Coronary artery disease	24 (19.0)	17 (18.1)	7 (21.9)	0.637
Diabetes mellitus	48 (38.1)	31 (33.0)	17 (53.1)	0.043
Neurologic disease	35 (27.8)	25 (26.6)	10 (31.3)	0.612
Chronic kidney disease	26 (20.6)	17 (18.1)	9 (28.1)	0.225
Infection diagnosis				
Pneumonia	74 (58.7)	58 (61.7)	16 (50.0)	0.245
Urosepsis	26 (20.6)	20 (21.3)	6 (18.8)	0.760
Blood stream infection	9 (7.1)	5 (5.3)	4 (12.5)	0.230
Intra-abdominal infection	11 (8.7)	6 (6.4)	5 (15.6)	0.145
Others*	6 (4.8)	5 (5.3)	1 (3.1)	1.000
Blood culture positivity	29 (23.0)	20 (21.3)	9 (28.1)	0.427
APACHE II	25.3 ± 7.7	24.0 ± 6.8	29.2 ± 8.8	0.001
SOFA score	9.9 ± 3.6	9.3 ± 3.5	11.6 ± 3.6	0.002

Data are presented as mean ± SD or number (percentage); APACHE II, Acute Physiology and Chronic Health Evaluation II; SOFA, Sequential Organ Failure Assessment

*including central nervous system infection (n=2), infective endocarditis (n=1), necrotizing fasciitis (n=1), osteomyelitis (n=1), and psoas muscle abscess (n=1).

+comparison of patients who survived and those who died within 28 days after admission

gin alfa (Xigris®, Eli Lilly, Indianapolis, IN) or anticoagulants for DIC treatment. JAAM DIC was found in 39 (31.0%) patients, and ISTH overt DIC was found in 10 (7.9%). All of the patients with ISTH overt DIC met the criteria for JAAM DIC. The patients with JAAM DIC or ISTH overt DIC had a significantly decreased platelet count, lengthened PT and aPTT, and increased levels of d-dimer and FDP compared to those without DIC. Fibrinogen levels were not significantly decreased in patients with either JAAM DIC or ISTH overt DIC.

The 28-day mortality rate of the study population was 25.4% (32 of 126 patients). Compared to the survivors, non-survivors had significantly higher median ISTH overt DIC scores (Figure 1A). There was no significant difference in the 28-day survival rate between patients with and without JAAM DIC (71.8% vs. 75.9%, P=0.552) (Figure 1B). Compared to patients without DIC, those with ISTH overt DIC had significantly decreased 28-day survival (76.7% vs. 50.0%, P=0.026) (Figure 1C).

Clinical characteristics of patients with sepsis-related JAAM DIC

Our data revealed that JAAM DIC was

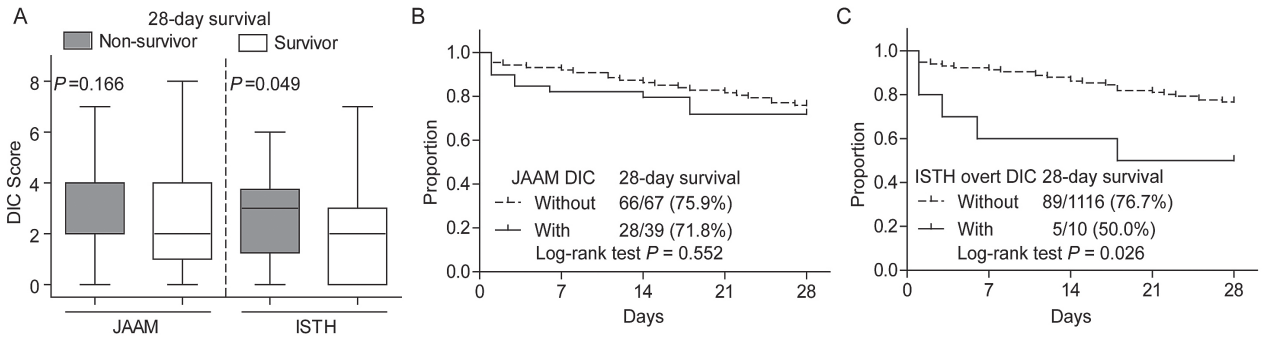

Fig. 1. Disseminated intravascular coagulation (DIC) and 28-day survival in patients with sepsis. (A) Compared to the survivors, the non-survivors had significantly higher International Society on Thrombosis and Haemostasis (ISTH) DIC scores (P=0.049, Mann-Whitney U test). However, the Japanese Association for Acute Medicine (JAAM) DIC scores were not significantly different between the survivors and non-survivors (P=0.166, Student's t-test). In the box plots, boxes represent the 25th to 75th percentiles, whiskers represent the lowest and highest values of the respective quartile, and dots represent outliers. (B) Patients with JAAM DIC did not have worse 28-day survival than those without JAAM DIC. (C) In contrast, patients with ISTH overt DIC had worse 28-day survival than those without ISTH overt DIC (50.0% vs. 76.7%, P=0.026, log-rank test)

significantly associated with intra-abdominal infections and other miscellaneous infections, mainly of soft tissue and neurological origin (Table 2). We further evaluated the association between JAAM DIC and acute dysfunction of organ systems other than the coagulation system, and found that hypotension, hyperbilirubinemia, and hypoperfusion were significantly associated with JAAM DIC. In addition, patients with JAAM DIC had significantly increased serum levels of creatinine and lactate (Figure 2) and increased SOFA scores, compared to those without DIC (Table 2).

Clinical characteristics of patients with sepsis-related ISTH overt DIC

Similar to the patients with JAAM DIC, those with ISTH overt DIC were significantly associated with intra-abdominal infections (Table 3). However, hyperbilirubinemia was the only organ dysfunction significantly associated with ISTH overt DIC. Of the laboratory indices of specific organ dysfunction, ISTH overt DIC was significantly associated with increased serum levels of total bilirubin and lactate (Figure 2) and increased SOFA scores (Table 3).

Sepsis-related DIC was associated with specific clinical characteristics

Multivariate logistic regression analysis was used to investigate specific clinical characteristics, including comorbidities, types of infection, and organ dysfunction, independently associated with increased risk of JAAM DIC or ISTH overt DIC (Table 4). The results revealed that hypotension (odds ratio [OR] 8.037, 95% confidence interval [CI] 1.496–43.175, P=0.015) and specific infection sources, particularly intra-abdominal infections (OR 8.952, 95% CI 1.765–45.395, P=0.008) and miscellaneous infections (OR 28.283, 95% CI 1.990–401.950, P=0.014), were significantly associated with increased risk of JAAM DIC, and that congestive heart failure (CHF) (OR 9.192, 95% CI 1.665–50.761, P=0.011) and hyperbilirubinemia (OR 6.525, 95% CI 1.311–32.481, P=0.022) were significantly associated with increased risk of overt DIC.

Table 2. Clinical Features of Patients with or Without Sepsis-Related JAAM DIC

Parameters	JAAM DIC				*P**
	Without		With		
Number	87		39		
Age	70.1 ± 16.6		71.6 ± 12.9		0.619
Sex					
Male	54	(62.1)	24	(61.5)	0.955
Female	33	(37.9)	15	(38.5)	
Comorbidities					
Congestive heart failure	4	(4.6)	6	(15.4)	0.068
Coronary artery disease	15	(17.2)	9	(23.1)	0.441
Diabetes mellitus	31	(35.6)	17	(43.6)	0.395
Neurologic disease	28	(32.2)	7	(17.9)	0.099
Chronic kidney disease	18	(20.7)	8	(20.5)	0.982
Infection diagnosis					
Pneumonia	60	(69.0)	14	(35.9)	<0.001
Urosepsis	16	(18.4)	10	(25.6)	0.353
Blood stream infection	7	(8.0)	2	(5.1)	0.720
Intra-abdominal infection	3	(3.4)	8	(20.5)	0.004
Others	1	(1.1)	5	(12.8)	0.011
Blood culture positivity	16	(18.4)	13	(33.3)	0.065
APACHE II	24.4 ± 6.7		27.5 ± 9.3		0.065
Acute organ dysfunction at admission					
Hypotension	63	(72.4)	37	(94.9)	0.004
Respiratory	16	(18.4)	6	(15.4)	0.681
Renal	33	(37.9)	22	(56.4)	0.053
Hyperbilirubinemia	5	(5.7)	9	(23.1)	0.011
Hypoperfusion	53	(60.9)	33	(84.6)	0.008
SOFA score at admission					
Total score	8.7 ± 3.2		12.5 ± 3.1		<0.001
Without hematologic score	8.4 ± 3.0		11.2 ± 2.8		<0.001

Data are presented as mean ± SD or number (percentage); JAAM DIC, Japanese Association for Acute Medicine disseminated intravascular coagulation; APACHE II, Acute Physiology and Chronic Health Evaluation II; SOFA, Sequential Organ Failure Assessment;
*Compared between patients with and without JAAM DIC: continuous variables using Student's t-test, and proportions using Pearson's χ^2 test or Fisher's exact test, as appropriate.

Discussion

This study found that specific infections and organ dysfunction in patients with sepsis were associated with DIC development. Intra-abdominal infections were significantly associated with increased risk of both JAAM and ISTH DIC. However, the association between DIC and acute organ dysfunction depended on the DIC scoring system.

Our data revealed that CHF is the only pre-admission comorbidity associated with DIC development. The exact mechanism that accounts for the association between CHF and

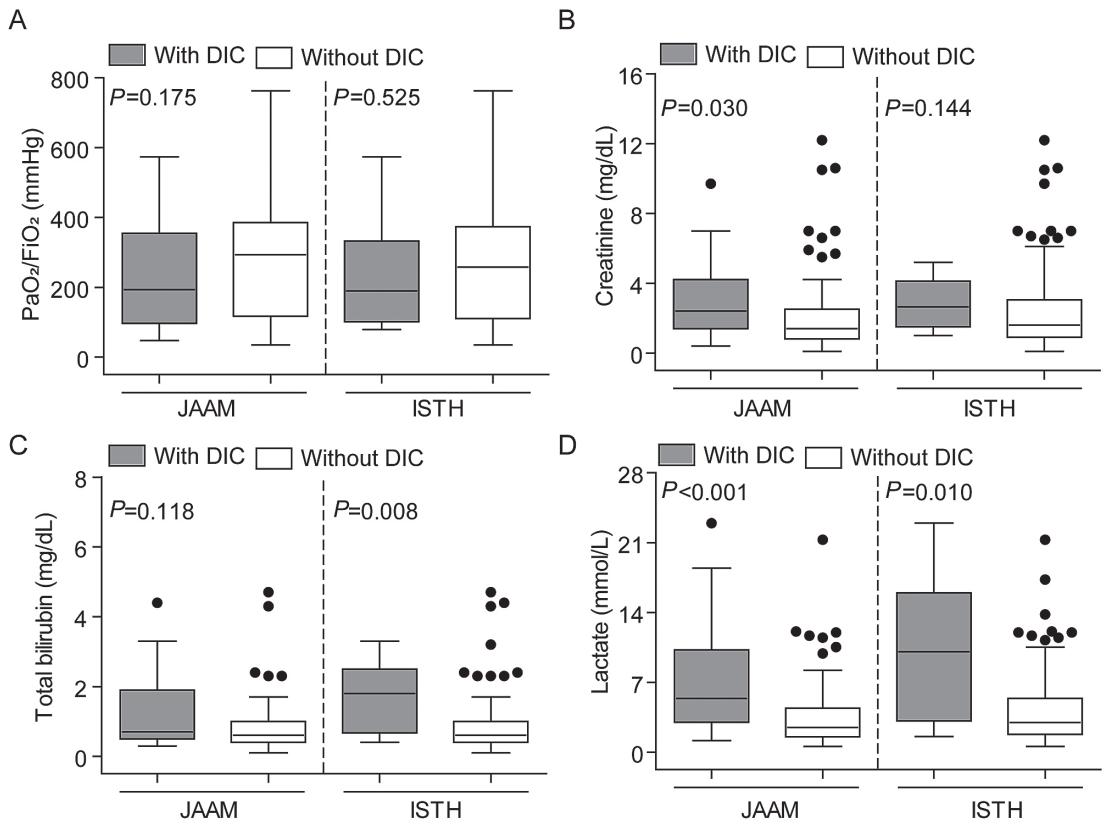

Fig. 2. Association between laboratory indices of organ dysfunction and disseminated intravascular coagulation (DIC). Patients with Japanese Association for Acute Medicine (JAAM) DIC, compared to those without DIC, had significantly increased levels of serum creatinine (P=0.030) and lactate (P<0.001). In addition, patients with International Society on Thrombosis and Haemostasis (ISTH) overt DIC were significantly associated with increased levels of serum total bilirubin (P=0.008) and lactate (P=0.010). Neither JAAM DIC nor ISTH overt DIC was significantly associated with decreased PaO_2/FiO_2 ratios. Patients with JAAM DIC vs. those without JAAM DIC were compared using Student's t-test; patients with ISTH overt DIC vs. those without ISTH overt DIC were compared using the Mann-Whitney U test. In the box plots, boxes represent the 25th to 75th percentiles, whiskers represent the lowest and highest values of the respective quartile, and dots represent outliers.

sepsis-related DIC is unclear. However, endothelial dysfunction in patients with CHF may predispose the patient to and exacerbate endothelial damage in sepsis, leading to DIC development [24-26]. Meanwhile, consistent with a previous study [14], we did not observe an association between DIC and respiratory dysfunction in our patients with sepsis. Sepsis-related DIC may be the consequence of systemic inflammation [3].

The development of multi-organ dysfunction in sepsis is caused by various mechanisms, such as hyperactive inflammation and mitochondrial injury [27]. The dominant pathophysiologic mechanism for the dysfunction of each organ system may be different, and the causal link between DIC and multi-organ dysfunction has yet to be elucidated [28]. It is not clear whether coagulation dysfunction and the development of DIC contribute to multi-organ failure in sepsis. In the current study, we found that patients with DIC tended to have intra-abdominal infections. In a post-hoc analysis of the Protein C Worldwide Evaluation in Severe Sepsis

Table 3. Clinical Features of Patients With or Without Sepsis-Induced ISTH overt DIC

	ISTH overt DIC				*P**
	Without		With		
Number	116		10		
Age	76	[29–95]	68	[58–87]	0.632
Sex					0.741
Male	71	(61.2)	7	(70.0)	
Female	45	(38.8)	3	(30.0)	
Comorbidities					
Congestive heart failure	7	(6.0)	3	(30.0)	0.032
Coronary artery disease	21	(18.1)	3	(30.0)	0.401
Diabetes mellitus	45	(38.8)	3	(30.0)	0.741
Neurologic disease	34	(29.3)	1	(10.0)	0.281
Chronic kidney disease	25	(21.6)	1	(10.0)	0.686
Infection diagnosis					
Pneumonia	69	(59.5)	5	(50.0)	0.740
Urosepsis	24	(20.7)	2	(20.0)	1.000
Blood stream infection	9	(7.8)	0	(0.0)	1.000
Intra-abdominal infection	8	(6.9)	3	(30.0)	0.043
Others	6	(5.2)	0	(0.0)	1.000
Blood culture positivity	25	(21.6)	4	(40.0)	0.237
APACHE II	25	[6–50]	27	[14–47]	0.597
Acute organ dysfunction defined for enrollment					
Hypotension	90	(77.6)	10	(100.0)	0.121
Respiratory	21	(18.1)	1	(10.0)	1.000
Renal	50	(43.1)	5	(50.0)	0.746
Hyperbilirubinemia	10	(8.6)	4	(40.0)	0.014
Hypoperfusion	77	(66.4)	9	(90.0)	0.168
SOFA score					
Total score	9.5	[2–20]	14.0	[8–16]	0.002
Without hematologic score	9.0	[2–18]	11.5	[6–15]	0.043

Data are presented as median [minimum–maximum] and number (percentage); ISTH overt DIC, International Society on Thrombosis and Haemostasis overt DIC; JAAM DIC, Japanese Association for Acute Medicine disseminated intravascular coagulation; APACHE II, Acute Physiology and Chronic Health Evaluation II; SOFA, Sequential Organ Failure Assessment

*Compared between patients with and without JAAM DIC: continuous variables using the Mann-Whitney U test, and proportions using Pearson's χ^2 test or Fisher's exact test, as appropriate.

(PROWESS) trial [29], surgical patients were found to be at a significantly increased risk of overt DIC [14]. Furthermore, in the PROWESS cohort, more surgical patients had infections other than pneumonia, especially intra-abdominal, soft tissue, and neurological infections [30]. Our findings thus are consistent with the findings of the PROWESS cohort. However, regarding the association between DIC and specific organ dysfunction and infection sources, the exact pathophysiological mechanisms are unknown, and further investigations are war-

Table 4. Multivariate Logistic Regression Models: Specific Organ Dysfunction and Infection Sources Associated with JAAM DIC or ISTH Overt DIC

Covariate	Estimate	SE	Odds ratio (95% CI)	*P*
JAAM DIC				
Infection diagnosis				
Intra-abdominal infection	2.192	0.828	8.952 (1.765-45.395)	0.008
Others	3.342	1.354	28.283 (1.990-401.950)	0.014
Organ dysfunction				
Hypotension	2.084	0.858	8.037 (1.496-43.175)	0.015
Hypoperfusion	1.030	0.552	2.800 (0.949-8.261)	0.062
ISTH overt DIC				
Comorbidity before admission				
Congestive heart failure	2.218	0.872	9.192 (1.665-50.761)	0.011
Infection diagnosis				
Intra-abdominal infection	1.370	0.880	3.936 (0.702-22.075)	0.119
Organ dysfunction				
Hyperbilirubinemia	1.876	0.819	6.525 (1.311-32.481)	0.022

JAAM DIC, Japanese Association for Acute Medicine disseminated intravascular coagulation; ISTH overt DIC, International Society on Thrombosis and Haemostasis overt DIC; SE, standard error; 95% CI, 95% confidence interval.

ranted to clarify this issue.

Several previous studies have reported inconsistent results regarding the association between the development of JAAM DIC and survival of patients with sepsis [7,21,23]. We found that JAAM DIC was not associated with decreased survival in patients with sepsis or septic shock. JAAM DIC may represent the early stage of DIC development, and the progression of DIC may be halted after initial treatment. In addition, only 7.9% of our patients had ISTH overt DIC, which is far lower than that reported in previous studies (ranging from 29% to 30%) [14,16]. Both advanced cancer and Child-Pugh C cirrhosis can predispose septic patients to the development of DIC [3,16]; however, patients with these co-morbidities were excluded from our study. Therefore, the occurrence of ISTH overt DIC in sepsis may be overestimated in previous studies. In addition, a recent study indicated that the incidence of ISTH overt DIC in critically ill patients has decreased over the last decade [31]. Taken together, the differences in the incidence of sepsis-related ISTH overt DIC between our and previous studies may be explained by differences in the characteristics of the study populations and changing epidemiology.

Some limitations of this study should be addressed. First, we did not record DIC scores after admission. However, Gando et al. reported that 87.5% of their JAAM DIC cases were diagnosed at the time of ICU admission [21], suggesting that most patients with sepsis with JAAM DIC would be identified at this time. In contrast, only 64.1% of the ISTH overt DIC cases in Gando et al.'s study were diagnosed at the time of ICU admission [21]. Thus, the actual occurrence of ISTH overt DIC in patients with severe sepsis may have been underestimated in the present study. Therefore, our results concerning ISTH overt DIC should be interpreted

with caution. Second, although we found an independent association between ISTH overt DIC and hepatic dysfunction in patients with severe sepsis, a previous study found that the development of ISTH overt DIC was also associated with renal and cardiovascular dysfunction, using a different definition of organ dysfunction [14]. Therefore, additional studies are needed to verify the independent association between hepatic dysfunction and ISTH overt DIC. Third, DIC is a pathophysiological process leading to both increased bleeding and a thrombotic tendency, and may lead to increased bleeding or thrombotic events in sepsis. Whether sepsis-related DIC will remarkably increase the risk of bleeding or thromboembolic events is unknown from our study, and should be further investigated in the future.

In conclusion, our findings indicate that DIC may be a unique feature in sepsis. Patients with sepsis tended to have DIC when they had specific infections, particularly intra-abdominal infections, or specific organ dysfunction, such as hypotension or hepatic dysfunction. Our results suggest that DIC may play a crucial role in the development of specific, but not all organ dysfunction, or that DIC may be just a reflection of disease severity. The exact clinical importance of DIC in sepsis needs to be re-defined, and the mechanisms and causality underlying our results require future investigation.

Conflicts of Interest

None of the authors have any conflicts of interest to declare.

Acknowledgments

Special thanks to Nai-Hua Cheng, Shu-Chuan Huang, Li-Min Lin, Shu-Ju Lu, Chen-Wei Lin, Shu-Hui Yang, Shu-Cheng Shen, Su-Chen Lin, Pao-Ling Chang, and Wei-Ru Chen for their help in patient recruitment and data collection.

References

1. Zeerleder S, Hack CE, Wuillemin WA. Disseminated intravascular coagulation in sepsis. Chest 2005; 128: 2864-75.
2. Aird WC. The role of the endothelium in severe sepsis and multiple organ dysfunction syndrome. Blood 2003; 101: 3765-77.
3. Levi M, Ten Cate H. Disseminated intravascular coagulation. N Engl J Med 1999; 341: 586-92.
4. Hartemink KJ, Hack CE, Groeneveld AB. Relation between coagulation/fibrinolysis and lactate in the course of human septic shock. J Clin Pathol 2010; 63: 1021-6.
5. Gando S, Kameue T, Nanzaki S, *et al*. Disseminated intravascular coagulation is a frequent complication of systemic inflammatory response syndrome. Thromb Haemost 1996; 75: 224-8.
6. Toh CH, Downey C. Performance and prognostic importance of a new clinical and laboratory scoring system for identifying non-overt disseminated intravascular coagulation. Blood Coagul Fibrinolysis 2005; 16: 69-74.
7. Kushimoto S, Gando S, Saitoh D, *et al*. Clinical course and outcome of disseminated intravascular coagulation diagnosed by Japanese Association for Acute Medicine criteria. Comparison between sepsis and trauma. Thromb Haemost 2008; 100: 1099-105.
8. Yeh YC, Wang MJ, Lin CP, *et al*. Enoxaparin sodium prevents intestinal microcirculatory dysfunction in endotoxemic rats. Crit Care 2012; 16: R59.
9. Slofstra SH, van 't Veer C, Buurman WA, *et al*. Low molecular weight heparin attenuates multiple organ failure in a murine model of disseminated intravascular coagulation. Crit Care Med 2005; 33: 1365-70.
10. Ranieri VM, Thompson BT, Barie PS, *et al*. Drotrecogin alfa (activated) in adults with septic shock. N Engl J Med 2012; 366:2055-64.
11. Warren BL, Eid A, Singer P, *et al*. Caring for the critically

ill patient. High-dose antithrombin III in severe sepsis: a randomized controlled trial. JAMA 2001; 286: 1869-78.

12. Abraham E, Reinhart K, Opal S, *et al*. Efficacy and safety of tifacogin (recombinant tissue factor pathway inhibitor) in severe sepsis: a randomized controlled trial. JAMA 2003; 290: 238-47.
13. Vincent JL, Francois B, Zabolotskikh I, *et al*. Effect of a recombinant human soluble thrombomodulin on mortality in patients with sepsis-associated coagulopathy: the SCARLET randomized clinical trial. JAMA 2019; 321: 1993-2002.
14. Dhainaut JF, Yan SB, Joyce DE, *et al*. Treatment effects of drotrecogin alfa (activated) in patients with severe sepsis with or without overt disseminated intravascular coagulation. J Thromb Haemost 2004; 2: 1924-33.
15. Dempfle CE, Wurst M, Smolinski M, *et al*. Use of soluble fibrin antigen instead of D-dimer as fibrin-related marker may enhance the prognostic power of the ISTH overt DIC score. Thromb Haemost 2004; 91: 812-8.
16. Voves C, Wuillemin WA, Zeerleder S. International Society on Thrombosis and Haemostasis score for overt disseminated intravascular coagulation predicts organ dysfunction and fatality in sepsis patients. Blood Coagul Fibrinolysis 2006; 17: 445-51.
17. Singh RK, Baronia AK, Sahoo JN, *et al*. Prospective comparison of new Japanese Association for Acute Medicine (JAAM) DIC and International Society of Thrombosis and Hemostasis (ISTH) DIC score in critically ill septic patients. Thromb Res 2012; 129: e119-25.
18. Chung KP, Chang HT, Huang YT, *et al*. Central venous oxygen saturation under non-protocolized resuscitation is not related to survival in severe sepsis or septic shock. Shock 2012; 38: 584-91.
19. Levy MM, Dellinger RP, Townsend SR, *et al*. The Surviving Sepsis Campaign: results of an international guideline-based performance improvement program targeting severe sepsis. Crit Care Med 2010; 38: 367-74.
20. Ferrer R, Artigas A, Suarez D, *et al*. Effectiveness of treatments for severe sepsis: a prospective, multicenter, observational study. Am J Respir Crit Care Med 2009; 180: 861-6.
21. Gando S, Iba T, Eguchi Y, *et al*. A multicenter, prospective validation of disseminated intravascular coagulation diagnostic criteria for critically ill patients: comparing current criteria. Crit Care Med 2006; 34: 625-31.
22. Taylor FB, Jr., Toh CH, Hoots WK, *et al*. Towards definition, clinical and laboratory criteria, and a scoring system for disseminated intravascular coagulation. Thromb Haemost 2001; 86: 1327-30.
23. Gando S, Saitoh D, Ogura H, *et al*. Natural history of disseminated intravascular coagulation diagnosed based on the newly established diagnostic criteria for critically ill patients: results of a multicenter, prospective survey. Crit Care Med 2008; 36: 145-50.
24. Varin R, Mulder P, Tamion F, *et al*. Improvement of endothelial function by chronic angiotensin-converting enzyme inhibition in heart failure: role of nitric oxide, prostanoids, oxidant stress, and bradykinin. Circulation 2000; 102: 351-6.
25. Chin BS, Conway DS, Chung NA, *et al*. Interleukin-6, tissue factor and von Willebrand factor in acute decompensated heart failure: relationship to treatment and prognosis. Blood Coagul Fibrinolysis 2003; 14: 515-21.
26. Iba T, Levy JH, Raj A, et al. Advance in the management of sepsis-induced coagulopathy and disseminated intravascular coagulation. J Clin Med 2019; 8.
27. Brealey D, Brand M, Hargreaves I, *et al*. Association between mitochondrial dysfunction and severity and outcome of septic shock. Lancet 2002; 360: 219-23.
28. Vincent JL, De Backer D. Does disseminated intravascular coagulation lead to multiple organ failure? Crit Care Clin 2005; 21: 469-77.
29. Bernard GR, Vincent JL, Laterre PF, *et al*. Efficacy and safety of recombinant human activated protein C for severe sepsis. N Engl J Med 2001; 344:699-709.
30. Barie PS, Williams MD, McCollam JS, *et al*. Benefit/risk profile of drotrecogin alfa (activated) in surgical patients with severe sepsis. Am J Surg 2004; 188: 212-20.
31. Singh B, Hanson AC, Alhurani R, *et al*. Trends in the incidence and outcomes of disseminated intravascular coagulation in critically ill patients (2004-2010) - A population based study. Chest 2012; 143: 1235-1242.

Meta-Analysis of Relationship Between EGFR Mutations, Risk of Brain Metastasis and Survival in NSCLC Patients

Ching-Han Lai[1,6], Sheng-Yuan Wang[1,6], Szu-Chun Yang[1], Yi-Lin Wu[2]
Fu-Chang Hu[3,4], Po-Lan Su[1], Jeng-Shiuan Tsai[1,5], Chien-Chung Lin[1,5]

Introduction: To investigate whether epidermal growth factor receptor (EGFR) mutations are associated with the risk of developing brain metastasis (BM) or with overall survival after BM in non-small cell lung cancer (NSCLC) patients.

Methods: We systematically performed meta-analyses and meta-regression to examine the associations. Seventeen studies involving 8,010 NSCLC patients were included for analysis.

Results: Meta-analysis of 12 studies (5,962 patients) yielded a pooled odds ratio of 1.70 (95% confidence interval (CI): 1.47–1.96, $p < 0.001$), and meta-regression indicated that patients with EGFR mutations had a higher risk of BM at initial diagnosis. Meta-analysis of 11 studies (3,170 patients) yielded a pooled odds ratio of 2.20 (95% CI: 1.76–2.75, $p < 0.001$), and meta-regression indicated that patients with EGFR mutations also had a higher risk of subsequent BM. Finally, meta-analysis of 5 studies yielded a pooled hazard ratio of 0.29 (95% CI: 0.22–0.39, $p < 0.001$), indicating EGFR mutations are associated with longer overall survival in NSCLC patients with BM.

Conclusion: Although EGFR mutations increased the risk of BM in NSCLC patients, they also predicted longer overall survival in those with BM. ***(Thorac Med 2021; 36: 106-122)***

Key words: EGFR mutation, brain metastasis, overall survival, NSCLC, meta-analysis, meta-regression

[1]Department of Internal Medicine, National Cheng Kung University Hospital, College of Medicine, National Cheng Kung University, Tainan, Taiwan
[2]Department of Nursing, National Cheng Kung University Hospital, College of Medicine, National Cheng Kung University, Tainan, Taiwan
[3]Graduate Institute of Clinical Medicine and School of Nursing, College of Medicine, National Taiwan University, Taipei, Taiwan
[4]International-Harvard Statistical Consulting Company, Taipei, Taiwan
[5]Institute of Clinical Medicine, National Cheng Kung University Hospital, College of Medicine, National Cheng Kung University, Tainan, Taiwan
[6]These authors contributed equally to this work. Acronyms: BM, brain metastasis; CT, computed tomography; EGFR, epidermal growth factor receptor; GAM, generalized additive model; GOF, goodness of fit; MRI, magnetic resonance image; NA, not applicable; NSCLC, non-small cell lung cancer; OS, overall survival; TKI, tyrosine kinase inhib
Address reprint requests to: Dr. Jeng-Shiuan Tsai, Department of Internal Medicine, National Cheng Kung University Hospital, College of Medicine, National Cheng Kung University, No.138 Sheng-Li Road, Tainan 704, Taiwan

Introduction

Brain metastases (BM) occur in 22%−54% of non-small cell lung cancer (NSCLC) patients and progress at various speeds. Although advances in systemic therapies have improved survival outcomes in patients with advanced NSCLC, BM is still an important cause of morbidity and mortality in NSCLC patients. Previous studies have attempted to identify the predictive factors of BM in NSCLC patients, including carcinoembryonic antigen levels [1], tumor size, lymph node involvement, and extracranial involvement [2]. BM is more common in patients with adenocarcinoma and undifferentiated NSCLC than in those with squamous cell lung cancer [3]. However, the predictive values of some recently identified molecular biomarkers for BM have not yet been verified [4-5].

The epidermal growth factor receptor (*EGFR*), a trans-membrane receptor for tyrosine kinase, is involved in various cellular processes. First-line treatment with tyrosine kinase inhibitors (TKIs) is recommended for patients with certain *EGFR* mutations. In NSCLC patients with *EGFR* mutations, treatment with TKIs results in better response rates (RR) and progression-free survival (PFS) than treatment with chemotherapy [6]. In contrast, NSCLC patients with wild-type *EGFR* do not benefit from TKIs. *EGFR* mutation status is thus crucial to the efficacy of TKIs.

Evaluation of risk factors for BM in NSCLC patients may help improve treatment decisions. For example, the presence of *EGFR* mutations that are associated with BM indicates that brain screening and surveillance are necessary. A recent study demonstrated that whole-brain radiotherapy might be more effective in NSCLC patients with *EGFR* mutations who have developed BM than in those with wild-type *EGFR* [7]. Another study showed that TKIs were more effective than chemotherapy in patients with *EGFR* mutations who developed asymptomatic BM [8]. However, differences in treatment outcomes in NSCLC patients with BM, depending on *EGFR* mutation status, remain [9-10]. In this meta-analysis, we therefore examined the effects of *EGFR* mutations on the risk of BM in NSCLC patients and on overall survival in NSCLC patients with BM.

Methods

Search strategy

This meta-analytic study was conducted according to the Preferred Reporting Items for Systematic Reviews and Meta-Analyses (PRISMA) Statement guidelines [11]. Three authors (CH Lai, SY Wang, and PL Su) independently searched the MEDLINE, PubMed, and Web of Science databases for clinical studies published between January 1, 2003 and July 31, 2017. Search terms included "lung cancer," "non-small cell lung cancer," "NSCLC," "lung adenocarcinoma," "epidermal growth factor receptor," "*EGFR*," "brain metastasis," "brain metastases," and "recurrence;" Boolean logic was used. A flow chart depicting the search strategy is shown in Figure 1. All studies referenced in each of the retrieved articles were also examined to identify any relevant studies missed in the primary search.

Study selection

Three reviewers (YL Wu, CH Lai, and SY Wang) independently scanned the titles and abstracts of all retrieved studies to identify those that were relevant. The inclusion criteria were:

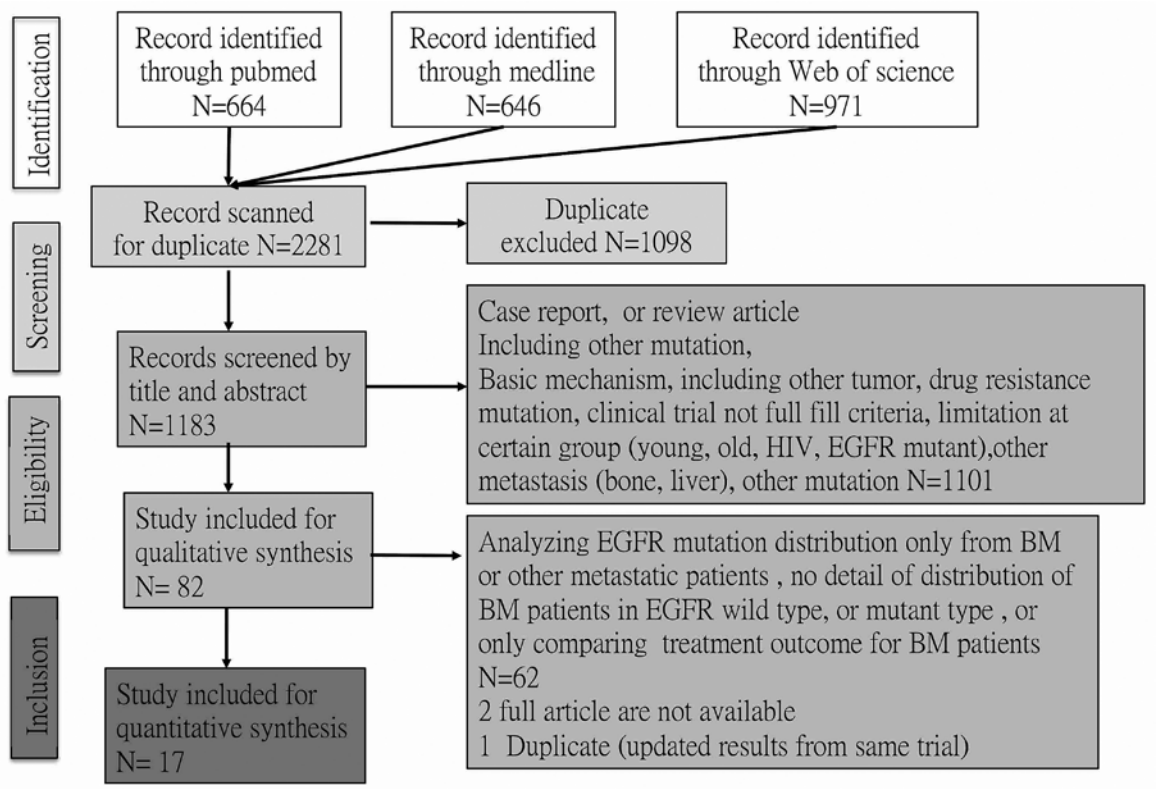

Fig. 1. Flow diagram of the study selection process (PRISMA 2009) [11]

(1) investigations of the association between *EGFR* mutations and lung cancer recurrence, and (2) investigations of the association between *EGFR* mutations and metastasis. After potentially relevant articles had been reviewed in full and additional information was requested from the authors by email, the same reviewers independently assessed the eligibility of all studies; any discrepancies were resolved by consulting with the 2 primary investigators (JS Tsai, CC Lin).

Data extraction

According to a pre-specified study protocol, 3 authors (PL Su, YL Wu and SC Yang) independently extracted the following data: authors, publication year, country, study design, and variation in clinical characteristics associated with *EGFR* mutations, BM, and survival (e.g., age, sex, smoking, and follow-up duration).

Assessing potential confounders

The "Reader's Guide to Critical Appraisal of Cohort Studies" [12] was used to assess potential confounding factors in each cohort study and to determine whether the study provided information on the distribution of potential confounding factors between patient groups. Discrepancies in these assessments were resolved through discussions among the authors or consultations with primary investigators (JS Tsai and CC Lin).

Statistical analysis

Meta-analysis and meta-regression analysis were performed by three authors (FC Hu, JS

Tsai, and CC Lin) using the metafor package of Viechtbauer in the free R software, Version 3.4.2 (R Foundation for Statistical Computing, Vienna, Austria). Two-sided p values ≤ 0.05 were considered statistically significant.

To examine the effect of *EGFR* mutations on BM in NSCLC patients and then evaluate the effect of *EGFR* mutations on overall survival of NSCLC patients with BM, we recorded the estimated individual-study odds ratio (OR) of BM given *EGFR* mutations in NSCLC patients, and the estimated individual-study hazard ratio (HR) of survival given *EGFR* mutations in NSCLC patients with BM from each collected study, with the corresponding 95% confidence intervals (CIs) as the measures of effect sizes. The reason for studying the ORs instead of central nervous system (CNS) progressions was that only a few studies compared the median time to CNS progression in *EGFR*-mutant versus wild-type patients (Supplementary Table 1). Yet, the estimated HRs of survival given *EGFR* mutations in NSCLC patients with BM were available in only 2 of the 5 collected studies with survival data; thus, we estimated the HRs from the reported group-specific median survival

Supplementary Table 1. Studies Comparing the Time to CNS Progression in *EGFR*-Mutant Versus Wild-type Patients

No	Author, year	Median months to CNS progression (EGFR+/EGFR-)
1	Yasunori Enomoto, 2013 [17]	NA
2	Daichi Fujimoto, 2014 [18]	NA
3	Dong-Yeop Shin, 2014 [28]	NA
4	Hiroaki Akamatsu, 2014 [16]	NA)
5	Jae Hyun Jeon, 2015 [27]	NA
6	Karmen Stanic, 2014 [13]	25.1/11.8
7	Bo Li, 2015 [23]	NA
8	Kosuke Tanaka, 2015 [20]	NA
9	Shigehiro Yagishita, 2015 [21]	NA
10	Toshihiko Iuchi, 2015 [63]	NA
11	Fred Hsu, 2016 [64]	NA
12	Guang Han, 2016 [65]	NA
13	Jian Guan, 2016 [24]	NA
14	Min Young Baek, 2016 [66]	13.4/8.8
15	Bao-Xiao Wang, 2017 [22]	NA
16	Vijaya Raj Bhatt,2017 [30]	NA
17	Shih-Hsin Hsiao, 2017 [29]	31.6/not reached

times in those 3 studies.

Let the median survival times of NSCLC patients with BM in the *EGFR*-mutant and wild-type groups be denoted by T_1 and T_2, respectively. It is usually assumed that T_1 and T_2 are exponentially distributed with the survival functions $S(t_1)$ and $S(t_2)$ with constant hazards λ_1 and λ_2, respectively. The survival function of an exponential distribution is simply $S(t) = \exp(-\lambda t)$. Thus, as an example, the hazard rate λ_1 of the *EGFR*-mutant group with a median survival time of 12.6 months in Study 6 [13] was estimated using the following calculations:

$$\exp(-\lambda_1 \times 12.6) = 0.5$$
$$-12.6\ \lambda_1 = -\log(2)$$
$$\lambda_1 = \log(2) / 12.6 = 0.0550$$

where "log" was the natural logarithm. And, the hazard rate λ_2 of the *EGFR* wild-type group with a median survival time of 6.8 months in Study 6 [13] was

$$\lambda_2 = \log(2) / 6.8 = 0.1019.$$

Then, the estimated HR for Study 6 was $\lambda_1 / \lambda_2 = 0.5396$. Similarly, we used the upper and lower limits of the 95% CIs of median overall survival to estimate the upper and lower limits of the 95% CIs of the HR for this study.

The log(OR) or log(HR) and the corresponding variances were computed using the escalc() function of the metafor package for each collected study in R, where "log" was the natural logarithm. Then, the meta-analyses and linear meta-regression analyses were performed using the rma() function of the metafor package in R. The weighted averages of (1) individual-study ORs of BM given *EGFR* mutations in NSCLC patients and (2) individual-study HRs of overall survival given *EGFR* mutations in NSCLC patients with BM were calculated respectively using the inverses of the variances of log(OR) or log(HR) as the weights from the selected studies as the fixed-effects estimates of the pooled effect measures of *EGFR* mutations. Heterogeneity was examined using the Chi-square Q test and the I^2 statistic (= total heterogeneity / total variability), where a p value of the Chi-square Q test < 0.15 or $I^2 > 50\%$ indicates a substantial amount of heterogeneity [14-15]. If the statistical test of heterogeneity or the I^2 statistic revealed substantial heterogeneity among the collected studies or that the effects of relevant covariates on the pooled effect measures should be explored based on substantive knowledge and investigators' insights, a fixed-effects linear meta-regression model for modelling log(OR) or log(HR) was fitted to the study-specific data by the weighted least squares (WLS) method to identify the important covariates (called the "moderators" in meta-analytic studies), which accounted for the observed heterogeneity or exerted significant effects on the pooled effect measures. Moreover, if the statistical test of heterogeneity in the residuals of the fixed-effects linear meta-regression model still revealed substantial heterogeneity among the collected studies, a mixed-effects linear meta-regression analysis of log(OR) or log(HR) would be conducted with the added random-effects to account for the unknown sources of heterogeneity.

To ensure a good quality of analysis, the model-fitting techniques for (1) variable selection, (2) goodness-of-fit (GOF) assessment, and (3) regression diagnostics and remedies were used in our meta-regression analyses. Specifically, with the aid of substantive knowledge, the stepwise variable selection procedure (including iterations between the forward and backward steps) was applied to obtain the candidate final

linear meta-regression model for log(OR) or log(HR). All the univariate significant and non-significant study-level covariates were put on the variable list to be selected. The significance levels for entry and for stay were set to 0.15 (or larger) to be conservative. Then, with the aid of substantive knowledge, the best candidate final linear meta-regression model was identified manually by dropping the covariates with a p value > 0.10, 1 at a time, until all regression coefficients were significantly different from 0. Generalized additive models (GAMs) were fitted to detect nonlinear effects of continuous covariates on log(OR) or log(HR), and identify appropriate cut-off point(s) for discretizing continuous covariates, if necessary, during the stepwise variable selection procedure. Next, the coefficient of determination (R^2) was calculated to assess the GOF of the fitted linear meta-regression model. Technically, the R^2 statistic ($0 \leq R^2 \leq 1$) equals the square of the Pearson correlation between the observed and predicted response values of the fitted linear regression model, and it usually indicates how much of the response variability is explained by the covariates included in the fitted linear regression model. Finally, the statistical tools of regression diagnostics were used for examination of publication bias (using the funnel plot and the regression test for funnel plot asymmetry).

Since randomized clinical trials are not feasible in investigating the effects of *EGFR* mutations on BM or survival, only observational retrospective or prospective studies could be conducted. Thus, the results of this meta-analytic study must be interpreted with caution.

Results

Characteristics of the selected studies

As shown in the flow diagram in Figure 1, our systematic search identified 2,281 articles from 3 databases. Among these, 1,098 were excluded due to duplications, 1,101 were excluded due to irrelevance after titles and abstracts were scanned, and 62 were excluded for other reasons after the full text was examined. Ultimately, 17 original articles were selected for this meta-analytic study.

The 17 studies in which associations between *EGFR* mutations and BM in patients with NSCLC at initial diagnosis and/or at recurrence were examined are listed in Table 1. The studies were published between 2013 and 2017 and involved a total of 8,010 NSCLC patients, with study-specific sample sizes ranging from 44 to 1,672. Most of the studies were conducted in Asia, including 6 in Japan [16-21], 4 in China [22-25], 3 in Korea [26-28], and 1 in Taiwan [29]; the remaining 3 studies were performed in the United States [30], Canada [31], and Slovenia [13]. The mean patient age ranged from 53.0 to 70.4 years old, the percentage of female patients from 27.3% to 60.0%, the *EGFR* mutation rate from 17.0% to 53.0%, and the Stage IV percentage from 0% to 100% among these studies. Five studies investigated associations between *EGFR* mutation and brain metastasis at diagnosis, and 4 focused on associations between *EGFR* mutation and subsequent brain metastasis. In addition, 7 studies investigated associations between *EGFR* mutation and brain metastasis both at and after initial diagnosis. Eleven studies demonstrated statistically significant positive associations between *EGFR* mutations and BM, while 4 failed to show and 2 did not mention such an association.

The 5 studies selected for examination of the association between *EGFR* mutations and overall survival in NSCLC patients with BM

Table 1. Details of the 17 Studies of Associations Between EGFR Mutations and BM at or Subsequent to Initial Diagnosis in NSCLC Patients

No	Author, year	Number of patients (n)	Country	Mean age	Sex (F,%)	EGFR mutation (%)	Stage 4 (%)	Image for BM	EGFR mutation assay	Association between BM and EGFR mutations
1	Yasunori Enomoto, 2013 [17]	95	Japan	70.4	40.0	36.8	100	MRI	RTPCR (PNA)	Non significant
2	Daichi Fujimoto, 2014 [18]	246	Japan	68.0	42.0	39.8	100	MRI	RTPCR (PNA)	Significant
3	Dong-Yeop Shin, 2014 [28]	314	Korea	64.0	51.9	43.9	48.7	MRI	Direct sequencing then pyrosequencing	Significant
4	Hiroaki Akamatsu, 2014 [16]	44	Japan	65.2	27.3	29.5	0	MRI	RTPCR (PNA-LNA PCR)	Significant
5	Jae Hyun Jeon, 2015 [27]	138	Korea	64.3	47.8	53.0	7.2	MRI or CT	RTPCR	Not mentioned
6	Karmen Stanic, 2014 [13]	629	Slovenia	64.0	48.2	21.8	60.2	MRI or CT	RTPCR (TheraScreen)	Significant
7	Bo Li, 2015 [23]	100	China	53.0	43.0	51.0	64.0	MRI	RTPCR	Not mentioned
8	Kosuke Tanaka, 2015 [20]	104	Japan	62.0	38.0	28.0	0	MRI or CT	RTPCR(PNA)	Not mentioned
9	Shigehiro Yagishita, 2015 [21]	198	Japan	60.0	30.2	17.0	0	MRI	RTPCR high-resolution melting analysis (HRMA)	Not mentioned
10	Toshihiko Iuchi, 2015 [63]	1127	Japan	67.0	34.8	29.4	32.6	MRI	RTPCR	Significant
11	Fred Hsu, 2016 [64]	543	Canada	66.0	60.0	22.3	100	MRI or CT	RTPCR	Significant
12	Guang Han, 2016 [65]	234	China	57.5	46.6	46.2	44.4	MRI	RTPCR (PNA)	Significant
13	Jian Guan, 2016 [24]	401	China	60.0	30.2	39.7	49.6	MRI or CT	RTPCR + sequencing	Significant
14	Min Young Baek, 2016 [66]	259	Korea	68.0	35.5	28.2	100	MRI	Sequencing then RT-PCR (PNA)	Significant
15	Bao-Xiao Wang, 2017 [22]	1672	China	68.1	42.4	27.8	NA	MRI or CT	Direct sequencing	Significant
16	Vijaya Raj Bhatt,2017 [30]	1522	USA	NA	35	29.7	90.7	MRI or CT	RTPCR	Significant
17	Shih-Hsin Hsiao, 2017 [29]	384	Taiwan	NA	47.4	48.4	NA	NA	Direct sequencing	Significant

Table 2. Details of the 5 Studies of Associations Between EGFR Mutations and Overall Survival in NSCLC Patients with BM

No	Author, year	Patients with mutated *EGFR*	Patients with wild-type *EGFR*	Median OS in mutated *EGFR* patients	Median OS in wild-type *EGFR* patients	Reported hazard ratio**	Imputed hazard ratio**
6	Karmen Stanic, 2014 [13]*	26	64	12.6	6.8	Not available	0.540
10	Toshihiko Iuchi, 2015 [63]*	104	157	Not available	Not available	0.448	--
11	Fred Hsu, 2016 [64]*	47	118	12.4 (5.2−26.1)	5.8 (4.4−7.5)	Not available	0.468
12	Guang Han, 2016 [65]*	48	28	23.8 (17.1−30.5)	14.2 (8.6−19.8)	Not available	0.597
14	Min Young Baek, 2016 [66]	27	40	25.7	3.8	0.278	--

* *EGFR* mutation was an independent prognostic factor in univariate and multivariate analysis.

** The "reported hazard ratio" is the value of the hazard ratio reported in the original article; the "imputed hazard ratio" is the value of the hazard ratio imputed from the median survival times reported in the original article. The imputation method is explained in the "Methods" section

are listed in Table 2. These studies involved a total of 659 NSCLC patients with BM, including 839 *EGFR*-mutant and 1,619 *EGFR* wild-type patients. Only 2 of the 5 studies reported estimated HRs; median overall survival times without HRs were reported in the other 3 studies.

EGFR mutations are associated with initial brain metastasis in NSCLC patients

We performed a fixed-effects meta-analysis of the 12 identified studies to examine the association between *EGFR* mutations and the risk of initial BM in NSCLC patients. As shown in the forest plot in Figure 2A, the weighted average OR of BM in mutated *EGFR* versus wild-type *EGFR* patients was 1.70 (95% CI: 1.47–1.96, $p < 0.001$), indicating that *EGFR* mutations are associated with an increased risk of BM in NSCLC patients. The heterogeneity of the ORs in these 12 studies was low, with I^2 (total heterogeneity / total variability) < 1% and Q (df = 11) = 14.7499 ($p = 0.1942 > 0.15$).

Moreover, we conducted a meta-regression analysis to investigate moderators (i.e., covariates or regressors) that might affect the ORs of BM, including average age at diagnosis, percentage of female patients, percentage of smoking, *EGFR* mutation percentage, Stage IV percentage, adenocarcinoma percentage, other metastasis percentage, brain imaging method, type of *EGFR* mutation assay, Asian vs. non-Asian patient population, and median follow-up time. Some of the covariates were reported to be associated with the frequency of *EGFR* mutations and may therefore have affected the ORs of BM [32-34]. And, in a large retrospective analysis using a database (a nationwide database of 18,973 surgically resected lung cancer patients), patients with an L858R mutation showed a lower risk of intracranial recurrences ($p = 0.003$) compared to those with an Exon 19 Del [35]. However, most of the studies included in the current meta-analysis used positive *EGFR* mutations without classification of the specific exon 19Del or L858R mutation, so we were unable to identify which type of *EGFR* mutation might affect the ORs of BM.

As shown in Supplementary Table 2, multivariate fixed-effects meta-linear regression analysis of log(OR) indicated that *EGFR* mutation percentage was the only moderator that affected the OR of BM. GAM plots revealed that *EGFR* mutation percentage had a non-linear effect on the predicted value of log(OR) of BM (Supplementary Figure 1A). Cut-off values of 30.0% and 47.4% were chosen accordingly to discretize it for meta-regression analysis, since the *EGFR* mutation percentage ranged from 22.0% to 51.0% among the 12 selected studies. Then, the studies with higher *EGFR*

Supplementary Table 2. Meta-regression Analysis of Brain Metastasis at Diagnosis From 12 Studies, Performed by Fitting a Fixed-Effects Linear Meta-Regression Model of log(odds ratio) with the Stepwise Variable Selection Method*.

Moderator	Estimate	Standard Error	*z* Value	*p* Value	95% Confidence Interval
Intercept	0.4376	0.0839	5.2126	<.0001	0.2731–0.6021
30.0% < Mutation percentage ≤ 47.4%	0.3836	0.1713	2.2392	0.0251	0.0478–0.7193

* The test of residual heterogeneity: χ^2 statistic QE (df = 10) = 9.7357, *p*-value = 0.4640 > 0.15. Thus, the fixed-effects linear meta-regression model was reported. Next, the test of all moderators: χ^2 statistic QM (df = 1) = 5.0142, *p*-value = 0.0251 < 0.05. Finally, the goodness-of-fit measure: $R^2 = 0.3126$. This meta-regression analysis was performed using the escalc() and rma() functions of the metafor package in R (version 3.4.2).

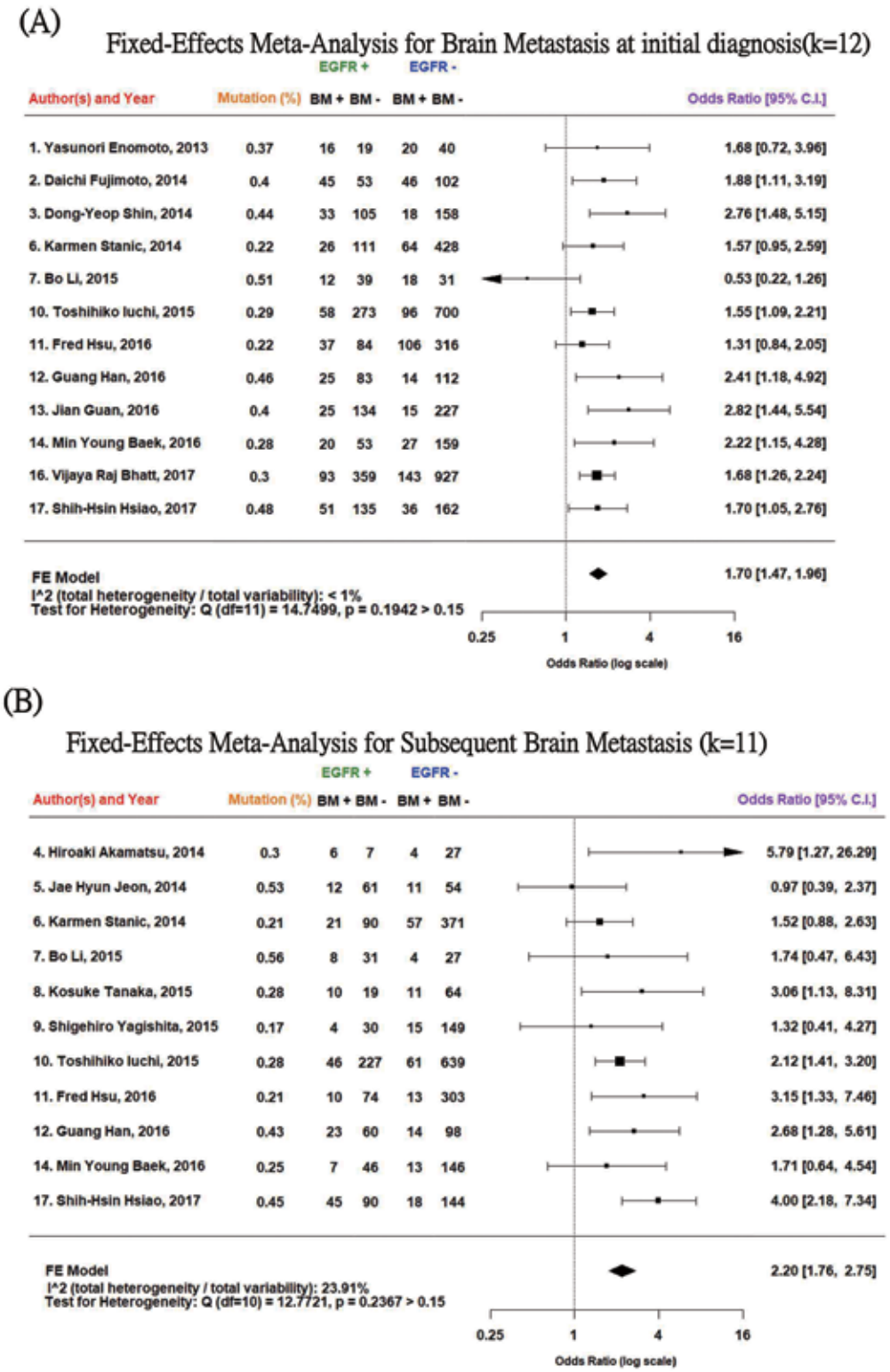

Fig. 2. (A) Fixed-effects meta-analysis of the association between EGFR mutations and the risk of brain metastasis (BM) at diagnosis in NSCLC patients. Squares and horizontal lines correspond to study-specific odds ratios (OR) and 95% confidence intervals (CI), respectively. (B) Fixed-effects meta-analysis of the association between EGFR mutations and the risk of subsequent BM in NSCLC patients. Squares and horizontal lines correspond to study-specific OR and 95% CI, respectively. The sizes of the data markers indicate the weight of each study in the meta-analysis. The diamond represents the pooled OR and its 95% CI.

mutation percentages (30.0% < *EGFR* mutation percentage ≤ 47.4%) had an estimated OR of 2.2732 (i.e., exp(0.4376 + 0.3836)), which was 1.4676 times higher (i.e., exp(0.3836)) than the estimated OR of 1.5490 (i.e., exp(0.4376)) in those with an *EGFR* mutation percentage ≤ 30%. However, 2 studies with an *EGFR* mutation percentage > 47.4% were exceptions [23, 27]. The non-significant result of the test for residual heterogeneity (QE (df = 10) = 9.7357, $p = 0.4640 > 0.15$) suggested that the fixed-effects linear meta-regression model of log(OR) sufficed for the needs of this analysis. The value of the GOF measure R^2 was 0.3126, indicating that the correlation between the reported and predicted study-specific log(OR) of BM from this fixed-effects linear meta-regression model equated 0.5591.

As shown in Supplementary Figure 2A, the funnel plot and the regression test for funnel plot asymmetry ($t = -1.2632$, df = 9, $p = 0.2383 > 0.05$) ruled out any publication bias after adjusting for the effects of moderators in the multivariate fixed-effects meta-linear regression analysis of log(OR). As shown in Supplementary Figure 3A, the quantile-normal

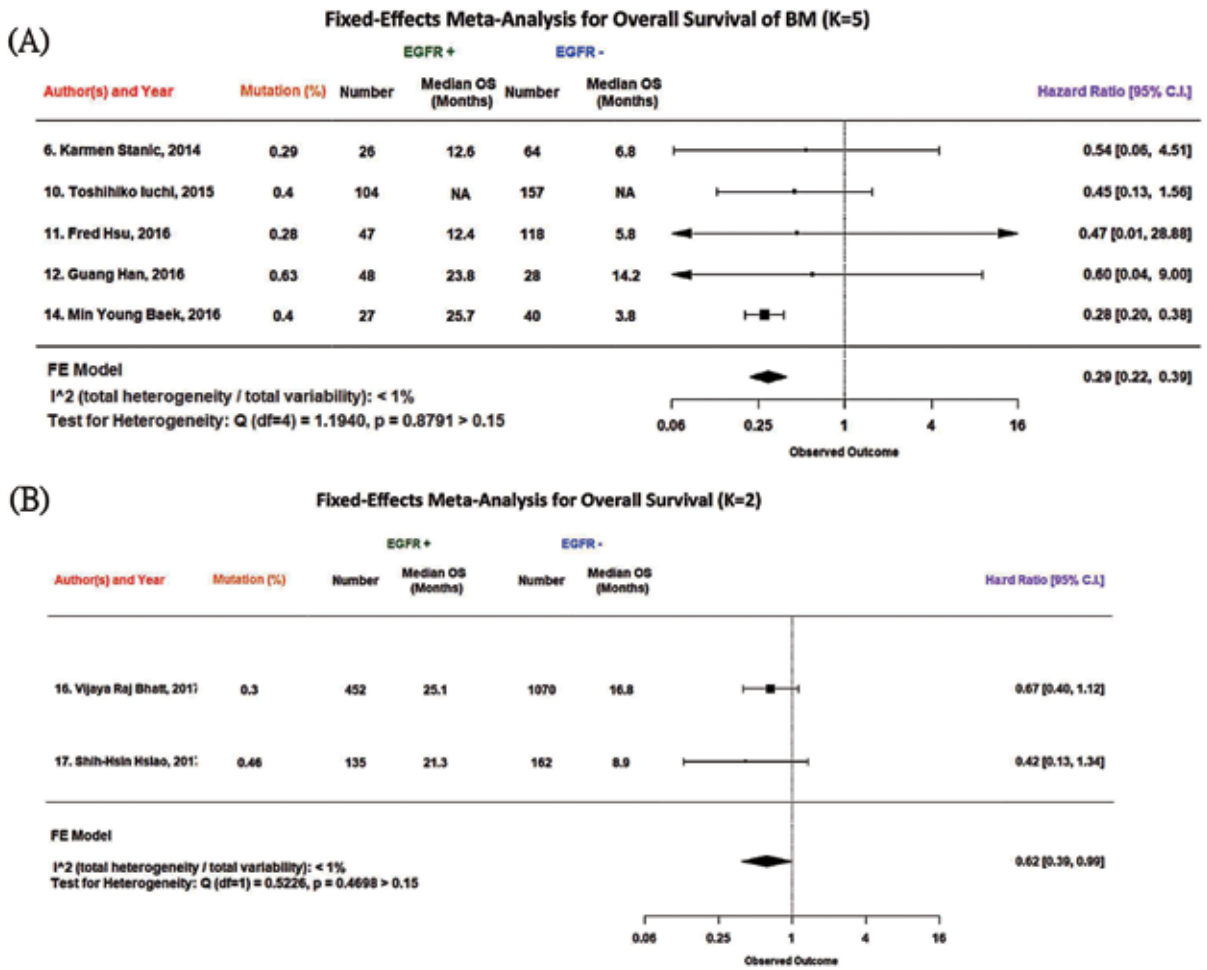

Fig. 3. Fixed-effects meta-analysis of the association between EGFR mutation and overall survival in NSCLC patients with brain metastasis (BM). Squares and horizontal lines correspond to study-specific hazard ratios (HR) and 95% confidence intervals (CI), respectively. The sizes of the data markers indicate the weight of each study in the meta-analysis. The diamond represents the pooled HR and its 95% CI.

plot supported the normality assumption for the fixed-effects linear meta-regression model of log(OR).

EGFR mutations were associated with subsequent BM in NSCLC patients

Next, we performed a fixed-effects meta-analysis of the 11 relevant studies to examine the association between *EGFR* mutations and the risk of subsequent BM in NSCLC patients. As shown in the forest plot in Figure 2B, the weighted average OR of BM in mutated EGFR versus wild-type *EGFR* patients was 2.20 (95% CI: 1.76–2.75, $p < 0.001$), indicating that *EGFR* mutations were associated with an increased risk of subsequent BM in NSCLC patients. The heterogeneity of the ORs in these studies was low, with I2 (total heterogeneity / total variability) of 23.91% and Q (df = 10) = 12.7721 ($p = 0.2367$).

Moreover, we conducted a meta-regression analysis to investigate moderators (i.e., covariates or regressors) that might affect ORs of BM. As shown in Supplementary Table 3, we found that the moderator affecting the OR of subsequent BM was the percentage of *EGFR* mutations ($p = 0.0386$). In Supplementary Figure 1B, GAM plots revealed that the *EGFR* mutation percentage had non-linear effects on the predicted value of log(OR) of BM. The cut-off values of 24.1% and 48.1% were chosen accordingly to discretize it for meta-regression analysis, since the *EGFR* mutation percentage ranged from 17.0% to 56.0% among the 11 studies. The studies with higher *EGFR* mutation percentages (24.1% < EGFR mutation percentage ≤ 48.1%) had an estimated OR of 2.6211 (i.e., exp(0.4730 + 0.4906)), which was 1.6333 times higher (i.e., exp(0.4906)) than the estimated OR of 1.6048 (i.e., exp(0.4730)) in those with an *EGFR* mutation percentage ≤ 24.1%. However, 2 studies with EGFR mutation percentages > 48.1% were exceptions [23, 27]. The non-significant result of the test for residual heterogeneity (QE (df = 9) = 8.4944, $p = 0.4852$) suggested that the fixed-effects linear meta-regression model of log(OR) sufficed for the needs of this analysis. The value of the GOF measure R^2 was 0.3756, indicating that the correlation between the reported and predicted study-specific log(OR) of BM from this fixed-effects linear meta-regression model equated 0.6129.

As shown in Supplementary Figure 2B, the funnel plot and the regression test for funnel plot asymmetry ($t = 0.7919$, df = 8, $p = 0.4513$) ruled out potential publication bias after adjusting for the effects of moderators in the multivariate fixed-effects meta-linear regression anal-

Supplementary Table 3. Meta-regression Analysis of Subsequent Brain Metastasis from 11 Studies, Performed by Fitting a Fixed-effects Linear Meta-Regression Model of log(odds ratio) with the Stepwise Variable Selection Method*.

Moderator	Estimate	Standard Error	*z* Value	*p* Value	95% Confidence Interval
Intercept	0.4730	0.1901	2.4877	0.0129	0.1003–0.8457
24.1% < Mutation percentage ≤ 48.1%	0.4906	0.2372	2.0682	0.0386	0.0257–0.9555

* The test of residual heterogeneity: χ^2 statistic QE (df = 10) = 8.4944, *p*-value = 0.4852 > 0.15. Thus, the fixed-effects linear meta-regression model was reported. Next, the test of all moderators: χ^2 statistic QM (df = 1) = 4.2776, *p*-value = 0.0386 < 0.05. Finally, the goodness-of-fit measure: $R^2 = 0.3756$. This meta-regression analysis was performed using the escalc() and rma() functions of the metafor package in R (version 3.4.2).

ysis of log(OR). And, in Supplementary Figure 3B, the quantile-normal plot barely supported the normality assumption for the fixed-effects linear meta-regression model of log(OR).

EGFR mutations are associated with longer overall survival in NSCLC patients with BM

Next, we performed a fixed-effects meta-analysis of the 5 relevant studies to examine the associations between *EGFR* mutations and overall survival in NSCLC patients with BM. As shown in the forest plot in Figure 3, NSCLC patients with BM in the *EGFR*-mutant group survived longer than those in the *EGFR wild*-type group (HR = 0.29, 95% CI: 0.22−0.29, $p < 0.001$). The heterogeneity of the HRs from these 5 studies was quite low, with I^2 (total heterogeneity / total variability) < 1% and Chi-square Q (df = 4) = 1.1940 ($p = 0.8791$). We also conducted a meta-regression analysis to examine moderators (i.e., covariates or regressors) that might affect the HRs of overall survival, but none were identified. As shown in Supplementary Figure 2C, the funnel plot and regression test for funnel plot asymmetry (QE (df = 6) = 1.1678, $p = 0.9784$) also ruled out potential publication bias in the fixed-effects meta-analysis of log(HR). Finally, as shown in Supplementary Figure 3C, the quantile-normal plot supported the normality assumption for the fixed-effects meta-linear regression analysis of log(OR).

Discussion

In this meta-analytic study, we found that *EGFR* mutations increased the risk of BM both at and after diagnosis in NSCLC patients, and that *EGFR* mutations were associated with better overall survival in NSCLC patients with BM.

Survival outcomes are poor in NSCLC patients with BM [36]. Resection of early-stage NSCLC offers patients the best chance of a cure, but post-resection recurrence rates remain high. Approximately 64% and 36% of NSCLC patients experience distant metastasis in a single or multiple organs, respectively [37]. The most common sites of distant metastasis are the brain [38] and bone [37, 39].

Although previous studies have examined the prognostic value of TNM stage, smoking index, and number of mediastinal lymph nodes dissected/sampled in NSCLC patients [40], none have evaluated the significance of *EGFR* mutations. Our data show that BM rates are higher in NSCLC patients with *EGFR* mutations than in those without mutations. Unfortunately, we were unable to evaluate the significance of TNM stage and mediastinal lymph node dissection surgery with regard to BM in this study, because most of the studies examined lacked the data. In addition, studies examining the impact of *ALK* rearrangements [41] or other mutations (*Kras*) [42] on BM were not included in this study, which prevented comparison of *EGFR* mutations to other mutations. Since *ALK* rearrangements are less common than *EGFR* mutations, and agents that target *Kras* mutations are not available for clinical use, *ALK* and *Kras* mutations are not routinely screened in clinical settings before first-line treatment for NSCLC [43]. However, our findings emphasize the importance of careful evaluation and early detection of BM.

Fixed-effects meta-analysis revealed that, compared to NSCLC patients with wild-type *EGFR*, the OR of developing BM after initial diagnosis was higher than the OR of having BM upon diagnosis in patients with *EGFR* mu-

tations (2.2 versus 1.7). Although previous studies have indicated that brain MRIs are of limited efficacy in patients with operable NSCLC, due to the low incidence of asymptomatic BM [44], another study emphasized that the incidence of silent BM is high in patients under 70 years of age, and especially those with adenocarcinoma, even in its early stages [45]. Our results reinforce the importance of brain imaging, especially for patients with *EGFR* mutations, even if NSCLC patients do not have BM at diagnosis. Furthermore, a recent study proposed that *EGFR*-TKIs might improve adjuvant treatments for NSCLC [46]; a number of associated clinical trials are ongoing [47].

The molecular mechanisms underlying this association between *EGFR* mutations and BM are unknown. Signaling downstream of *EGFR* or activation of other pathways might help explain how *EGFR* mutation-harboring NSCLC easily metastasizes to the brain. Mutant *EGFR* can activate the gp130/JAK/STAT3 pathway by upregulating IL-6 [48], and STAT3 promotes lung-to-brain metastases [49]. STAT3 also regulates VEGF, which is upregulated by *EGFR* signaling, to create an environment that promotes BM [50]. Other pathways, such as Met, are also activated by the EGF receptor through MAPK, and enhance invasion and BM in NSCLC patients [51]. Moreover, activation of C/EBPβ-LIP/CUG-binding protein 1 (CUGBP1) [52] and phosphoinositide 3-kinase/protein kinase B/phospholipase C γ [53] by *EGFR* promotes BM. Although the mechanisms described in these studies might contribute to the increased risk of BM in NSCLC patients with *EGFR* mutations, additional studies are needed to determine how *EGFR* mutations affect BM at the molecular level.

Several studies have investigated factors that affect the prognosis of BM; these factors include surgical resection, neurofunction class, extent of metastasis, and whole brain irradiation [2, 54, 55]. Evidence suggests that 1st generation *EGFR*-TKIs can penetrate the blood–brain barrier [56-57], and that 2nd generation *EGFR*-TKIs may be an effective first-line treatment for BM in patients with *EGFR* mutations [8]. A meta-analysis also found that *EGFR*-TKIs are an effective treatment for NSCLC patients with BM, particularly those with activating *EGFR* mutations [58]. Although the 3rd generation *EGFR*-TKI osimertinib has been shown to have superior brain penetration in 1st-line and 2nd-line treatment for *EGFR*-mutant lung cancer [59-60], the high cost of osimertinib presents an economic burden and limits its use in patients with *EGFR* mutations. A recent study also highlighted that osimertinib for T790M-mutant NSCLC may not be cost-effective [61]. For those countries in which osimertinib is unaffordable and not reimbursed by health insurance, the impact of *EGFR* mutations on BM and subsequent survival still merits investigation.

In this study, median survival was better in *EGFR*-mutant patients with BM than in those with wild-type *EGFR*. Moreover, *EGFR* mutations were identified as an independent prognostic factor. Thus, *EGFR* mutations should be considered a prognostic factor in lung cancer patients with BM. However, we were not able to investigate other factors that may affect prognosis in NSCLC patients with BM, such as extracranial metastasis [62], tumor size [25], lymph node involvement [25], and treatment strategy [13, 31]. We were also unable to evaluate whether various *EGFR*-TKIs have different levels of efficacy on BM. The treatment strategies employed in the 5 selected studies are

Supplementary Table 4. Treatment Strategy in the 5 Included Studies

No	Author, year	Treatment strategy
2	Daichi Fujimoto, 2014 [18]	*EGFR*+ (First-line chemotherapy: 53% TKIs, 42% platinum combination, 3% single-agent, and 2% no chemotherapy), *EGFR*− (First-line chemotherapy; 3% TKIs, 60% platinum combination, 22% single-agent, and 15% no chemotherapy).
10	Toshihiko Iuchi, 2015 [63]	Treatment for the brain metastasis EGFR+ (Surgery 15.1%, Chemotherapy 9.7%, and TKI 61.3%), *EGFR*− (Surgery 22.6%, Chemotherapy 33.3%, and TKI 7.7%).
11	Fred Hsu, 2016 [64]	*EGFR*+ (Chemotherapy 49%, TKI 81%), *EGFR*− (Chemotherapy 49%, TKI 48%).
12	Guang Han, 2016 [65]	Treatment for the brain metastasis: *EGFR*+ (Radiotherapy 61.4%, Chemotherapy 50%, and TKI 91.3%), *EGFR*− (Surgery 38.6%, Chemotherapy 50%, and TKI 8.3%).
14	Min Young Baek, 2016 [66]	*EGFR*+ (TKI: 48.7% at first line, 40.7% at second line, and 7.4% at third line; Chemotherapy: Not available).

listed in Supplementary Table 4.

Conclusion

In summary, this meta-analysis revealed that *EGFR* mutations are a risk factor for BM in NSCLC patients, but are also associated with improved survival in NSCLC patients with BM.

Funding

This work was financially supported by MOHW106-TDU-B-211-144-004 from the Ministry of Health and Welfare, Taiwan, MOST 104-2314-B-006-046-MY3 and MOST105-2314-B-076-MY2 from the Ministry of Science and Technology, Taiwan, and NCKUH-10503002 from National Cheng Kung University Hospital, Taiwan.

References

1. Lee DS, Kim YS, Jung SL, *et al*. The relevance of serum carcinoembryonic antigen as an indicator of brain metastasis detection in advanced non-small cell lung cancer. Tumour Biol 2012; 33(4): 1065-1073.
2. Owen S, Souhami L. The management of brain metastases in non-small cell lung cancer. Front Oncol 2014; 4: 248.
3. Mujoomdar A, Austin JH, Malhotra R, *et al*. Clinical predictors of metastatic disease to the brain from non-small cell lung carcinoma: primary tumor size, cell type, and lymph node metastases. Radiology 2007; 242(3): 882-888.
4. Su H, Lin Z, Peng W, *et al*. Identification of potential biomarkers of lung adenocarcinoma brain metastases via microarray analysis of cDNA expression profiles. Oncol Lett 2019; 17(2): 2228-2236.
5. Choi H, Puvenna V, Brennan C, *et al*. S100B and S100B autoantibody as biomarkers for early detection of brain metastases in lung cancer. Translational Lung Cancer Res 2016; 5(4): 413-419.
6. Lee CK, Wu YL, Ding PN, *et al*. Impact of specific epidermal growth factor receptor (*EGFR*) mutations and clinical characteristics on outcomes after treatment with EGFR tyrosine kinase inhibitors versus chemotherapy in EGFR-mutant lung cancer: a meta-analysis. J Clin Oncol 2015; 33(17): 1958-1965.
7. Gow CH, Chien CR, Chang YL, *et al*. Radiotherapy in lung adenocarcinoma with brain metastases: effects of activating epidermal growth factor receptor mutations on clinical response. Clin Cancer Res 2008; 14(1): 162-168.
8. Schuler M, Wu YL, Hirsh V, *et al*. First-line afatinib versus chemotherapy in patients with non-small cell lung

cancer and common epidermal growth factor receptor gene mutations and brain metastases. J Thorac Oncol 2016; 11(3): 380-390.

9. Hendriks LE, Smit EF, Vosse BA, *et al*. EGFR mutated non-small cell lung cancer patients: more prone to development of bone and brain metastases? Lung Cancer 2014; 84(1): 86-91.
10. Luo D, Ye X, Hu Z, *et al*. *EGFR* mutation status and its impact on survival of Chinese non-small cell lung cancer patients with brain metastases. Tumour Biol 2014; 35(3): 2437-2444.
11. Shamseer L, Moher D, Clarke M, *et al*. Preferred reporting items for systematic review and meta-analysis protocols (PRISMA-P) 2015: elaboration and explanation. BMJ 2015; 350: g7647.
12. Mamdani M, Sykora K, Li P, *et al*. Reader's guide to critical appraisal of cohort studies: 2. Assessing potential for confounding. BMJ 2005; 330(7497): 960-962.
13. Stanic K, Zwitter M, Hitij NT, *et al*. Brain metastases in lung adenocarcinoma: impact of *EGFR* mutation status on incidence and survival. Radiol Oncol 2014; 48(2): 173-183.
14. Higgins JP, Thompson SG, Deeks JJ, *et al*. Measuring inconsistency in meta-analyses. BMJ 2003; 327(7414): 557-560.
15. Patsopoulos NA, Evangelou E, Ioannidis JP. Sensitivity of between-study heterogeneity in meta-analysis: proposed metrics and empirical evaluation. Int J Epidemiol 2008; 37(5): 1148-1157.
16. Akamatsu H, Kaira K, Murakami H, *et al*. The impact of clinical outcomes according to *EGFR* mutation status in patients with locally advanced lung adenocarcinoma who received concurrent chemoradiotherapy. Am J Clin Oncol 2014; 37(2): 144-147.
17. Enomoto Y, Takada K, Hagiwara E, *et al*. Distinct features of distant metastasis and lymph node stage in lung adenocarcinoma patients with epidermal growth factor receptor gene mutations. Respir Investigat 2013; 51(3): 153-157.
18. Fujimoto D, Ueda H, Shimizu R, *et al*. Features and prognostic impact of distant metastasis in patients with stage IV lung adenocarcinoma harboring EGFR mutations: importance of bone metastasis. Clin Exp Metastasis 2014; 31(5): 543-551.
19. Iuchi T, Shingyoji M, Itakura M, *et al*. Frequency of brain metastases in non-small-cell lung cancer, and their association with epidermal growth factor receptor mutations. Int J Clin Oncol 2015; 20(4): 674-679.
20. Tanaka K, Hida T, Oya Y, *et al. EGFR* mutation impact on definitive concurrent chemoradiation therapy for inoperable stage III adenocarcinoma. J Thorac Oncol 2015; 10(12): 1720-1725.
21. Yagishita S, Horinouchi H, Katsui Taniyama T, *et al*. Epidermal growth factor receptor mutation is associated with longer local control after definitive chemoradiotherapy in patients with stage III nonsquamous non-small-cell lung cancer. Int J Rad Oncol, Biol, Physics 2015; 91(1): 140-148.
22. Wang BX, Ou W, Mao XY, *et al*. Impacts of *EGFR* mutation and EGFR-TKIs on incidence of brain metastases in advanced non-squamous NSCLC. Clin Neurol Neurosurg 2017; 160: 96-100.
23. Li B, Sun SZ, Yang M, *et al*. The correlation between EGFR mutation status and the risk of brain metastasis in patients with lung adenocarcinoma. J Neuro-oncol 2015; 124(1): 79-85.
24. Guan J, Chen M, Xiao N, *et al*. *EGFR* mutations are associated with higher incidence of distant metastases and smaller tumor size in patients with non-small-cell lung cancer based on PET/CT scan. Med Oncol (Northwood, London, England) 2016; 33(1): 1.
25. Han G, Bi J, Tan W, *et al*. A retrospective analysis in patients with EGFR-mutant lung adenocarcinoma: is EGFR mutation associated with a higher incidence of brain metastasis? Oncotarget 2016; 7(35): 56998-57010.
26. Baek MY, Ahn HK, Park KR, *et al*. Epidermal growth factor receptor mutation and pattern of brain metastasis in patients with non-small cell lung cancer. Korean J Intern Med 2018; 33(1): 168-175.
27. Jeon JH, Kang CH, Kim HS, *et al*. Prognostic and predictive role of epidermal growth factor receptor mutation in recurrent pulmonary adenocarcinoma after curative resection. Eur J Cardio-thorac Surg: official journal of the European Association for Cardio-thoracic Surgery 2015; 47(3): 556-562.
28. Shin DY, Na, II, Kim CH, *et al*. *EGFR* mutation and brain metastasis in pulmonary adenocarcinomas. J Thorac Oncol: official publication of the International Association for the Study of Lung Cancer 2014; 9(2): 195-199.

29. Hsiao SH, Chou YT, Lin SE, *et al*. Brain metastases in patients with non-small cell lung cancer: the role of mutated-EGFRs with an exon 19 deletion or L858R point mutation in cancer cell dissemination. Oncotarget 2017; 8(32): 53405-53418.
30. Bhatt VR, D'Souza SP, Smith LM, *et al*. Epidermal growth factor receptor mutational status and brain metastases in non-small-cell lung cancer. J Global Oncol 2017; 3(3): 208-217.
31. Hsu F, De Caluwe A, Anderson D, *et al*. *EGFR* mutation status on brain metastases from non-small cell lung cancer. Lung Cancer 2016; 96: 101-107.
32. Girard N, Sima CS, Jackman DM, *et al*. Nomogram to predict the presence of EGFR activating mutation in lung adenocarcinoma. Eur Respir J 2012; 39(2): 366.
33. Ellison G, Zhu G, Moulis A, *et al. EGFR* mutation testing in lung cancer: a review of available methods and their use for analysis of tumour tissue and cytology samples. J Clin Pathol 2013; 66(2): 79-89.
34. Choi YH, Lee JK, Kang HJ, *et al*. Association between age at diagnosis and the presence of *EGFR* mutations in female patients with resected non-small cell lung cancer. J Thorac Oncol 2010; 5(12): 1949-1952.
35. Suda K, Mitsudomi T, Shintani Y, *et al*. Clinical impacts of EGFR mutation status: analysis of 5780 surgically resected lung cancer cases. Ann Thorac Surg 2021 Jan;111(1):269-276.
36. Schuette W. Treatment of brain metastases from lung cancer: chemotherapy. Lung Cancer 2004; 45 Suppl 2: S253-257.
37. Hung JJ, Jeng WJ, Hsu WH, *et al*. Prognostic factors of postrecurrence survival in completely resected stage I non-small cell lung cancer with distant metastasis. Thorax 2010; 65(3): 241-245.
38. Martini N, Bains MS, Burt ME, *et al*. Incidence of local recurrence and second primary tumors in resected stage I lung cancer. J Thorac Cardiovasc Surg 1995; 109(1): 120-129.
39. Yoshino I, Yohena T, Kitajima M, *et al*. Survival of non-small cell lung cancer patients with postoperative recurrence at distant organs. Ann Thorac Cardiovasc Surg 2001; 7(4): 204-209.
40. Hung JJ, Jeng WJ, Hsu WH, *et al*. Predictors of death, local recurrence, and distant metastasis in completely resected pathological stage-I non-small-cell lung cancer. J Thorac Oncol 2012; 7(7): 1115-1123.
41. Rangachari D, Yamaguchi N, VanderLaan PA, *et al*. Brain metastases in patients with EGFR-mutated or ALK-rearranged non-small-cell lung cancers. Lung Cancer 2015; 88(1): 108-111.
42. Doebele RC, Lu X, Sumey C, *et al*. Oncogene status predicts patterns of metastatic spread in treatment-naive nonsmall cell lung cancer. Cancer 2012; 118(18): 4502-4511.
43. Selinger CI, Rogers TM, Russell PA, *et al*. Testing for ALK rearrangement in lung adenocarcinoma: a multicenter comparison of immunohistochemistry and fluorescent in situ hybridization. Mod Pathol 2013; 26(12): 1545-1553.
44. Yohena T, Yoshino I, Kitajima M, *et al*. Necessity of preoperative screening for brain metastasis in non-small cell lung cancer patients without lymph node metastasis. Ann Thorac Cardiovasc Surg 2004; 10(6): 347-349.
45. de Cos Escuin JS, Menna DM, Gonzalez MA, *et al*. Silent brain metastasis in the initial staging of lung cancer: evaluation by computed tomography and magnetic resonance imaging. Arch Bronconeumol 2007; 43(7): 386-391.
46. Huang Q, Li J, Sun Y, *et al*. Efficacy of *EGFR* tyrosine kinase inhibitors in the adjuvant treatment for operable non-small cell lung cancer by a meta-analysis. Chest 2016; 149(6): 1384-1392.
47. Lourdes LS, Jalal SI, Hanna N. Adjuvant epidermal growth factor receptor inhibitors in non-small cell lung cancer. Oncologist 2015; 20(9): 975-978.
48. Gao SP, Mark KG, Leslie K, *et al*. Mutations in the *EGFR* kinase domain mediate STAT3 activation via IL-6 production in human lung adenocarcinomas. J Clin Invest 2007; 117(12): 3846-3856.
49. Singh M, Garg N, Venugopal C, *et al*. STAT3 pathway regulates lung-derived brain metastasis initiating cell capacity through miR-21 activation. Oncotarget 2015; 6(29): 27461-27477.
50. Lindeman NI, Cagle PT, Beasley MB, *et al*. Molecular testing guideline for selection of lung cancer patients for *EGFR* and ALK tyrosine kinase inhibitors: guideline from the College of American Pathologists, International Association for the Study of Lung Cancer, and Association for Molecular Pathology. J Mol Diagn 2013;

15(4): 415-453.
51. Breindel JL, Haskins JW, Cowell EP, *et al*. EGF receptor activates MET through MAPK to enhance non-small cell lung carcinoma invasion and brain metastasis. Cancer Res 2013; 73(16): 5053-5065.
52. Baldwin BR, Timchenko NA, Zahnow CA. Epidermal growth factor receptor stimulation activates the RNA binding protein CUG-BP1 and increases expression of C/EBPbeta-LIP in mammary epithelial cells. Mol Cell Biol 2004; 24(9): 3682-3691.
53. Nie F, Yang J, Wen S, *et al*. Involvement of epidermal growth factor receptor overexpression in the promotion of breast cancer brain metastasis. Cancer 2012; 118(21): 5198-5209.
54. Rodrigus P, de Brouwer P, Raaymakers E. Brain metastases and non-small cell lung cancer. Prognostic factors and correlation with survival after irradiation. Lung Cancer 2001; 32(2): 129-136.
55. Sen M, Demiral AS, Cetingoz R, *et al*. Prognostic factors in lung cancer with brain metastasis. Radiother Oncol 1998; 46(1): 33-38.
56. Broniscer A, Panetta JC, O'Shaughnessy M, *et al*. Plasma and cerebrospinal fluid pharmacokinetics of erlotinib and its active metabolite OSI-420. Clin Cancer Res 2007; 13(5): 1511-1515.
57. Bai H, Han B. The effectiveness of erlotinib against brain metastases in non-small cell lung cancer patients. Am J Clin Oncol 2013; 36(2): 110-115.
58. Fan Y, Xu X, Xie C. *EGFR*-TKI therapy for patients with brain metastases from non-small-cell lung cancer: a pooled analysis of published data. Onco Targets Ther 2014; 7: 2075-2084.
59. Soria JC, Ohe Y, Vansteenkiste J, *et al*. Osimertinib in untreated *EGFR*-mutated advanced non-small-cell lung cancer. N Engl J Med 2018; 378(2): 113-125.
60. Yang JC-H, Cho BC, Kim D-W, *et al*. Osimertinib for patients (pts) with leptomeningeal metastases (LM) from *EGFR*-mutant non-small cell lung cancer (NSCLC): updated results from the BLOOM study. J Clin Oncol 2017; 35(15_suppl): 2020-2020.
61. Wu B, Gu X, Zhang Q. Cost-effectiveness of osimertinib for *EGFR* mutation-positive non-small cell lung cancer after progression following first-line *EGFR* TKI therapy. J Thorac Oncol 2018; 13(2): 184-193.
62. Eichler AF, Kahle KT, Wang DL, *et al*. *EGFR* mutation status and survival after diagnosis of brain metastasis in nonsmall cell lung cancer. Neuro Oncol 2010; 12(11): 1193-1199.
63. Iuchi T, Shingyoji M, Sakaida T, *et al*. The incidence and clinical feature of brain metastasis from non-small cell lung cancer, and their associations with *EGFR* mutation. Eur J Cancer 2013; 49: S787-S787.
64. Hsu F, De Caluwe A, Anderson D, *et al. EGFR* mutation status on brain metastases from non-small cell lung cancer. Lung Cancer 2016; 96: 101-107.
65. Han G, Bi J, Tan W, *et al*. A retrospective analysis in patients with *EGFR*-mutant lung adenocarcinoma: is *EGFR* mutation associated with a higher incidence of brain metastasis? Oncotarget 2016; Aug 30;7(35): 56998-57010
66. Baek MY, Ahn HK, Park KR, *et al*. Epidermal growth factor receptor mutation and pattern of brain metastasis in patients with non-small cell lung cancer. Korean J Intern Med 2018 Jan;33(1): 168-175.

Pulmonary Tuberculosis with Mediastinal Involvement Mimicking Lung Cancer on Chest Images: A Case Report

Ming-Hung Chang[1], Shian-Chin Ko[2]

Although the incidence of tuberculosis is declining, it is still the most common notifiable infectious disease in Taiwan. Tuberculosis is known as a great imitator. Atypical clinical presentations will mislead us and delay the diagnosis. Here, we present the case of a patient with pulmonary tuberculosis and huge mediastinal lymphadenopathy, who was initially diagnosed as having advanced lung cancer. Histologic and microbiologic evidence led to the final accurate diagnosis. We should maintain a high index of clinical suspicion for tuberculosis in areas of high prevalence, such as Taiwan. Biopsy and culture remain the gold standard for the definitive diagnosis of tuberculosis. ***(Thorac Med 2021; 36: 123-128)***

Key words: pulmonary tuberculosis, mediastinal lymphadenopathy, chest imaging

Introduction

Worldwide, tuberculosis (TB) is 1 of the top 10 causes of death, and the leading cause from a single infectious agent [1]. In Taiwan, through the efforts of the central government's public health department, TB prevalence and mortality have continued to decline over the years. The prevalence rate of TB has been reduced by 46% during the past 13 years [2]. According to the statistical data of Taiwan's Ministry of Health and Welfare, TB was the 23rd leading cause of death in Taiwan in 2018 [3]. However, TB is still the most common notifiable infectious disease in Taiwan and cannot be ignored.

Early diagnosis and prompt treatment are the most important methods to control TB. However, TB is a great imitator. The symptoms of pulmonary TB are nonspecific, and there is great variability in the radiographic findings. Differentiating the diagnosis of TB and that of malignancy is often the doctor's dilemma.

Case Report

This 53-year-old woman presented to out chest clinic with the chief complaints of chronic productive cough and exertional dyspnea for

[1]Department of Internal Medicine, Chi Mei Hospital, Tainan City, Taiwan
[2]Division of Chest Medicine, Chi Mei Hospital, Tainan City, Taiwan
Address reprint requests to: Dr. Shian-Chin Ko, Division of Chest Medicine, Department of Internal Medicine, Chi Mei Hospital, No.901, Zhonghua Rd., Yongkang Dist., Tainan City 710, Taiwan (R.O.C.)

about 2 months. The sputum was mucoid, whitish and medium in amount. She felt short of breath when climbing upstairs to the 3rd floor. There was no fever, chest pain, cold sweating or body weight loss.

The patient had no major medical disorder, such as hypertension or diabetes. She had had asthma in her childhood, but she experienced no further attacks as an adult. She had smoked 0.5 packs a day for 15 years, but quit 20 years ago. She was a housekeeper and had no travel or contact history within the half year before the onset of illness. The patient did not remember having been exposed to TB. The people around her had no similar symptoms.

On arrival to our OPD, she was alert, but chronically ill-looking. Her vital signs were stable: BT 35.8℃, RR 16 breaths/min, PR 65 beats/min, BP 104/74 mm Hg, and SpO_2 95% on room air. On chest auscultation, the breathing sounds were decreased and inspiratory scattered crackles were heard in the left lower lung field.

The blood test results were as follows: leukocyte count: 4,100/μL, hemoglobin: 12.3 g/dL, platelet count: 201×10^3/μL, glucose: 108 mg/dL, aspartate transaminase (AST): 21 U/L, alanine transaminase (ALT): 9 U/L, creatinine: 0.75 mg/dL, blood urea nitrogen: 18 mg/dL, sodium concentration: 142.8 mmol/L, potassium concentration: 3.90 mmol/L, chloride concentration: 107.9 mmol/L, immunoglobulin (Ig) E 248.3 IU/mL (ref <100), and an eosinophil count < 50 /μL (ref 50-350).

Chest radiography showed a consolidated lesion in the left lower lobe and an enlarged left hilar shadow (Figure 1). Under the impression of lung tumor or atelectasis, the patient was admitted for further investigation. After admission, chest computed tomography (CT) scan revealed infiltrations with tree-in-bud signs in the right upper and left lower lobes. A left lower lobe lung mass, 8.3×9.0×3.0 cm in size, with inhomogeneous contrast enhancement and calcified plaques, extended to the left upper lobe and mediastinum. Atelectasis of the left lower lobe with a significant fluid-bronchogram was noted. There were also multiple small nodules in the bilateral lung fields. Left hilar and mediastinal lymphadenopathy was also found. Lung cancer with clinical stage T4N2M1a, stage IVa, was diagnosed based on the radiologist's report (Figure 2).

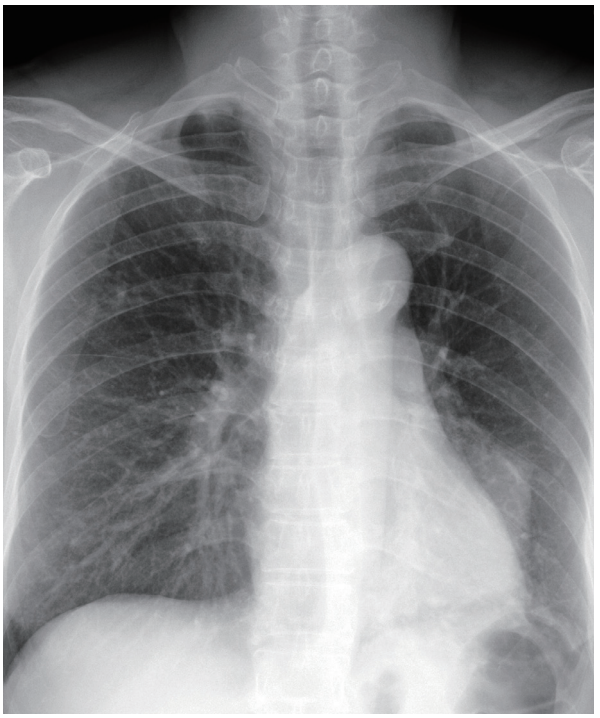

Fig. 1. Chest radiography at initial presentation showed consolidation in the left retrocardiac area and hyperlucency in the left upper lung field, suggestive of left lower lobe collapse. Enlargement of the left hilar shadow was also found.

Bronchoscopy was performed for histologic confirmation and staging of the suspected lung cancer. It showed that the carinal angle was fixed and widening. Total obstruction of the orifice of the left lower lobe bronchus and stenosis

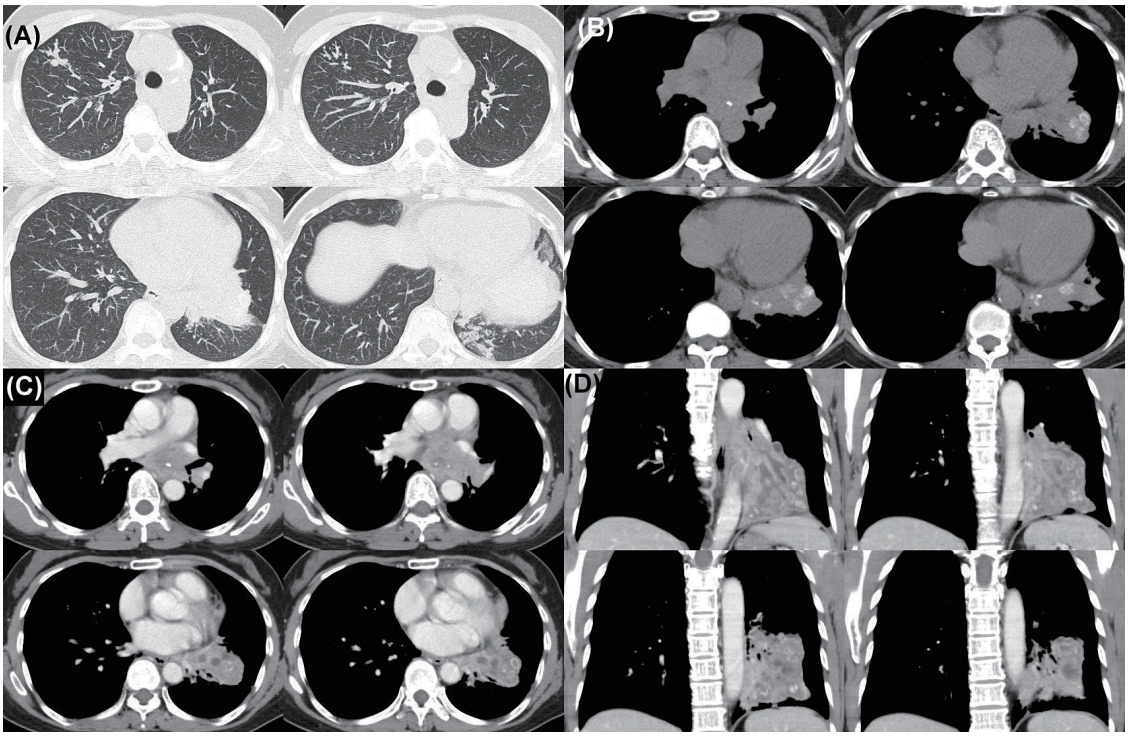

Fig. 2. Chest CT scan at initial diagnosis showed: (A) Some infiltrations with tree-in-bud signs in the right upper lobe and left basal lung in the lung window, in addition to the left lower lobe consolidation; (B) Some calcified plaques within the lesion were found in the non-contrasted soft tissue window; (C) After contrast enhancement, the soft tissue window showed a left lower lobe mass, 8.3×9.0×3.0 cm in size, extending to the left upper lobe and mediastinum. Some low-attenuation areas within the lesion were suggestive of secretion retention due to proximal airway obstruction. There were bilateral multiple tiny nodules and enlarged lymph nodes in the left hilum and mediastinum; (D) The coronal reconstruction view revealed significant fluid-bronchograms, which represented bronchial obstruction.

of the left upper lobe bronchus due to mucosal swelling and external compression were found. The mucosa had an irregular surface and erythematous change with many rice-like nodules. There were copious tenacious whitish secretions with many cheese-like materials (Figure 3). Bronchoscopic biopsy revealed multiple pieces of necrotic tissue with inflammatory exudates. Numerous mycobacterial microorganisms in necrotic tissue were highlighted by acid-fast stain (Figure 4). Mycobacterium tuberculosis quantitative polymerase chain reaction (PCR) was positive. Culture from bronchoalveolar lavage finally yielded *Mycobacterium tuberculosis complex*.

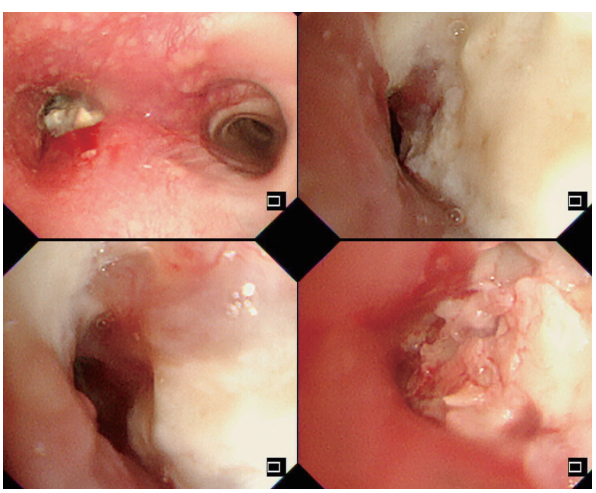

Fig. 3. Bronchoscopy showed widening of the carinal angle with overlying erythematous swollen mucosa. The left main bronchus was stenotic with copious cheese-like materials and tenacious secretions. After removal of the debris and secretions, an endobronchial tumor-like lesion with an irregular surface was revealed.

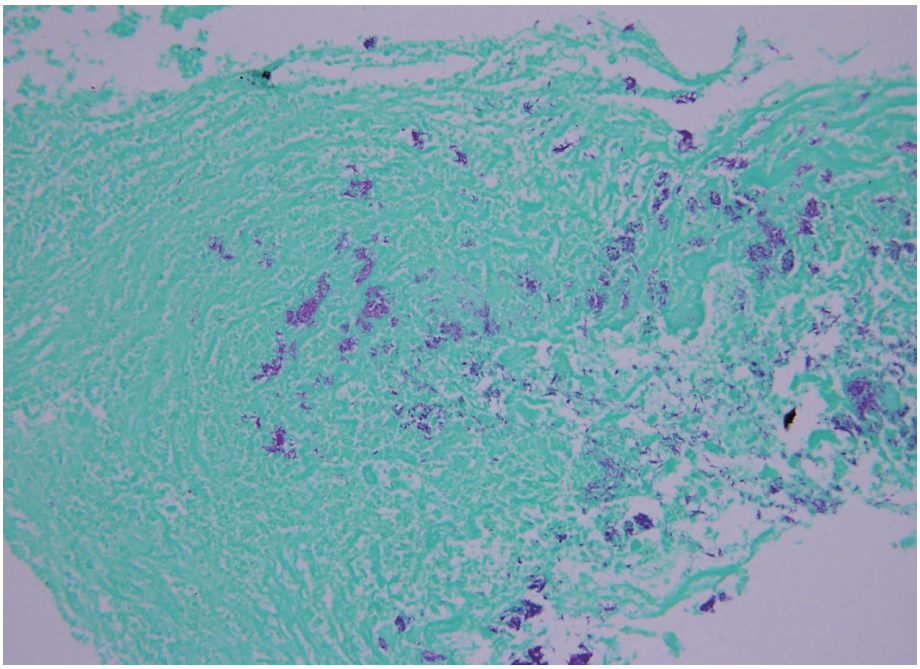

Fig. 4. Histological examination with acid-fast stain (400×) showed many clustered acid-fast bacilli (AFB) in the necrotic tissue and inflammatory exudates.

After confirmation of the pulmonary TB diagnosis, combined anti-TB therapy with isoniazid, rifampicin, ethambutol and pyrazinamide was immediately initiated. The drug susceptibility test revealed that the *M. tuberculosis* isolate was susceptible to all first-line anti-TB drugs. After 6 months of anti-TB therapy, the follow-up chest CT scan revealed marked shrinkage of the left lower lobe lesion and mediastinal lymphadenopathy with residual fibro-calcified lesions (Figure 5). The patient completed a 9-month anti-TB treatment course uneventfully.

Discussion

Although the incidence of TB is decreasing, it is still a healthcare problem in Taiwan. TB has the highest prevalence rate and greatest number of mortality cases among the notifiable infectious diseases in Taiwan. According to official statistics, there are nearly 9,000 newly diagnosed TB cases in Taiwan every year [2].

The lung is the major organ affected by *M. tuberculosis,* and pulmonary TB accounts for about 85% of TB cases. However, *M. tuberculosis* can also cause infection in almost all other organs and tissues in the body. Up to 25% of

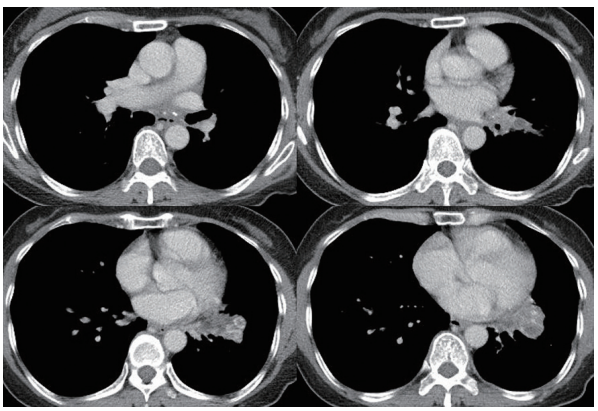

Fig. 5. Chest CT scan after more than 6 months of anti-TB treatment showed marked shrinkage of the left lower lobe consolidation and mediastinal lymphadenopathy. Some fibrocalcified lesions were left behind.

TB cases present extrapulmonary involvement. This is caused by the hematogenous and lymphatic spread of the *M. tuberculosis* bacillus to other organs. Pulmonary TB is reported in 18-42% of patients with extrapulmonary TB, as in our case. Among cases of extrapulmonary TB, the incidence of lymph node TB is second to that of TB pleuritis [4].

Early diagnosis and proper treatment are keys to preventing *M. tuberculosis* transmission. However, TB is well known as a diagnostic chameleon and can also resemble malignancy. In the thorax, TB can manifest as a pulmonary infiltrate and/or mediastinal lymphadenopathy [5].

In our case, advanced lung cancer was first suspected because of severe mediastinal involvement. Benign diseases such as TB and sarcoidosis can also cause mediastinal lymphadenopathy [6]. Mediastinal tuberculous lymphadenitis is more common in childhood and primary TB. It causes lipid inflammation and the development of matting and conglomeration around the lymph nodes. There is lung-parenchymal involvement in 80% of patients with mediastinal TB lymphadenitis [7]; in our case, there were tree-in-bud lung lesions. Other chronic infections can also cause similar lesions. Chronic melioidosis was reported to have cavitary lung lesions and mediastinal lymphadenopathy [8]. Despite the highly suggestive diagnosis of malignancy using radiographic findings, a tissue biopsy should be performed for all patients, if possible, given the fact that the management options are widely different.

CT is a valuable complementary technique in the evaluation of mediastinal lymphadenopathy. There are 3 CT patterns of nodal involvement in TB. In the early course of the disease, the nodes are homogeneous in attenuation and contrast enhancement. As the disease progresses, the second and most common pattern, a node with a central area of necrosis, presents as a center of low attenuation with an enhancing rim. The low-attenuated center indicates caseation or liquefaction necrosis. The enhancing rim is representive of granulation tissue with inflammatory hypervascularity and hyperpermeability. The third pattern is a fibrocalcified node that is usually seen in patients who have been treated. Fibrotic strands and calcified spots are characteristic [9]. Central necrosis, fibrosis and calcified spots were also evident in the CT images of our case.

Bronchoscopy can play a primary role in the pulmonary TB diagnosis of patients who cannot cough up qualified sputum or who have negative sputum examination results [10]. A reliable specimen can be obtained by bronchoalveolar lavage (BAL). Bronchoscopic forceps biopsy can accurately diagnose endobronchial TB. A definite diagnosis was obtained for our patient by bronchoscopy. In addition to traditional lavage and biopsy, endobronchial ultrasound-guided transbronchial needle aspiration (EBUS-TBNA) may be useful in the setting of isolated intrathoracic lymphadenopathy [11]. Nucleic acid amplification (NAA) testing of sputum and tissue can facilitate an early diagnosis and differentiate TB from nontuberculous mycobacteria. In a systematic review and meta-analysis, the sensitivity and specificity of the Xpert MTB/RIF assay with lymph nodes were 83% and 94%, respectively [12]. In our case, TB-PCR showed positive for the biopsied tissue. A combination of EBUS-TBNA and NAA can increase the diagnostic rate in cases of mediastinal lymphadenopathy [13]. Tracheal or bronchial stenosis and lung atelectasis are the common complications of tracheobronchial TB.

In our case, left lower lobe collapse was evident on chest CT images. Balloon dilatation and bronchial stent by bronchoscopy may be the feasible treatment modalities [14].

Lung cancer and pulmonary TB can coexist in the same patient, and even in the same pulmonary lobe [15]. Even if TB has been diagnosed, the lesion should be followed up during anti-TB treatment. If the lesion does not shrink as expected, re-biopsy should be considered. Fortunately, in our case, the lung lesion decreased in size after anti-TB therapy.

In conclusion, TB and lung cancer have been confused and misdiagnosed for centuries, especially in countries with a low TB incidence. The atypical symptoms and imaging findings of some TB patients are diagnostic challenges [16]. We reported a patient with presumed lung cancer due to imaging findings, who turned out to have pulmonary TB instead. Microbiologic and histopathologic examinations, the gold-standard diagnostic methods for TB, should be performed in a timely manner to prevent a delay in diagnosis.

References

1. Global Tuberculosis Report 2018, World Health Organization (WHO) https://www.who.int/tb/publications/global_report/en/.
2. Infectious Diseases Statistics Inquiry System - Centers for Disease Control and Prevention (CDC) https://nidss.cdc.gov.tw/ch/SingleDisease.aspx?dc=1&dt=3&disease=010.
3. Statistics Department of the Ministry of Health and Welfare: Death statistics in 2018 https://www.mohw.gov.tw/dl-55956-b1722374-0580-4af8-b043-ae906b9d4634.html.
4. Golden MP1, Vikram HR. Extrapulmonary tuberculosis: an overview. Am Fam Physician 2005;72(9): 1761-8.
5. Hammen I. Tuberculosis mimicking lung cancer. Respir Med Case Rep 2015;16(C): 45-7.
6. Nin CS, de Souza VV, do Amaral RH, *et al*. Thoracic lymphadenopathy in benign diseases: A state of the art review. Respir Med 2016;112: 10-7.
7. Mehrian P, Moghaddam AM, Tavakkol E, *et al*. Determining the lymphadenopathy characteristics of the mediastinum in lung CT scan of children with tuberculosis. Int J Mycobacteriol 2016;5(3): 306-12.
8. Chan HP, Yip HS. Mediastinal lymphadenopathy: melioidosis mimicking tuberculosis. Trop Med Health 2015;43(2): 93-4.
9. Moon WK, Im JG, Yu IK, *et al*. Mediastinal tuberculous lymphadenitis: MR imaging appearance with clinicopathologic correlation. AJR Am J Roentgenol 1996;166(1): 21-5.
10. Mondoni M, Repossi A, Carlucci P, *et al*. Bronchoscopic techniques in the management of patients with tuberculosis. Int J Infect Dis 2017;64: 27-37.
11. Hassan T, McLaughlin AM, O'Connell F, *et al*. EBUS-TBNA performs well in the diagnosis of isolated thoracic tuberculous lymphadenopathy. Am J Respir Crit Care Med 2011;183(1): 136-7.
12. Denkinger CM, Schumacher SG, Boehme CC, *et al*. Xpert MTB/RIF assay for the diagnosis of extrapulmonary tuberculosis: a systemic review and meta-analysis. Eur Respir J 2014;44(2): 435-46.
13. Eom JS, Mok JH, Lee MK, *et al*. Efficacy of TB-PCR using EBUS-TBNA samples in patients with intrathoracic granulomatous lymphadenopathy. BMC Pulm Med 2015;15: 166.
14. Pathak V, Shepherd RW, Shojaee S. Tracheobronchial tuberculosis. J Thorac Dis 2016;8(12): 3818-25.
15. Kim YI, Goo JM, Kim HY, *et al*. Coexisting bronchogenic carcinoma and pulmonary tuberculosis in the same lobe: radiologic findings and clinical significance. Korean J Radiol 2001;2(3): 138-44.
16. Manca S, Fois AG, Santoru L, *et al*. Unusual clinical presentation of thoracic tuberculosis: the need for a better knowledge of illness. Am J Case Rep 2015;16: 240-4.

Marked Improvement in Pulmonary Function after Nintedanib Treatment in a Patient with Rapid Progressive Fibrosing Interstitial Lung Disease

Yen-Kun Ko[1], Chih-Yi Liu[2], Po-Ju Chen[3], Ming-Hong Yen[4]

A 62-year-old male, a smoker with rapid progressive fibrosing interstitial lung disease, developed exertional dyspnea and dry cough lasting for 1 year, with a decreased forced vital capacity (FVC) of 300 mL during the last 6 months. High-resolution computed tomography (HRCT) and the surgical lung biopsy pathology report showed a fibrosing pattern that lay somewhere between that of usual interstitial pneumonia and that of non-specific interstitial pneumonia. Twenty-one months after starting nintedanib therapy, the predicted FVC value increased 20% and the ground-glass opacity and consolidation on HRCT improved. The FVC value was subsequently maintained above baseline for 28 months. We concluded that the rapid improvement of the patient indicated a super-responder to nintedanib therapy. ***(Thorac Med 2021; 36: 129-134)***

Key words: progressive fibrosing interstitial lung disease, pulmonary function test, high-resolution computed tomography, nintedanib

Introduction

The term interstitial lung disease (ILD) encompasses a large group of over 200 pulmonary disorders, and of them, idiopathic pulmonary fibrosis (IPF) is a classic fibrosing ILD. There is a larger group of patients with differing clinical ILD diagnoses who develop a progressive fibrosing phenotype during the course of their disease; this was described as progressive fibrosing interstitial lung disease (PF-ILD) by Flaherty *et al* [1]. About 18~32% of patients diagnosed with non-IPF ILDs would develop progressive fibrosis in the USA [2].

Nintedanib is a small-molecule multikinase inhibitor that targets intracellular receptors of fibroblasts, and platelet-derived and vascular endothelial growth factor receptors [3-4]. In patients with PF-ILD (including usual interstitial pneumonia (UIP)-like or other fibrotic patterns), treatment with nintedanib has been reported to reduce the annual decline in forced vital capacity (FVC) by approximately 50% compared with a placebo over the course of 1 year [5-6].

[1]Division of Respiratory Therapy & Chest Medicine, Sijhih Cathay General Hospital
[2]Division of Pathology, Sijhih Cathay General Hospital
[3]Department of Surgery, Sijhih Cathay General Hospital
[4]Division of Thoracic Surgery, Cathay General Hospital
Address reprint requests to: Dr. Ming-Hong Yen, Department: Division of Thoracic Surgery, Cathay General Hospital
Address: Cathay General Hospital No.280, Sec. 4, Ren'ai Rd., Da'an Dist., Taipei City, Taiwan

To our knowledge, few previous case reports have described ILD patients who were super-responders to nintedanib. We report the case of a patient with rapidly deteriorating PF-ILD for whom treatment with nintedanib yielded remarkable improvements in FVC and high-resolution computed tomography (HRCT) findings.

Case Report

A 62-year-old male who was a trunk driver had smoked 1 pack of cigarettes a day for over 30 years. He had been well before, and then experienced shortness of breath and dry cough for 1 year. He had been prescribed oral prednisolone 5 mg/day, clarithromycin 1 g/day, a fixed-dose combination of evohaler (salmeterol 100 μg/day and fluticasone propionate 1000 μg/day), and quit smoking for 6 months, but the symptoms progressed.

He was then referred to a pulmonary physician in a regional hospital. Fine crackles were audible in the bilateral basilar lung region, and the FVC value decreased from 2.1 l/min to 1.8 l/min (from 62% to 53.3% of predicted). HRCT of the chest revealed progressive peribronchovascular reticulation with consolidation, fibrotic change and traction bronchiectasis in both lungs, predominantly at the peripheral and lower lung fields, without the presence of honeycombing (Figure 1A, B). Fibrosing obstructive pneumonia or non-specific interstitial pneumonia (NSIP), and "probable UIP" without a honeycombing pattern of IPF were considered [7-8].

No underlying condition that could have caused ILD was identified, and all of the examined autoantibodies (including ANA, RA, anti-Jo1, anti-Scl-70) were negative. Surgical lung biopsy (SLB) was advised to reach a definitive diagnosis.

In the histopathological exam, the section of the right lower lung revealed diffuse homogeneous alveolar wall thickening with infiltration of mononuclear cells and slight hyperplastic type 2 pneumocytes, compatible with fibrotic NSIP. There was mild interstitial inflammation and prominent fibrotic change, with a UIP-like pattern. Fibroblastic foci were also noted. These results showed a fibrosing pattern lying somewhere between UIP and NSIP, and a distinction could not be made with certainty (Figure 2).

PF-ILD was diagnosed based on the risk factor of smoking, the clinical symptoms, a rapid decline in FVC, and features of possible UIP or fibrosing NSIP on HRCT and SLB. The patient was treated with 150 mg nintedanib administered twice daily, and all other medications were withheld. After treatment with nintedanib for 6 months, the patient had no respiratory symptoms and HRCT images showed reduced areas of ground-glass opacity (GGO) and consolidation (Figure 1C).

Twenty-one months after treatment, HRCT images revealed continued regression of the PF-ILD (Figure 1D) and an improvement in FVC from 1.8L to 2.5L, or 20.7% (Figure 3).

During treatment, we noted grade 1 mild elevation of liver enzymes, which recovered by reducing the dose of nintedanib by half for 2 weeks. Diarrhea occurring less than 2 times/day continued, but was tolerable.

Discussion

Idiopathic pulmonary fibrosis (IPF) is an ILD of unknown cause with progressive deterioration in lung function and a 5-year survival rate of 20% [7].

A. Six months before treatment

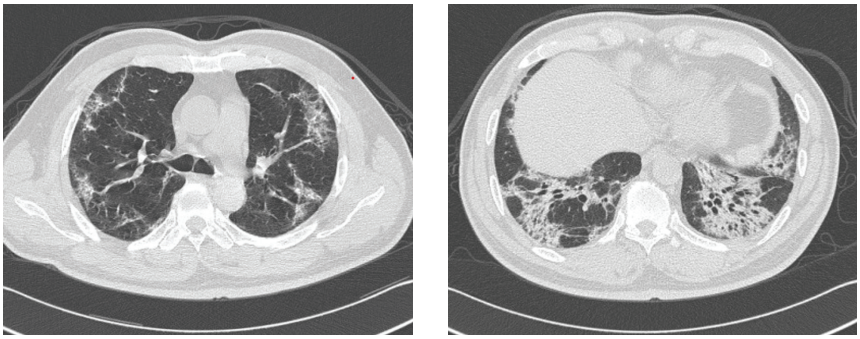

B. Just before treatment

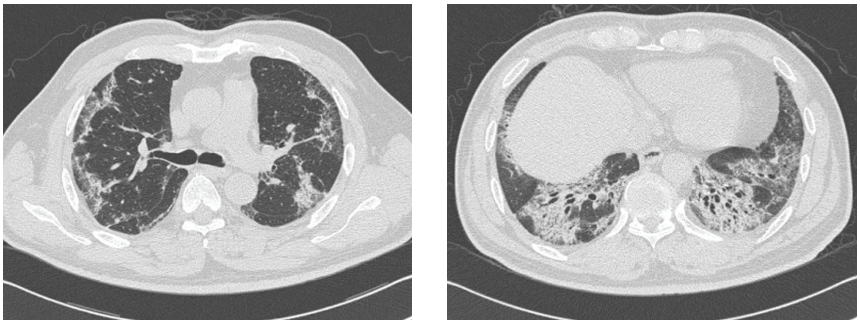

C. Six months after treatment

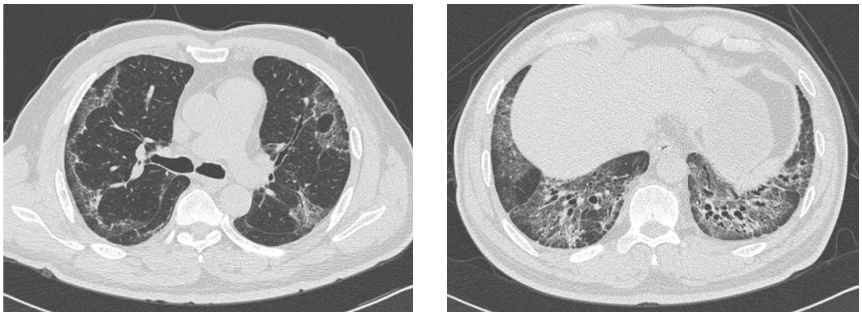

D. Twenty-eight months after treatment

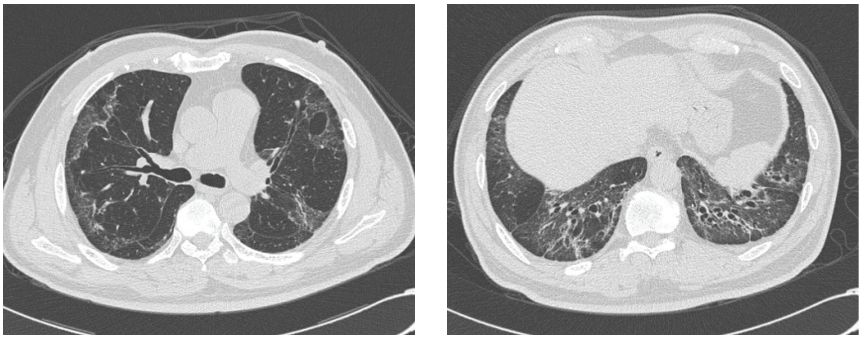

Fig. 1. Serial HRCT images at the carina level and at the lower lobe level. (A) Six months before treatment; (B) Just before initiating nintedanib therapy; (C) Six months after starting treatment; (D) Twenty-eight months after starting treatment. HRCT images showed reductions in the area of ground-glass opacities and consolidation compared to the images obtained before treatment.

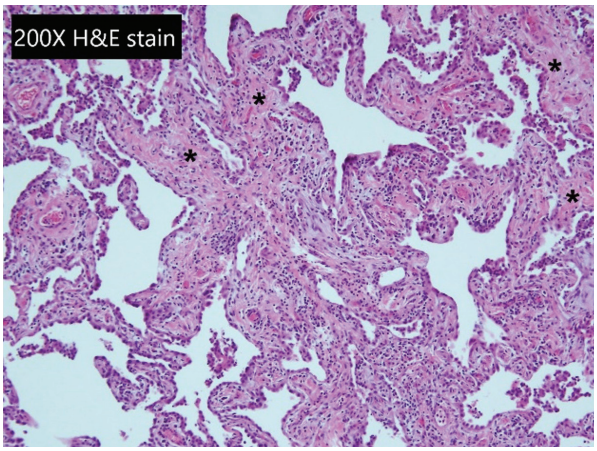

Fig. 2. Histopathology A surgical lung biopsy was obtained from the right lower lobe. There was mild interstitial inflammation and prominent fibrotic change, with a UIP-like pattern. Fibroblastic foci (*) were also noted. These results showed a fibrosing pattern lying somewhere between UIP and NSIP that could not be distinguished with certainty. (hematoxylin & eosin stain; x200 magnification).

PF-ILD has demonstrated a number of similarities to IPF, with the disease being defined by the presence of progressive pulmonary fibrosis, worsening respiratory symptoms, declining lung function, resistance to immunomodulatory therapies and, ultimately, early mortality [9].

Among patients with PF-ILD (including a UIP-like fibrotic pattern or others), the annual rate of decrease in FVC after 52 weeks of treatment was significantly lower among those who received nintedanib (-80.8 ml/yr) than among those who received placebo (-187.8 ml/yr) in the INBUILD study [6]. FVC in untreated patients with IPF has been reported to decrease 150 to 200 mL per year on average, similar to patients with PF-ILD [10].

In addition, the manifestations of fibrosing ILD that are associated with these diseases can overlap substantially with those of IPF, with radiographic and histologic patterns that meet the criteria for UIP, which was once considered the hallmark of IPF. As such, there is a lack of a diagnostic marker that would distinguish fibrosing ILD from IPF [9],

We report a patient with PF-ILD without an acute exacerbation episode, who had a rapid decline of 300 ml in FVC during a 6-month period under steroid treatment and a smoking cessation. The positive effects of nintedanib were

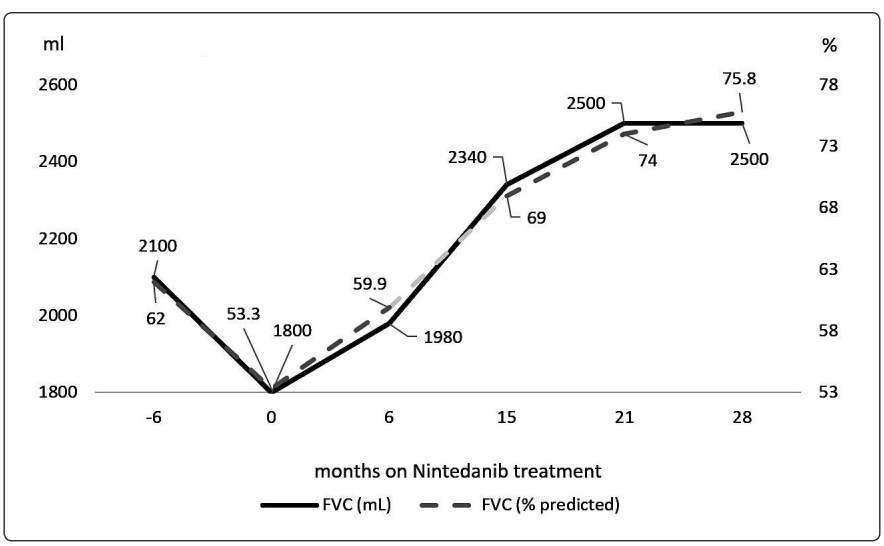

Fig. 3. Changes in forced vital capacity (FVC) and predicted FVC values during treatment.
FVC decreased 300 ml (8.7% of predicted) within 6 months before treatment and improved by up to 700 ml (20% of predicted) after 21 months of nintedanib treatment

clearly demonstrated by the clinical parameters, including FVC, HRCT findings, and clinical symptoms. In this case, FVC had improved by up to 20% when tested 21 months after initiation of treatment with nintedanib. Given these changes in FVC, the patient was regarded as a super-responder to nintedanib [11].

Flaherty et al. reported that in some IPF patients (24.8%) whose FVC improved or did not decline, median improvements in FVC at week 52 were 77 mL in the nintedanib treatment group [12]. The mechanisms underlying improvement in FVC in patients with IPF are unknown and no related data have been reported for PF-ILD.

In the INBUILD study, the FVC decline and therapeutic effect of nintedanib on maintaining FVC were similar in PF-ILD patients with a UIP-like fibrotic pattern or others [6]. A decline in FVC or an increase in fibrotic changes on HRCT in patients with ILDs reflects disease progression and is predictive of mortality [2].

An analysis of serial CT images may be useful for assessing the treatment efficacy of anti-fibrotic agents for IPF. Iwasawa et al. classified the CT lung field into normal, GGO, consolidation, emphysema, and fibrosis patterns [13]. The increase in GGO and fibrous pattern lesions and the decrease in the normal lung capacity of the antifibrotic agent (pirfenidone)-treatment group were also significantly less than that of the control. In previous case reports of IPF involving a super-responder to anti-fibrotic agents, the HRCT images showed a reduction in the areas of GGO [11, 14] and consolidation [11]. In the present case, the patient was without honeycombing on baseline HRCT, and showed improvement in GGO and consolidation 6 months after treatment.

The most frequently reported adverse event (over 60%) with nintedanib treatment is diarrhea, which was mild or moderate in intensity, and led to premature discontinuation of the medication in less than 5% of patients [5, 6]. About 11.4% of patients under nintedanib treatment in the INBUILD trials had elevated levels of liver enzymes [6]. In our patient, we noted grade 1 mild elevation of liver enzymes for about 2 weeks and diarrhea continued, but was tolerable without discontinuation of nintedanib treatment.

The median survival times for patients with non-IPF ILDs with progressive fibrosis in the USA, from the onset of symptoms to death, was estimated to be 61~80 months [2]. But the prognosis for an improvement in FVC with anti-fibrotic agent treatment is unknown. We believe that nintedanib improved the prognosis in our case because the FVC improved up to 20%. In addition, nintedanib remained tolerable for our patient 28 months after the start of therapy and FVC remained above baseline without respiratory symptoms.

In conclusion, we reported a patient with PF-ILD who was classified as a super-responder to nintedanib. A change in FVC and findings on HRCT images may be useful for assessing the efficacy of nintedanib. Further research is therefore highly warranted to identify predictive factors and the prognosis for an improvement in FVC in the subgroup patients with PF-ILD.

Acknowledgments

This case report was presented in part in the ILD casebook, Page 25, published by TSPCCM 2019. (https://drive.google.com/drive/folders/1rwnPasMr8wbPC78RG2OIBjE8xG46cjBi?usp=sharing)

References

1. Flaherty KR, Brown KK, Wells AU, *et al*. Design of the PF-ILD trial: a double-blind, randomised, placebo-controlled phase III trial of nintedanib in patients with progressive fibrosing interstitial lung disease. BMJ Open Respir Res 2017; 4(1): e000212.
2. Wijsenbeek M, Kreuter M, Olson A, *et al*. Progressive fibrosing interstitial lung diseases: current practice in diagnosis and management. Curr Med Res Opin 2019; 35(11): 2015-2024.
3. Richeldi L, Cottin V, Flaherty KR, *et al*. Design of the INPULSIS™ trials: two phase 3 trials of nintedanib in patients with idiopathic pulmonary fibrosis. Respir Med 2014; 108(7): 1023-1030.
4. Hilberg F, Roth GJ, Krssak M, *et al*. BIBF 1120: triple angiokinase inhibitor with sustained receptor blockade and good antitumor efficacy. Cancer Res 2008; 68(12): 4774-4782.
5. Richeldi L, Du Bois RM, Raghu G, *et al*. Efficacy and safety of nintedanib in idiopathic pulmonary fibrosis. N Eng J Med 2014; 370(22): 2071-2082.
6. Flaherty KR, Wells AU, Cottin V, *et al*. Nintedanib in progressive fibrosing interstitial lung diseases. N Engl J Med 2019; 381(18): 1718-1727.
7. Raghu G, Collard HR, Egan JJ, *et al*. An official ATS/ERS/JRS/ALAT statement: idiopathic pulmonary fibrosis: evidence-based guidelines for diagnosis and management. Am J Respir Crit Care Med 2011; 183(6): 788-824.
8. Raghu G, Remy-Jardin M, Myers JL, *et al*. Diagnosis of idiopathic pulmonary fibrosis. an official ATS/ERS/JRS/ALAT clinical practice guideline. Am J Respir Crit Care Med 2018; 198(5): e44-e68.
9. Goldberg HJ. Understanding progressive fibrosing interstitial lung disease through therapeutic trials. N Engl J Med 2019; 381(18): 1775-1777.
10. Klingsberg RC, Mutsaers SE, Lasky JA. Current clinical trials for the treatment of idiopathic pulmonary fibrosis. Respirology 2010; 15(1): 19-31.
11. Nakano A, Ohkubo H, Fukumitsu K, *et al*. Remarkable improvement in a patient with idiopathic pulmonary fibrosis after treatment with nintedanib. Intern Med 2019; 58(8): 1141-1144.
12. Flaherty KR, Kolb M, Vancheri C, *et al*. Stability or improvement in forced vital capacity with nintedanib in patients with idiopathic pulmonary fibrosis. Eur Respir J 2018; 52(2): 1702593.
13. Iwasawa T, Ogura T, Sakai F, *et al*. CT analysis of the effect of pirfenidone in patients with idiopathic pulmonary fibrosis. Eur J Radiol 2014; 83(1): 32-38.
14. Miyamoto A, Morokawa N, Takahashi Y, *et al*. Marked improvement with pirfenidone in a patient with idiopathic pulmonary fibrosis. Japan Soc Intern Med 16; 55(6): 657-661.

Pulmonary Adenocarcinoma Presenting as a Simple Cystic Lung Lesion: A Case Report

Po-Pin Cheng[1], Luga Lee[2], Jen-Jyh Lee[1,2], Bee-Song Chang[1,2], Chih-Bin Lin[1,2]

A pulmonary cyst is defined as a round, thin-walled (often less than 2 mm thick) parenchymal lucency that may contain air, fluid or a solid. A pulmonary cyst should be differentiated from a pulmonary cavity because the 2 entities often have very different etiologies. The differential diagnoses of lung cyst observed on HRCT or chest CT can range from isolated lung diseases to multisystem diseases. Primary lung cancer presenting as a cystic airspace lung lesion is relatively rare, and is often misdiagnosed or the diagnosis is delayed due to the poorly understood pathogenesis and sometimes subtle image changes. It is imperative that the underlying reason be sought when pulmonary cysts are identified on CT. We present the case of a 54-year-old male with a pulmonary cystic lung lesion at the upper segment of the right lower lobe that was eventually proved to be adenocarcinoma. ***(Thorac Med 2021; 36: 135-138)***

Key words: pulmonary cyst, adenocarcinoma of the lung

Introduction

A pulmonary cyst is defined as a round and thin walled (often less than 2 mm thick) parenchymal lucency or area of low attenuation that may contain air, fluid or a solid [1]. A pulmonary cyst should be differentiated from a pulmonary cavity because the 2 entities often have very different etiologies. A cavity is a gas-filled space which is often produced by emptying the necrotic part of the lesion, and contains a fluid level [1]. Differential diagnoses of lung cysts observed on high-resolution computed tomography (CT) or chest CT can range from isolated lung diseases to multisystem diseases [2]. Primary lung cancer presenting as a cystic airspace lung lesion is relatively rare, and is often misdiagnosed or the diagnosis is delayed due to the poorly understood pathogenesis and sometimes subtle image changes. When pulmonary cysts are identified on CT, it is imperative that the underlying reason be sought. We present the case of a 54-year-old male with a pulmonary cystic lung lesion in the upper segment of the right lower lobe that was eventually proved to be adenocarcinoma.

[1]Buddhist Tzu Chi General Hospital, Hualien, Taiwan
Address: 707, Sec. 3, Chung-Yang Rd. Hualien 970, Taiwan, R.O.C
[2]Buddhist Tzu Chi Medical Foundation and Tzu Chi University
Address reprint requests to: Dr. Chih-Bin Lin, Buddhist Tzu Chi General Hospital, No. 701, Sec. 3, Jhongyang Rd. Hualien 97004, Taiwan

Case Report

The patient was a 54-year-old male non-smoker with hypertension, who was admitted to our hospital due to a cystic lesion growing in the upper segment of the right lower lobe, as noted on serial chest CT images. The patient was noted to have a small cystic lung lesion measuring about 1 cm x 0.7 cm in the upper segment of the right lower lobe on low-dose CT (Figure 1) during a health check-up about 4 years prior (2014). The patient had no complaints about fever, cough or significant body weight loss. Physical examinations, complete blood count and blood chemistry panel results were unremarkable. Sputum acid-fast stains and cultures were found to be negative. Standing chest x-ray revealed no suspicious pulmonary lesions. The follow-up low-dose lung CT examinations in 2018 showed continued enlargement of the cystic lesion with a thickening cyst wall, irregular margin and septation (Figure 2). No other emerging lung cysts, nodules, or mediastinal lymphadenopathy was noted on low-dose lung CT. Malignant cystic lung lesion was highly suspected, so the patient opted to undergo a right lower lobe lobectomy using single-port video-assisted thoracic surgery (VATS) with lymph nodes dissection, rather than CT-guided transthoracic needle biopsy. The pathology report of the cystic lung lesion later confirmed it to be a mixed-type adenocarcinoma (Figure 3), pT1cN0M0. Immunohistochemical stain results included: TTF-1 (+), napsin-A (+), and CK7(+). The patient underwent a complete tumor resection, and no further chemotherapy was used. Follow-up positron emission tomography (PET) scan performed in 2019 showed no residual or new lung lesions.

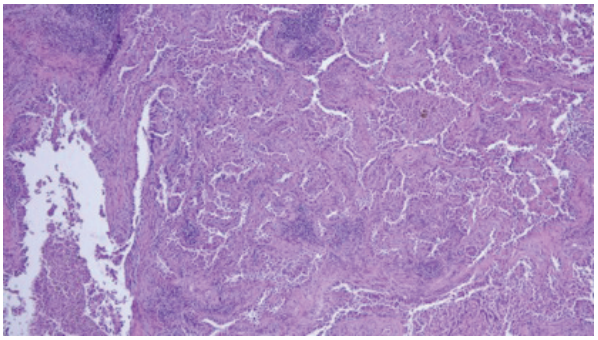

Fig. 1. Chest CT performed in June 2014 showing a 1 cm x 0.7 cm cystic lesion at the right lower lobe.

Fig. 2. Chest CT performed in October 2018 showing an enlarged cystic lesion, 2.2 cm x 1.7 cm in size, with septation at the right lower lobe.

Fig. 3. Histopathology of the cystic lung lesion performed in December 2018 confirmed adenocarcinoma.

Discussion

The lungs normally do not develop simple cyst(s) like other solid organs, such as the kidney or liver. Consequently, any cystic lesions of the lungs will require careful investigation [2]. The Fleischner Society defined cyst as a "thin-walled (<2 mm), spherical parenchymal lucency interfaced with the normal lung" and cavity as a "gas-filled space within a pulmonary consolidation, mass, or nodule, typically thick-walled (>2 mm) and more irregularly shaped than a cyst;" the 2 must be differentiated because a cavitary lesion has a higher risk of malignancy [1]. Primary lung cancers arising in association with cystic air space are uncommon. The prevalence of this condition is as yet unknown [3]. The distinguishing radiological features of pulmonary cystic lesions that point to malignancy include rapid growth with increased and uneven wall thickening [4]. abutting nodule(s) inside or outside the cystic wall, spiculation and septation [5]. The imaging features of the cystic lesion on the low-dose chest CT of our patient showed enlargement and septation, which was indicative of possible malignancy. The patient had no history of acute or chronic pulmonary infections which could potentially cause cystic wall thickening or irregularity.

Patients with cystic lesions suspected to be malignant should undergo percutaneous needle biopsy (3) to determine the nature of the lesion. Fluorodeoxyglucose (FDG)-PET may help strengthen the suspicion of malignancy [6]. However, a negative FDG-PET result does not rule out malignancy unless the solid component of the cystic lung lesion is greater than 8 mm [7].

The majority of primary cystic lung cancers are found to be adenocarcinoma, which often co-exists with pulmonary emphysema found in current or former smokers [6-7]. Cystic lung cancers show a slower growth rate than lung cancers arising from solid nodules [1]. Although malignant cystic lung cancers have a higher risk of a delayed diagnosis, no evidence has shown that this group of patients has a worse prognosis [3].

It is still uncertain whether malignant cystic lung cancer arises from pre-existing cystic lesions or that a microscopically small malignancy forms a check-valve which may result in cyst formation [6]. Despite currently insufficient information on the pathogenesis of malignant cystic lung cancer, any lung cysts without clear clinical or radiological characteristics pointing toward a benign lesion should be treated as lung cancer until proven otherwise.

References

1. Hansell DM, Bankier AA, MacMahon H, et al. Fleischner Society: glossary of terms for thoracic imaging. Radiology 2008; 246: 697-722.
2. Beddy P, Babar J, Devaraj A, Practical approach to cystic lung disease on HRCT. Insights Imaging 2011; 2(1): 1-7.
3. Sheard S, Moser J, Sayer C, et al. Lung cancers associated with cystic airspaces: underrecognized features of early disease. RadioGraphics 2018; 38: 704-717.
4. Farooqi AO, Cham M, Zhang L, et al. Lung cancer associated with cystic airspaces. Am J Roentgenol 2012; 199: 781-786.
5. Hasegawa M, Sone S, Takashima S, et al. Growth rate of small lung cancers detected on mass CT screening. Br J Radiol 2000; 73: 1252-1259.
6. Mets OM, Cornelia M, Schaefer-Prokop CM, et al. Cyst-related primary lung malignancies: an important and relatively unknown imaging appearance of (early) lung cancer. Eur Respir Rev 2018; 27: 180079.
7. Fintelmann FJ, Brinkmann JK, Jeck WR, et al. Lung cancers associated with cystic airspaces: natural history, pathologic correlation, and mutational analysis. J Thorac Imaging. 2017; 32: 176-188.

8. Deng H, Zhang J, Zhao S, *et al*. Thin-wall cystic lung cancer: a study of 45 cases. Oncol Letters 2018; 16: 755-760.
9. Aberle DR, Adams AM, Amanda M, et al. National Lung Screening Trial Research Team: reduced lung-cancer mortality with low-dose computed tomographic screening. New Engl J Med 2011; 365(5): 395-409.
10. Ye MX, Zhao YL, Zhang J, Quistes pulmonares como manifestación radiológica de enfermedades benignas y malignas: errores en el diagnóstico. Arch Bronconeumol 2012; 48: 138.

Disseminated Mycobacterium abscessus Infection in a Patient with Invasive Thymoma: A Case Report

Fan-Yi Chuang[1], Jia-Yi Feng[1,2], Yu-Chung Wu[2,3], Wei-Juin Su[1,2]

Nontuberculous mycobacteria (NTM) can be isolated from a variety of environmental sources. These free-living organisms have potential to cause a variety of infections, such as lung disease, soft tissue infection, and disseminated disease. Treatment for NTM can include anti-mycobacterial therapy and surgical management. Here, we present a case of dyspnea after recent median sternotomy, with disseminated NTM infection. ***(Thorac Med 2021; 36: 139-146)***

Key words: nontuberculous mycobacteria (NTM), *M. abscessus subspecies massiliense*, disseminated infection, invasive thymoma

Introduction

Nontuberculous mycobacteria (NTM) are widely distributed in the environment and can cause infections in humans exposed to the bacterial reservoirs, such as soil and natural or drinking water. This species is known to cause a broad spectrum of diseases in the human body, which more frequently present as lung disease, lymphadenitis, skin and soft tissue infections (SSTIs) and disseminated infection, often leading to mortality and morbidity. The incidence and prevalence of pulmonary NTM disease has been increasing [1]; it has become a health issue worldwide, and presents a greater disease burden than even tuberculosis in many geographic regions.

Up to now, more than 170 species of NTM have been identified [2], with many of them being documented as capable of causing disease in both immunocompromised and immunocompetent patients. All NTM species are characterized by a slow growth rate compared to other bacterial pathogens, but can still be further divided into rapidly growing and slowly growing organisms. Rapidly growing mycobacteria

[1]Department of Chest Medicine, Taipei Veterans General Hospital, Taipei, Taiwan
[2]School of Medicine, National Yang-Ming University, Taipei, Taiwan
[3]Department of Thoracic Surgery, Taipei Medical University Hospital, Taipei, Taiwan
Address reprint requests to: Dr. Jia-Yi Feng, Division of Pulmonary Immunology and Infectious Disease, Department of Chest Medicine, Taipei Veterans General Hospital, Taipei, Taiwan, No. 201, Sec.2, Shih-Pai Rd., Beitou District, Taipei City 11217, Taiwan, R.O.C.

(RGM) usually grow in less than 1 week after initial isolation, and the most clinically relevant species are *Mycobacterium abscessus (M. abscessus) complex* (including the subspecies: *abscessus, massiliense, and bolletii), M. fortuitum*, and *M. chelonae*. Both slow-growing and rapid-growing organisms have diverse manifestations from colonization to disseminated diseases. In this report, we present a case of disseminated *M. abscessus subspecies massiliense* infection with lung, pleural, sternum, and pericardium involvement.

Case Report

A 51-year-old female presented to our emergency department with symptoms of dyspnea. She worked as a hairdresser and lived with her family in Taoyuan County in Taiwan. She was a non-smoker and did not drink alcohol. She was non-diabetic and in good health until she underwent median sternotomy surgery for an anterior mediastinal tumor 2 months prior to her present hospital visit. The initial presentation was pain in the left shoulder and chest that had persisted for approximately 2 years. A chest X-ray (Figure 1A) and chest computed tomography (CT) scan (Figure 2A) showed a 7-cm irregular mass in the anterior mediastinum with bilateral pulmonary centrilobular opacities. Since respiratory symptoms were insignificant, evaluation of the pulmonary infiltrations was not pursued preoperatively. The patient underwent extended thymectomy, partial pericardiectomy, angioplasty, left upper lobe S3 segmentectomy, and artificial pericardium patch repair. The pathology was reported as invasive thymoma. Postoperative recovery was smooth and she was discharged on the 8th day postoperatively.

Approximately 2 days prior to this admis-

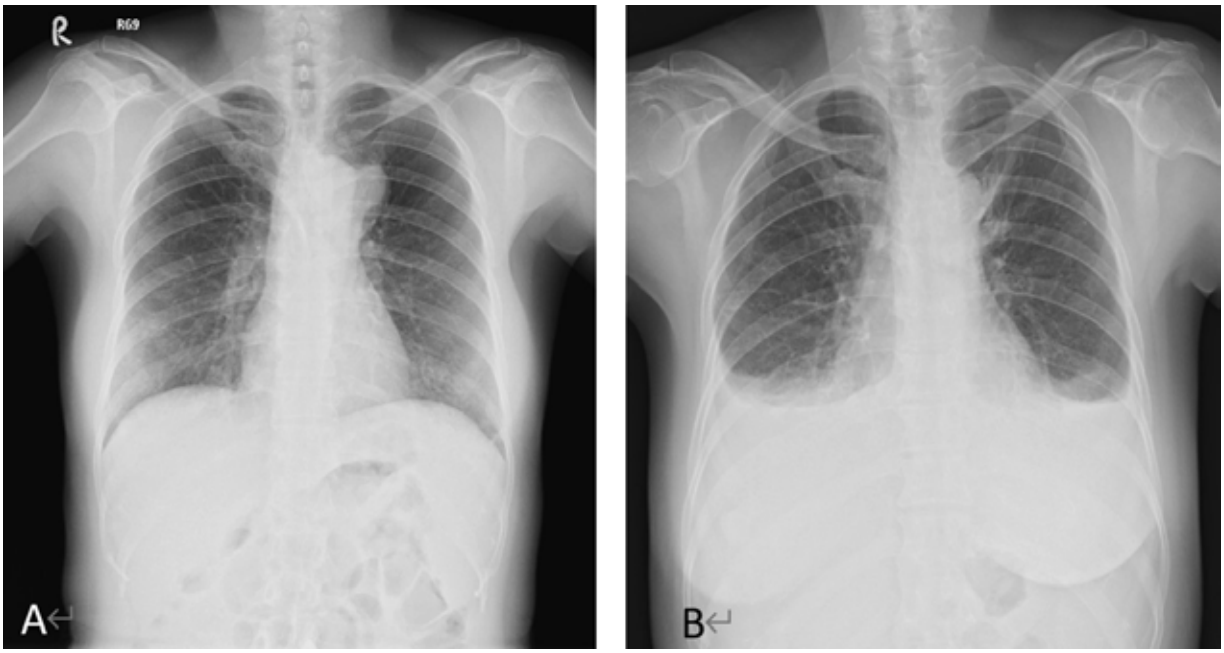

Fig. 1. Chest X-ray obtained before surgery showing (panel A) an anterior mediastinal tumor abutting the aortic arch. Before the present admission, bilateral pleural effusion, cardiomegaly, and increased pulmonary infiltrations were noted in the lung fields 2 months after surgery (panel B).

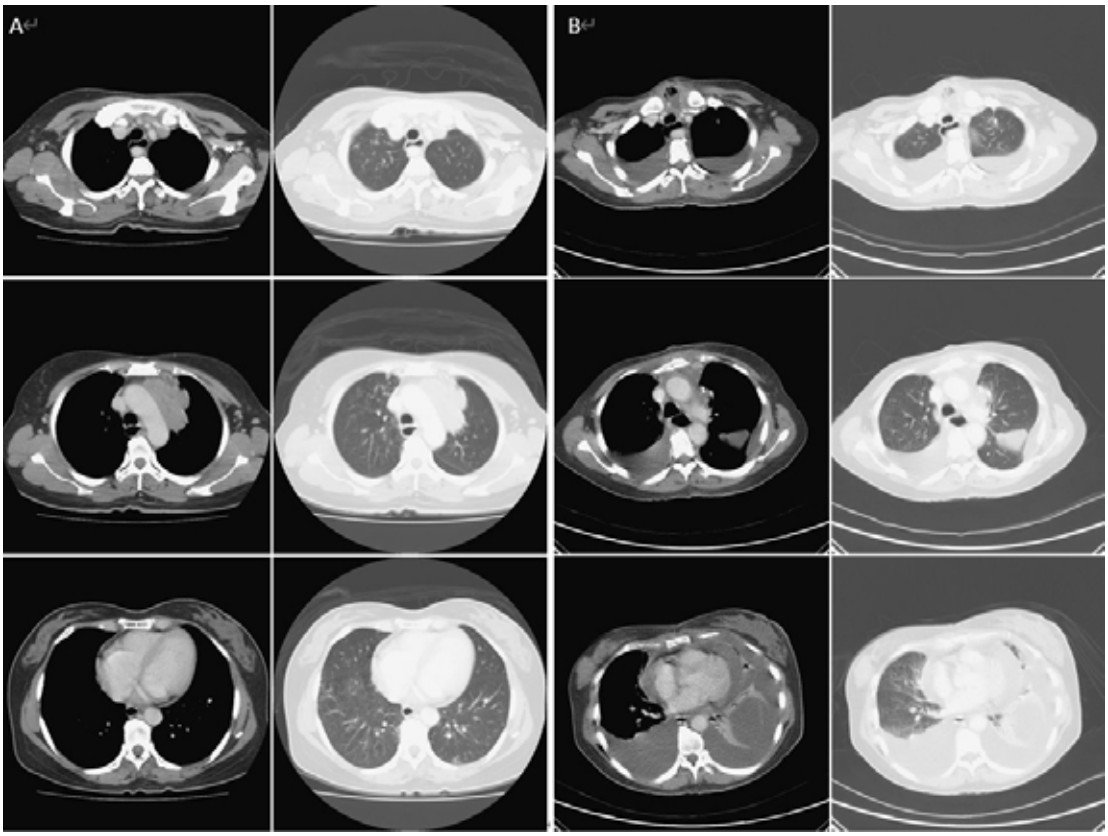

Fig. 2. Chest computed tomography (CT) obtained before surgery (panel A) showing an anterior mediastinal tumor and bilateral centrilobular opacities. Chest CT scans obtained before the present admission (panel B) showing gas accumulation in the sternotomy wound, bronchiectasis, centrilobular opacities in both lung fields, and bilateral pleural and pericardial effusion.

sion, the patient developed progressive shortness of breath. The symptoms developed gradually, without precipitating, exacerbating, or relieving factors. In addition, limb edema was also noted bilaterally. At the emergency department, her blood pressure was 144/103 mmHg, her pulse rate was 126 beat per minute, her respiratory rate was 22 per minute, and her body temperature was 37.1°C. Her oxygen saturation was 94% while breathing ambient air. An electrocardiogram showed sinus tachycardia, and chest X-ray revealed bilateral pleural effusion with increased infiltration in both lung fields (Figure 1B). Cardiomegaly was also observed. Laboratory data revealed leukocytosis (WBC 12600/cumm) with a left shift and an elevated C-reactive protein level (14.64 mg/dL). Diagnostic thoracocentesis of pleural effusion was performed at the emergency room and showed lymphocyte-predominant exudates with 73% lymphocytes and lactate dehydrogenase (LDH) levels of 400 mg/dL (serum LDH: 304 mg/dL).

Tube thoracotomy with pig-tail catheter placement was performed for bilateral pleural effusion drainage, and cefmetazole antibiotic was prescribed as empiric therapy. A chest CT scan reported gas accumulation in the sternotomy wound, accumulation of bilateral pleural effusion, and pericardial effusion with bronchiectasis and centrilobular opacities in both lung fields (Figure 2B). The acid-fast bacilli staining of pleural effusion and sputum were positive,

and the nucleic acid amplification test was negative for *M. tuberculosis*. Cytology of pleural effusion was negative for malignant cells. The level of complement component 3 and 4 were low (C3: 52.3, C4: 7.0 mg/dL). Tests for autoimmune disease showed positive results for antinuclear antibodies (1:160 diffuse type) and anti-double strand DNA antibody (138 IU/mL), and weak positive results for anticardiolipin antibody (12 MPL-U/mL). In addition, a serological test revealed that the patient was a hepatitis B virus (HBV) carrier. CT-guided pericardiocentesis was also performed for pigtail placement, and pericardial fluid analysis showed 79% lymphocytes and LDH levels of 1435 mg/dL. Mycobacterium culture of specimens from pleural effusion and sputum showed growth of *M. abscessus* after 8 days of culture. Subsequent genotyping confirmed the subspecies *M. abscessus massiliense*. Chemotherapy for *M. massiliense* was then started with combined therapy of parenteral imipenem, amikacin, moxifloxacin and oral clarithromycin. Video-assisted thoracic surgery for deloculation of pleural effusion and wedge resection of the left lower lung lobe were then performed. In addition, wound debridement was done after median sternotomy surgery for invasive thymoma. Tissue culture of the pleura, pericardium, lung and sternotomy wound were all reported positive for *M. abscessus*.

A peripherally inserted central catheter was implanted in the left arm for medication infusion, and intravenous therapy was continued. Mycobacterium culture of the patient's sputum showed negative conversion after 5 weeks of treatment. She was discharged after 6 weeks of treatment for *M. abscessus*. Intramuscular administration of amikacin was maintained for 8 weeks. Oral moxifloxacin and clarithromycin were prescribed as maintenance therapy.

Liver function test results remained within normal limits during treatment, but an abdomen sonography reported chronic liver parenchymal disease with a cirrhotic appearance, splenomegaly and the presence of ascites. A high HBV viral load test was detected (150,000,000 IU/mL). Entecavir was prescribed for treatment of HBV-related cirrhosis by a gastrointestinal specialist. In addition, persistent positive ANA, anti-dsDNA, anti-phospholipid antibody and low complement (C3/C4), with an episode of autoimmune hemolytic anemia with a positive direct Coomb's test were observed during follow-up. Systemic lupus erythematosus (SLE) was diagnosed and azathioprine and prednisolone (10 mg per day) were prescribed by a rheumatologist.

After 16 months of antibiotic treatment, the follow-up chest CT scan showed stationary bronchiectasis with regression of pulmonary centrilobular opacities (Figure 3). We discontinued the maintenance treatment and her condition was generally stable on follow-up clinic visits.

Discussion

M. abscessus complex is a group of rapidly-growing multi-drug resistant mycobacterium species [3]. Based on genome sequencing, the complex can be further divided into 3 subspecies: *M. abscessus abscessus, M. abscessus massiliense* and *M. abscessus bolletii*. The global isolation and prevalence of *M. abscessus complex* infection is diverse. According to recent research, *M. abscessus/chelonae* infection is the 2nd most common NTM pulmonary disease in the United States [4], secondary only to Mycobacterium avium complex, and accounts

Fig. 3. Chest X-ray obtained after 12 months of maintenance therapy (panel A) showing regression of pleural effusion and pericardial effusion. Chest CT scan (panel B) showing stationary bronchiectasis with improvement in pulmonary centrilobular opacities.

for 2-13% of NTM incidence. *M. abscessus* complex is more commonly detected in East Asia, and comprises 17.2% of all clinical NTM isolates in Taiwan [5]. The incidence of *M. abscessus bolletii* is rare [6], but the subspecies *M. abscessus abscessus* and *M. abscessus massiliense* both commonly cause human diseases [7].

M. abscessus complex usually causes pulmonary disease, SSTIs, central nervous system infection and occasionally, disseminated disease. Disseminated *M. abscessus* complex infection is more likely to occur in immunocompromised patients, such as hosts with acquired immune deficiency syndrome, anti-interferon-γ immunodeficiency syndrome [8] and malignancy. In a case series and literature review, about 8% of cancer patients with RGM disease had disseminated disease [9]. Disseminated infections were seen mostly in patients with hematologic malignancies (83% of cases). Among

RGM, *M. abscessus* complex (46%) was the most common species, followed by *M. chelonae* (27%) and *M. fortuitum* (23%). In a retrospective cohort of 725 SLE patients [10], NTM disease was not uncommon, with a prevalence of 1.5%. Among the 11 patients with NTM disease, most of them had skin and soft tissue infection and 1 had disseminated infection. Nevertheless, NTM infection was found to develop in the late disease course, rather than with the first presentation of a lupus diagnosis in the series. Initially, we thought that our patient was immunocompetent. However, during treatment, the patient was diagnosed with HBV-related cirrhosis and SLE, and therefore, we presumed that she was already immunocompromised before this infection. We did not check for anti-interferon antibody, and thus it is uncertain whether the patient also had concomitant anti-interferon immunodeficiency syndrome.

NTM species identification should be done after diagnosis. Molecular methods such as polymerase chain reaction are reliable for differentiation of RGM [11]. However, there are still no available commercial DNA probes for *M. abscessus* complex. Meanwhile, *M. abscessus* complex identified as "*M. chelonae/abscessus complex*" or "*M. abscessus*" may be inadequate without accurate subspecies identification. *M. abscessus* complex includes the subspecies *abscessus, massiliense*, and *bolletii*. Inducible drug resistance and treatment outcomes differ between subspecies [12], and thus may influence the treatment strategy chosen by physicians. In our case, subspecies identification was carried out after diagnosis of disseminated *M. abscessus* complex infection, which included identification of the subspecies as *massiliense*.

M. abscessus complex is resistant to most antibiotics and to anti-tuberculosis chemotherapy. Susceptibility testing with macrolides (clarithromycin), aminoglycosides (amikacin), fluoroquinolones, doxycycline, tigecycline, cefoxitin, imipenem, cotrimoxazole and linezolid was recommended by The Clinical and Laboratory Standard Institute [13]. Recent studies have questioned the important role of macrolides in the management of RGM, because of inducible resistance to clarithromycin in *M. abscessus subsp. abscessus*, due to the *erythromycin ribosomal methylase* (*erm*[41]) gene. This specific gene was present in *M. abscessus* complex, but absent in *M. chelonae* [14]. *M. abscessus* subsp. massiliense had a non-functional copy of the *erm*(41) gene, and thus the rate of clarithromycin resistance was lower in *M. massiliense* than in M. abscessus subsp. abscessus. An alternative mechanism leading to acquired macrolide resistance occurs via a point mutation in the *rrl* gene, which encodes the peptidyl transferase domain of the 23S rRNA. The *rrl* gene point mutation at nucleotides 2058 and 2059 was responsible for a high level of macrolides resistance in *M. abscessus* complex, even in the absence of a functional erm(41) [15-16].

Optimal regimens for adult patients with *M. abscessus* complex pulmonary disease are still lacking. According to the most recent British Thoracic Society guidelines published in 2017 [17], sensitivity to macrolides should be determined before the initiation of treatment. For macrolide-sensitive isolates, initial therapy with $\geq$ 4 weeks of macrolide-based therapy in combination with intravenous amikacin, tigecycline and imipenem, followed by a continuation phase with nebulized amikacin and macrolide in combination with 1-3 oral antibiotics is recommended. Unfortunately, macrolide susceptibility testing is not routinely performed in clinical practice in most institutes in Taiwan, including

our hospital. However, our in-house subspecies identification revealed that the isolate in our patient was *M. abscessus subsp. massiliense*. Therefore, we included macrolide in our regimen, which demonstrated a good treatment response. This highlights the importance of having subspecies identification and/or macrolides susceptibility tests in the management of patients with *M. abscessus*-complex pulmonary disease.

There is still a lack of consensus around the optimal treatment for M. abscessus complex infections in extrapulmonary organs, and thus the choice of treatment may rely on reported case series [7]. Surgical debridement of infective foci or abscess drainage may be beneficial in patients with skin and soft tissue infection, bacteremia and disseminated infections. The minimum length of therapy was 4 months in mild diseases, with at least 2 weeks of intravenous therapy. Continuation therapy for at least 4 weeks after a negative blood culture for bacteremia was recommended. The treatment outcome of NTM disease was satisfactory in SLE patients, and the therapy duration varied from 10 to 42 weeks for different sites of infection [10]. In our patient, surgical wound infection with *M. abscessus* was also noted, and therefore wound debridement was performed in the initial phase of our treatment. We also optimized the antibiotics duration and the treatment outcome was favorable.

In summary, we successfully treated an immunocompromised patient with disseminated *M. abscessus subsp*. massiliense infection. Our success was attributed to the rapid identification of the infection based on microbial culture evidence from the sputum, pleural effusion, pericardium and wound, and to an optimal combination therapy. Subspecies identification of *M. abscessus* complex plays a crucial role in the therapy strategy and prediction of macrolide susceptibility. Although the compromised immunity and disseminated infection indicate a higher treatment failure rate, our patient had a good outcome after long-term, complete maintenance therapy.

References

1. 3rd FJ. Current epidemiologic trends of the nontuberculous mycobacteria (NTM). Curr Environ Health Rep 2016; Jun;3(2):161-167. doi: 10.1007/s40572-016-0086-z.
2. AC. P. List of prokaryotic names with standing in nomenclature. Genus Mycobacterium. http://www.bacterio.net/mycobacterium.html (Accessed on August 8, 2019).
3. Brown-Elliott BA, Wallace RJ Jr. Clinical and taxonomic status of pathogenic nonpigmented or late-pigmenting rapidly growing mycobacteria. Clin Microbiol Rev 2002; Oct; 15(4): 716-746. doi: 10.1128/CMR.15.4.716-746.2002.
4. Prevots DR, Shaw PA, Strickland D, *et al*. Nontuberculous mycobacterial lung disease prevalence at four integrated health care delivery systems. Am J Respir Crit Care Med 2010; 182(7): 970-976.
5. Lai CC, Tan CK, Chou CH, *et al*. Increasing incidence of nontuberculous mycobacteria, Taiwan, 2000-2008. Emerg Infect Dis 2010;16(2): 294-296.
6. Benwill JL, Wallace RJ. Mycobacterium abscessus: challenges in diagnosis and treatment. Curr Opin Infect Dis 2014; 27(6): 506-510.
7. Lee MR SW, Hung CC, Yu CJ, *et al*. Mycobacterium abscessus complex infections in humans. Emerg Infect Dis 2015 Sep;21(9):1638-1646. doi: 10.3201/2109.141634.
8. Browne SK BP, Chetchotisakd P, Suputtamongkol Y, *et al*. Adult-onset immunodeficiency in Thailand and Taiwan. N Engl J Med 2012;367(8): 725-734.
9. Redelman-Sidi G SK. Rapidly growing mycobacteria infection in patients with cancer. Clin Infect Dis 2010;51: 422.
10. M. Y. Mok, S. S. Y. Wong, T. M. Chan, *et al*, Non-

tuberculous mycobacterial infection in patients with systemic lupus erythematosus, Rheumatology 2007;46(2), 280-284. doi: 10.1093/rheumatology/kel206.

11. Huebner RE GR, and Tokars JI. Current practices in mycobacteriology: results of a survey of state public health laboratories. J Clin Microbiol 1993;31(4): 771.
12. Koh WJ, Jeon K, Lee NY, *et al*. Clinical significance of differentiation of Mycobacterium massiliense from Mycobacterium abscessus. Am J Respir Crit Care Med 2011;183(3): 405-410. doi: 10.1164/rccm.201003-0395OC. PubMed PMID: 20833823.
13. Clinical and Laboratory Standards Institute (CLSI). Susceptibility testing of mycobacteria, nocardiae, and other aerobic actinomycetes. Approved standard—second edition. CLSI document M24–A2. Wayne (PA): The Institute; 2011.
14. Nash KA, Brown-Elliot BA, Wallace RJ Jr. A novel gene, erm(41), confers inducible macrolide resistance to clinical isolates of Mycobacterium abscessus but is absent from Mycobacterium chelonae. Antimicrob Agents Chemotherapy 2009 Apr; 53(4): 1367-1376.
15. Wallace RJ Jr, Meier A, Brown BA, *et al*. Genetic basis for clarithromycin resistance among isolates of Mycobacterium chelonae and Mycobacterium abscessus. Antimicrob Agents Chemother 1996;40(7): 1676-1681. doi: 10.1128/AAC.40.7.1676.
16. Faiza Mougari FB, Flora Crockett, Rachid Nessar, *et al*. Selection of resistance to clarithromycin in Mycobacterium abscessus subspecies. Antimicrob Agents Chemother 2017;61, Article e00943–16. doi: 10.1128/AAC.00943-16.
17. Charles S Haworth JB, Toby Capstick, Andrew J Fisher, *et al*. British Thoracic Society guidelines for the management of non-tuberculous mycobacterial pulmonary disease (NTM-PD). Thorax 2017;72: ii1-ii164.